JGR Solid Earth

FEATURE ARTICLE
10.1029/2018JB016459

GRAND CHALLENGES CENTENNIAL COLLECTION
AGU100 ADVANCING EARTH AND SPACE SCIENCE

Timescales and Processes of Methane Hydrate Formation and Breakdown, With Application to Geologic Systems

C. D. Ruppel[1] and W. F. Waite[1]

[1]U.S. Geological Survey, Woods Hole, MA, USA

Abstract Gas hydrate is an ice-like form of water and low molecular weight gas stable at temperatures of roughly −10°C to 25°C and pressures of ~3 to 30 MPa in geologic systems. Natural gas hydrates sequester an estimated one sixth of Earth's methane and are found primarily in deepwater marine sediments on continental margins, but also in permafrost areas and under continental ice sheets. When gas hydrate is removed from its stability field, its breakdown has implications for the global carbon cycle, ocean chemistry, marine geohazards, and interactions between the geosphere and the ocean-atmosphere system. Gas hydrate breakdown can also be artificially driven as a component of studies assessing the resource potential of these deposits. Furthermore, geologic processes and perturbations to the ocean-atmosphere system (e.g., warming temperatures) can cause not only dissociation, but also more widespread dissolution of hydrate or even formation of new hydrate in reservoirs. Linkages between gas hydrate and disparate aspects of Earth's near-surface physical, chemical, and biological systems render an assessment of the rates and processes affecting the persistence of gas hydrate an appropriate Centennial Grand Challenge. This paper reviews the thermodynamic controls on methane hydrate stability and then describes the relative importance of kinetic, mass transfer, and heat transfer processes in the formation and breakdown (dissociation and dissolution) of gas hydrate. Results from numerical modeling, laboratory, and some field studies are used to summarize the rates of hydrate formation and breakdown, followed by an extensive treatment of hydrate dynamics in marine and cryospheric gas hydrate systems.

Key Points:
- Gas hydrates are widespread, store large amounts of carbon, and are susceptible to degradation under warming ocean-atmosphere conditions
- Gas hydrate formation and breakdown rates are generally limited by mass transport and heat transport processes, respectively
- Hydrate dissolution, not dissociation, is the more common breakdown process; sufficient dissolved gas in adjacent fluids is necessary for hydrate to persist

Supporting Information:
- Supporting Information S1

Correspondence to:
C. D. Ruppel,
cruppel@usgs.gov

Citation:
Ruppel, C. D., & Waite, W. F. (2020). Timescales and processes of methane hydrate formation and breakdown, with application to geologic systems. *Journal of Geophysical Research: Solid Earth*, *125*, e2018JB016459. https://doi.org/10.1029/2018JB016459

Received 12 DEC 2019
Accepted 20 MAY 2020
Accepted article online 4 JUN 2020

1. Introduction

The vast deposits of methane hydrates in marine sediments and in permafrost areas (Figure 1) are often considered a potential future resource since they concentrate natural gas that could contribute to society's energy supplies if the gas could be economically extracted (Collett, 2002; Collett et al., 2009). At the same time, the susceptibility of natural gas hydrates to degradation when subjected to increasing temperatures has led to concerns about potential outgassing of methane as the oceans and the atmosphere continue to warm in the 21st century (Archer, 2007; Bangs et al., 2005; Biastoch et al., 2011; Harvey & Huang, 1995; Phrampus et al., 2014; Ruppel, 2011; Ruppel & Kessler, 2017; Stranne et al., 2016). In both cases, the rate of gas hydrate dissociation and the factors limiting the liberation of methane gas from hydrate are critical for quantifying the ultimate outcomes—how much gas is released in response to destabilization of the deposits and over which timescales.

Assessing the breakdown of gas hydrate and, conversely, its formation under natural conditions is an American Geophysical Union Centennial Grand Challenge with implications for ocean and atmospheric chemistry (Denman et al., 2007), geohazard assessments (Dugan & Sheahan, 2012; Hornbach et al., 2004; Mienert et al., 2005), global climate history (Dickens et al., 1997), the carbon cycle (Dickens, 2003), marine hydrogeology (Chatterjee et al., 2014; Jain & Juanes, 2009; Pecher et al., 2010; Roberts, 2001; Tryon et al., 1999, 2002), and energy resource studies (Collett, 2002; Holder et al., 1984; Li et al., 2016). A key goal of this paper is to build the reader's intuition about the response of natural gas hydrate reservoirs to dynamic processes occurring at or near the Earth's surface over the full range of relevant timescales.

This paper first reviews background information about gas hydrate and then discusses the thermodynamic controls on gas hydrate stability. This is followed by a description of the kinetic and mass and heat transfer processes related to hydrate formation and breakdown, with an emphasis on the most significant factors for

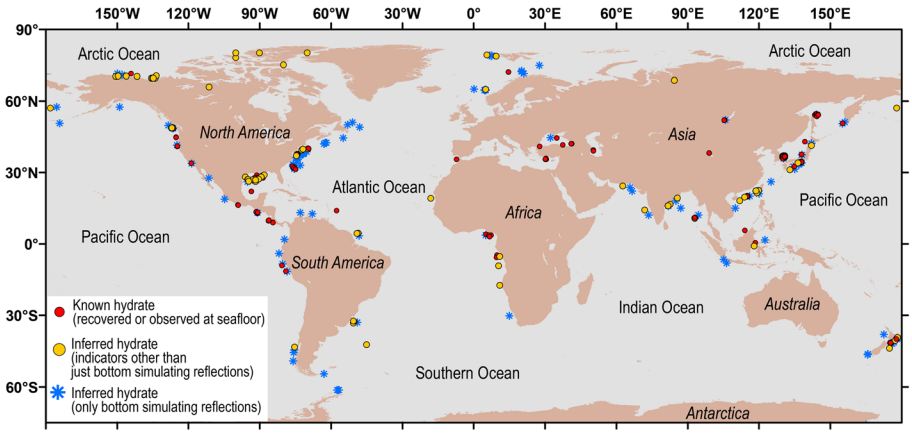

Figure 1. Global map of recovered or observed gas hydrate (red circles) and inferred gas hydrate (yellow circles and blue symbols) as of the end of 2019 from the preliminary U.S. Geological Survey database (Waite et al., 2020). The recovered hydrate is biased toward shallow deposits accessible by coring and drilling. Hydrate is inferred primarily based on bottom simulating reflections, borehole logs, and chlorinity anomalies associated with pore water freshening of recovered cores as hydrate dissociates. Blue symbols denote inferences based only on bottom simulating reflections and are plotted within the region of the bottom simulating reflection. Yellow circles signify inferences based on at least one other indicator of gas hydrate, sometimes in addition to bottom simulating reflections.

natural systems. We then review the rates of gas hydrate formation, dissolution, and dissociation using the results of molecular modeling, laboratory experiments, and some field observations. Finally, we discuss gas hydrate formation and breakdown processes, rates, and driving forces relevant to gas hydrate in geologic systems in marine and cryospheric settings. The paper concludes with a summary of critical points about phase changes in gas hydrate systems from a geoscience perspective.

2. Gas Hydrate Background

To set the stage for exploring Grand Challenge questions related to the formation and degradation of gas hydrate, this section first reviews fundamentals about single crystal gas hydrate and then discusses gas hydrate stability conditions and the application of theoretical stability models to natural systems. In this paper, natural systems are distinguished from gas hydrate formed as the result of human activities such as the installation of seafloor infrastructure or the production or transport of hydrocarbons.

2.1. Basic Characteristics

Gas hydrate, which often resembles opaque water ice, forms when water and low-molecular weight gas (e.g., methane, ethane, propane, carbon dioxide, and/or hydrogen sulfide) combine at high enough pressure (usually 3 to 30 MPa) and cold enough temperature (usually less than 25°C). Natural gas hydrate that is visible to the naked eye is always an agglomeration of many gas hydrate crystals that have formed in sediment pores, between sediment grains, in void spaces within sediments, at the seafloor, or on the surface of gas bubbles ascending through the marine water column.

Since gas hydrate often contains organic molecules in the form of hydrocarbon gases, it is not formally classified as a mineral. Nonetheless, gas hydrate structures are described using the crystallographic terminology applied to minerals. Gas hydrate typically forms one of two crystallographic structures, termed structure I (sI) and structure II (sII), within the cubic (isometric) system. Structure I gas hydrate is the most common type found in nature so far and is popularly rendered as a single water cage with 12 pentagonal and 2 hexagonal faces surrounding a gas molecule (see discussion in Sloan & Koh, 2007). The entire sI gas hydrate unit cell actually consists of six of these structures enclosing larger gas cages joined to two pentagonal dodecahedra enclosing smaller guest gas cages, for a total of 46 water molecules and 8 potential gas guest cages (or sites). Methane (CH_4), the most important hydrate-forming gas, can occupy both the small and large cages of sI gas hydrate. Figure 2a shows a scanning electron micrograph of an euhedral methane hydrate crystal synthetized in the laboratory in the presence of sand (Stern et al., 2004).

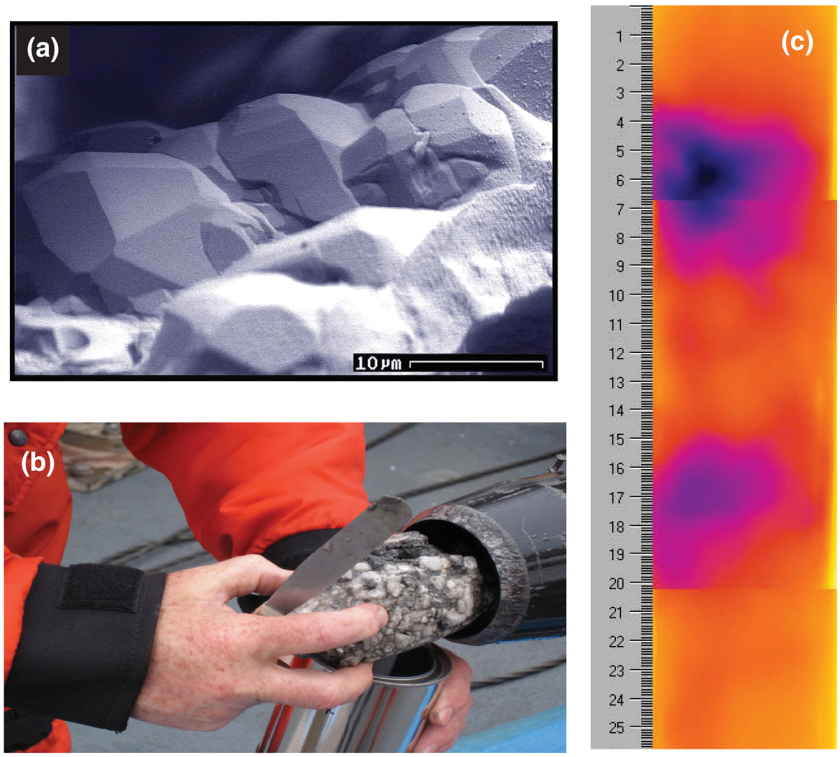

Figure 2. Gas hydrate imagery. (a) Euhedral methane hydrate crystals synthesized in the laboratory and imaged by scanning electron microscopy from Stern et al. (2004). (b) Chunks of gas hydrate (white) with sediment (gray) recovered during piston coring in the Arctic Ocean. Photograph by J. Fitzpatrick, USGS. (c) Thermal infrared image of sediment in a core immediately after recovery from the Indian Ocean during the first National Gas Hydrate Program drilling expedition (Collett et al., 2015). The blue area indicates endothermic dissociation of gas hydrate. Scale in cm.

Two other structures of gas hydrate are known to occur naturally on Earth, and both have larger cages and more complicated forms than sI. Structure II (sII) gas hydrate is the second most abundant type so far discovered in natural settings, and its water cages can accommodate higher-order hydrocarbon gases (e.g., ethane and propane), which have larger molecular sizes than methane. The sII unit cell contains 136 water molecules and has 16 pentagonal dodecahedra (small guest gas sites) linked to 8 water cages with 12 pentagonal and 4 hexagonal faces (large sites). Although sII hydrate is stable even when only the large cages are filled, naturally occurring sII hydrate often has a helper gas such as CH_4 in the small cages. Several studies have highlighted the coexistence of sI and sII gas hydrate in molecular dynamics (MD) simulations (Vatamanu & Kusalik, 2006), laboratory experiments (Ranieri et al., 2017; Schicks & Ripmeester, 2004), and natural reservoirs (Kida et al., 2006; Klapp et al., 2010; Paganoni et al., 2016; Qian et al., 2018; Schicks, 2018; Subramanian et al., 2000). In terms of spatial distribution on Earth, sI gas hydrates dominate those recovered to date, probably because most samples are obtained at shallow depths where methane is the predominant gas (e.g., Figure 2b). sII gas hydrates, which form where gas is supplied by thermogenic, multigas sources (e.g., Hadley et al., 2008; Paganoni et al., 2016), could be more prevalent deep in reservoirs, particularly in areas associated with conventional oil and gas resources.

Structure H (sH) gas hydrate was discovered only ~30 years ago (Ripmeester et al., 1987) and has 34 water molecules per unit cell. sH can accommodate both small (e.g., CH_4, hydrogen sulfide [H_2S]) and large gas molecules and is stabilized only when small gas molecules are present in the appropriate sites and the concentration of larger hydrocarbons is high (e.g., Tohidi et al., 2001). Because sH hydrate can accommodate larger and more complex hydrocarbon molecules than sII, it could theoretically form in thermogenic basins or in pipelines or vessels used in transport or processing of mixed hydrocarbons (Mehta & Sloan, 1996). The few natural samples of sH hydrate so far discovered have been found near migration pathways for thermogenic hydrocarbons (Chapman et al., 2004; Sassen & MacDonald, 1994). Tohidi, Anderson, et al. (2001) show

that sII hydrate, not sH, is the most stable form in the presence of complex hydrocarbon mixtures, which may include gas condensates, volatile oils, and black oils. sH hydrate is therefore not expected to be volumetrically important in global hydrate reservoirs.

Regardless of the gas hydrate structure, the water cages are often not fully occupied by gas molecules. For example, a water cage may form with no encased gas molecule, and gas molecules can move in and out of the cages after hydrate has formed. Considering cage occupancy (which is also cast as "hydrate number") yields more accurate calculations for the total amount of gas trapped in hydrates and improves certain thermodynamic property estimates of methane-water systems. As an example, the ideal case with complete cage occupancy for sI hydrate has only 5.75 water molecules per methane (8 cage sites per 46 water molecules). In naturally formed or laboratory formed sI gas hydrate, however, the ratio is often 6 to 6.2 water molecules for each methane molecule (Circone et al., 2005a; Kida et al., 2015, 2019), a 4–7% reduction in the amount of methane per cubic meter of gas hydrate relative to the ideal case.

2.2. General Stability Conditions (Thermodynamics)

The pressure-temperature (P-T) conditions needed for hydrate stability prevail in modern marine sediments at water depths greater than a few hundred meters. Such conditions can also be found in and beneath permanently frozen ground (permafrost; Collett et al., 2011; Dallimore & Collett, 1995; Majorowicz et al., 2008; Ruppel, 2015), beneath some continental ice sheets (Lamarche-Gagnon et al., 2019; Wadham et al., 2012), and in the sediments that floor Lake Baikal (Kida et al., 2006; Scholz et al., 1993), the world's deepest freshwater lake. However, gas hydrate is not ubiquitous in sediments that occupy the appropriate P-T space because hydrate formation also requires gas in excess of its solubility in pore waters. This point has sometimes been missed when researchers calculated the potential "container size" for gas hydrates or, in other terms, how much of the global sedimentary section could potentially host gas hydrate. As discussed by Boswell and Collett (2011), Beaudoin et al. (2014), Ruppel and Kessler (2017), and others, calculations assuming that gas hydrate fills all appropriate P-T space have been the source of some of the larger published estimates of methane sequestered in global gas hydrate deposits or methane released when gas hydrate reservoirs dissociate. Nonetheless, methane hydrate is still estimated to sequester about one sixth of the world's methane (Boswell & Collett, 2011).

Forming and maintaining gas hydrate requires either sustained methane generation in situ or gas migration into the hydrate stability zone in either vapor phase or dissolved form. Methane, the most common guest gas molecule so far found in recovered gas hydrates, primarily forms from microbial breakdown of organic carbon. Gas hydrate is thus missing from sediments in the deeper parts of many ocean basins, which are typically starved of organic carbon. Gas hydrate also forms where thermogenic gases, including thermogenic methane, migrate into the hydrate stability zone from deeper conventional hydrocarbon reservoirs. This process is occurring now in petroleum basins such as the northern Gulf of Mexico (e.g., Brooks et al. 1984; Portnov et al., 2019). Such gas migration also explains the formation of gas hydrate at high northern latitudes during Pleistocene glaciations when gas that had reached the shallower sedimentary section overlying deep conventional reservoirs "froze" as gas hydrate during global cooling events (Dai et al., 2011; Majorowicz et al., 2008).

In the rest of this paper, the term gas hydrate refers to a clathrate hydrate structure that hosts gas molecules. Frequently, we use the term hydrate as shorthand for gas hydrate, and, unless otherwise specified, hydrate is used specifically to mean methane hydrate.

2.3. Thermodynamics: Equations of State

An equation of state (EOS) describes the phase boundary separating gas hydrate from other gas phases (vapor or liquid) as a function of pressure, temperature, and the availability of water and methane for an equilibrium thermodynamic state. The availability of a particular component is often described in EOS derivations by an activity (liquid) or fugacity (gas) parameter. The activity or availability of water can be thought of as the effective concentration of water in the full, nonideal system consisting of water plus dissolved salts and gas in its dissolved, vapor, or solid (hydrate) phase. Similarly, the fugacity or availability of methane in the gas phase can be thought of as the effective partial pressure of methane. Fundamentally, the EOS shows how hydrate stability depends on P-T conditions and whether enough water and gas are present to form the hydrate. Because gas hydrate formation depends on methane availability, an EOS for gas hydrate is naturally

linked to the solubility of methane in pore fluids in the presence of gas hydrate or vapor phase gas. The determination of the EOS and of methane solubility are often presented side by side in research papers.

The EOS for a given type of gas hydrate is a function of the hydrate-forming gases that are present, the salinity of the pore water, the size of pore spaces, and other factors. Higher-order hydrocarbons (e.g., ethane or C2, and propane or C3) form hydrates over a broader range of temperatures than pure methane (C1) (Sloan & Koh, 2007). Saline pore waters exercise an inhibitory effect that shifts the standard P-T curve for methane hydrate to lower temperatures (De Roo et al., 1983; Dickens & Quinby-Hunt, 1994; Liu & Flemings, 2006; Maekawa, 2001; Ruppel et al., 2005; Sloan & Koh, 2007), reducing the region of hydrate stability. Elevated capillary pressures in fine-grained sediments also inhibit hydrate formation (Clennell et al., 1999; Duan et al., 2011; Henry et al., 1999; Liu & Flemings, 2011), although the scarcity of free water (low activity of water) in such low-permeability media may dominate the inhibitory effect in these sediments (e.g., Liu & Flemings, 2007).

Predicting gas hydrate degradation processes, which encompass dissociation (Figure 2c) and dissolution, and formation processes requires accurate EOS and solubility curves for methane hydrate in the presence of pore fluids. At the time of the most rapid evolution in this field, there were relatively few studies that constrained methane hydrate stability (Dickens & Quinby-Hunt, 1994) and methane solubility (Davie & Buffett, 2001; Servio & Englezos, 2002) under conditions relevant to geologic systems. Verifying EOS has therefore been challenging and sometimes requires substantial interpolation from laboratory conditions to the more generic conditions captured by the EOS modeling approaches or equations. Even for the most common sI (methane-only) hydrate, differences in published EOS-based predictions of P-T conditions at the phase boundary can translate to variations of tens of meters for the predicted base of the gas hydrate stability zone in nature (e.g., Waite et al., 2019).

Here we discuss the EOS used most widely in the hydrates research community without considering commercial codes used in the energy industry. Table 1 summarizes these EOS and provides mathematical fitting functions that can be used by researchers for comparing the details of the EOS. Figure 3 compares the key EOS. The end of this section makes recommendations about application of the EOS in hydrate studies.

1. CSMGem: Programs distributed by Sloan and Koh (2007) are widely used by gas hydrate researchers to constrain hydrate stability conditions. Based on a Gibbs energy minimization (GEM) approach and a fit to empirical data (Dickens & Quinby-Hunt, 1994), the program yields the P-T conditions for the hydrate phase transition in the presence of salt or other inhibitors and also determines the equilibrium composition of the components even outside the hydrate stability field. Duan et al. (2011) note that CSMGem fits experimental data well but that its calculations are only valid up to pressures of 40–50 MPa. Naturally occurring gas hydrates are nearly always at lower pressure than this limit, rendering the CSMGem tool a good option for initial calculations. CSMGem does not take into account porous media phenomena.
2. Tishchenko et al. (2005) provide closed-form equations to calculate the stability conditions for methane hydrate and the solubility of methane in seawater systems up to 20°C and over a range of pressures and salinities that encompass natural systems. They estimate their phase change predictions have a maximum uncertainty of ±0.04 MPa (corresponding to ~4 m shallower or deeper in a hydrostatically pressured deepwater reservoir) for dissociation pressure at the most extreme temperature and salinity conditions they examine. Tishchenko et al. (2005) adopt a simplified approach to calculating the total activity of water in the system, rendering it as a function of the known activity of water in seawater. They also explicitly incorporate the interaction of the dissolved methane with ions in the fluid phase using a Pitzer approach (Pitzer, 1991). The formulation also includes changes in the activity of water in seawater with increased pressure, which is ignored by some other researchers and could cause an error in equilibrium pressure determinations on the order of their estimated accuracy (~0.03 MPa or 3 m). Although the compressibility of solid hydrate has almost no effect on predicted equilibrium conditions, Tishchenko et al. (2005) also take this factor into account. They postulate that variations in the hydrate number, which is a function of pressure and temperature, could be a critical source of uncertainty for their calculations but show that the effect is small. Tishchenko et al. (2005) make two further contributions of importance for scientists interested in natural gas hydrate reservoirs. First, they note that the widely cited 1.1°C

Journal of Geophysical Research: Solid Earth

10.1029/2018JB016459

Table 1
Mathematical Approximations to the Equations of State (EOS) in Terms of Pressure and Temperature for the sI Methane Hydrate-Water System With Various Fluid Phases and Porous Media[a]

EOS Name	Reference	Conditions[b]	Mathematical fits to EOS (pressure P in MPa; temperature T in °C)[c]
D&Q (experimental)	Dickens and Quinby-Hunt (1994)	Bulk 33.5‰ NaCl	$\log_{10}P = -0.0001584T^2 + 0.04733T + 0.4552$ $T = 123.2P^{0.069189} - 132.5$ T (° C) = [0, 11]; up to 10 MPa
CSMGem (Gibbs free energy)	Sloan and Koh (2007)	Bulk 35‰ NaCl	$\log_{10}P = 0.0001716T^2 + 0.04605T + 0.4626$ $T = -166.6P^{-0.06013} + 156.3$ T (°C) = [0, 27]
Tishchenko (first principles)	Tishchenko et al. (2005), Equation 24	Bulk 35‰ NaCl	$\log_{10}P = 0.0004238T^2 + 0.04114T + 0.4723$ $T = -81.36P^{-0.148} + 69.34$ T (°C) = [0, 20]
Duan (first principles)	Duan, Moeller, & Weare (1992)[d]	Bulk pure water	$\log_{10}P = 0.0004485T^2 + 0.03836T + 0.4231$ [0, 25] $T = -103.5P^{-0.1114} + 93.02$ T (°C) = [−2, 30]
	Duan and Sun (2006)[d]	Bulk 35‰ NaCl	$\log_{10}P = 0.0002462T^2 + 0.04417T + 0.4619$ [−2, 27] $T = -135.7P^{-0.07707} + 125.0$ T (°C) = [−2, 27]
	Duan et al. (2011)	Pure water; 9.2 nm cylindrical capillaries[e]	$\log_{10}P = 0.0005355T^2 + 0.04234T + 0.6174$ $T = -68.28P^{-0.197} + 51.58$ T (°C) = [−3, 18]
	Duan et al. (2011)	Pure water; 15.8 nm cylindrical capillaries[e]	$\log_{10}P = 0.0005682T^2 + 0.03925T + 0.5376$ $T = -65.52P^{-0.215} + 50.21$ T (°C) = [−3, 18]
	Duan et al. (2011)	Pure water; 30.6 nm cylindrical capillaries[e]	$\log_{10}P = 0.0005095T^2 + 0.034866T + 0.4829$ $T = -68.89P^{-0.1974} + 55.35$ T (°C) = [−3, 18]

[a]All mathematical fits were done using the Curve Fitting toolbox in Matlab 2019a. R^2 in all cases was at least 0.99. [b]"Bulk" indicates that the EOS was determined in the presence of water only (no porous medium). [c]Numbers in brackets indicate the temperature range over which the fits are considered valid. For Dickens and Quinby-Hunt (1994), this corresponds to the range in which they determined the stability boundary in their experiments. For Tishchenko et al. (2005), they report the given range as the one for which their formulation is applicable. For Duan et al. (2011), the range is that of the graph from which the original curves were digitized for fitting. [d]The original phase stability pairs (P, T) used for the fits were recorded by the authors several years ago using the online calculator of Duan and coworkers available at the time of publication of Duan and Sun (2006). [e]Stability curve was digitized from Figure 9a of Duan et al. (2011) and then fit by the functions shown at the right.

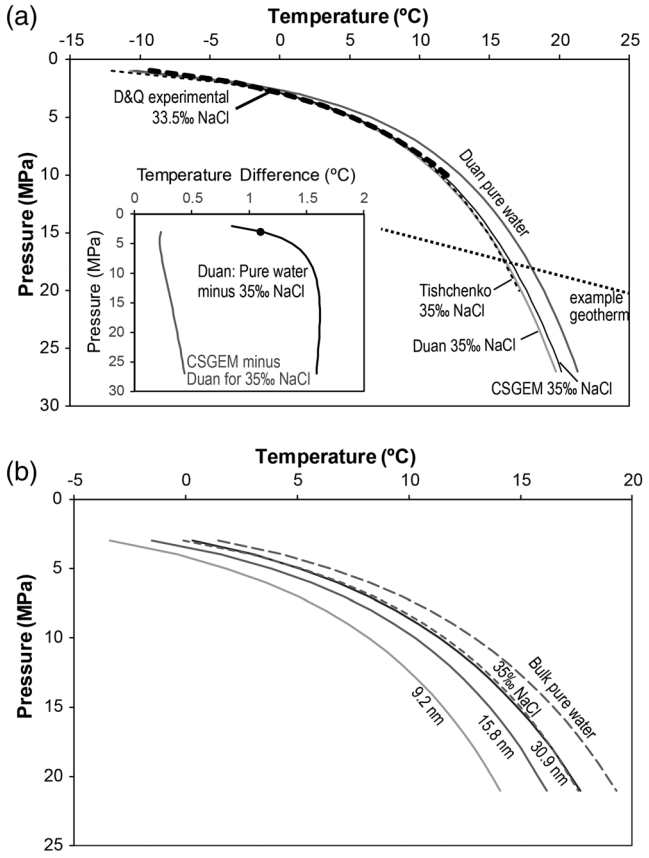

Figure 3. Comparison of various equations of state (EOS) for sI methane hydrate. Mathematical fits plotted here are given in Table 1. (a) EOS for sI methane hydrate for pure water ("Duan pure water" after Duan, Moeller, & Weare, 1992; dark gray curve) and 35‰ NaCl pore waters from Tishchenko et al. (2005), Duan and Sun (2006), and Sloan and Koh (2007). The EOS from CSMGem (Sloan & Koh, 2007), shown as the solid black line, was calibrated to fit the data of Dickens and Quinby-Hunt (1994), which is labeled "D&Q experimental" and shown as a thick dashed line. Those data were only acquired to 10 MPa. The Tishchenko et al. (2005) curve, shown as short dashes, is plotted only in the P-T range considered valid by that study. Thick dotted line shows a nominal geotherm of 30°C/km starting from the seafloor at 1,500 m water depth (~15 MPa) and ~6°C. Inset: The difference in temperature as a function of pressure between EOS for pure water and 35‰ NaCl (black curve) from the Duan formulations and between CSMGem and Duan for the 35‰ NaCl case (gray curve). The circle marks the nominal 1.1°C difference between sI methane hydrate stability in pure and saline waters as discussed by (Dickens & Quinby-Hunt, 1994). (b) Capillary pressure in porous sediments alters the EOS in the same way as the addition of saline pore waters. For pure water and cylindrical pores of 9.2, 15.8, and 30.9 nm (Duan et al., 2011), the inhibitory effect on hydrate stability can be even greater than that of nominal seawater (35‰ NaCl).

difference between the equilibrium P-T curve for pure water and seawater conditions as described by Dickens and Quinby-Hunt (1994), who used a salinity of 33.5‰, should actually be greater based on first principles calculations (Figure 3a). They estimate that the phase change in pure water occurs at temperatures 1.32°C higher at 3 MPa and 1.72°C higher at 30 MPa when compared to seawater with salinity of 35‰. Second, they expand on the work of Dickens and Quinby-Hunt (1997) to calculate the EOS for methane hydrate in equilibrium with sulfate-depleted pore waters. This provides a more complete parameterization of the gas hydrate stability field than is possible with an EOS that ignores the zone of anaerobic methane oxidation/sulfate reduction in the near-seafloor sediments.

3. The most sustained contributions to first principles development of EOS for the aqueous methane and methane hydrate system were made by Z. Duan and colleagues from 1992 to 2011. The early papers provided an EOS for methane and constraints on methane solubility in ionic systems (Duan, Moeller, Greenberg, et al., 1992; Duan, Moeller, & Weare, et al., 1992; Duan & Weare, 1992), and are still widely used by researchers to calculate methane fugacity. Duan and Mao (2006) updated the methane solubility framework, leading to greater accuracy than the older formulation (Duan, Moeller, Greenberg, & Weare, 1992). Sun and Duan (2005) published the results of an ab initio model for determining cage occupancy (hydrate number) and phase equilibrium for methane, as well as CO_2, hydrate. This approach eliminated reliance on Kihara potentials when generating Langmuir constants, a procedure that has been common in many models for determination of water activity. This ab initio approach also addressed one of the concerns raised by Tishchenko et al. (2005) about a potential source of uncertainty in their own work. Duan and Sun (2006) then incorporated the ab initio results of Sun and Duan (2005) into a new phase equilibria model that relied on the Pitzer approach for the interaction between methane and electrolytic pore fluids. Their formulation is less empirical than that of Tishchenko et al. (2005). In a final paper in this series, Duan et al. (2011) modify the earlier theoretical phase equilibrium framework and include capillary forces arising in porous media (section 2.4). They adopt a variant of the Gibbs-Thomson approach first used by Clennell et al. (1999) and Henry et al. (1999) in their consideration of porous media-methane hydrate interaction. Until a few years ago, the EOS from Duan and Sun (2006) and Duan et al. (2011) were available in online calculators that have since been removed from public access. This paper's authors had results from these online calculators stored in spreadsheets for use in other projects and fit these results to produce some of the equations given in Table 1.

Figure 3 shows a comparison among the three commonly used sI methane hydrate EOS for bulk seawater conditions along with a plot of the mathematical relationship supplied by Dickens and Quinby-Hunt (1994) to fit their experimental data and a pure water EOS from Duan, Moeller, and Weare (1992). As noted by Tishchenko et al. (2005), the difference between the pure water and seawater EOS is greater than the ~1.1°C estimated by Dickens and Quinby-Hunt (1994) for pressures greater than ~3 MPa (roughly corresponding to 300 m water depth). For most of the pressure range corresponding to deepwater marine reservoirs (>7 MPa), the offset between the two 35‰ NaCl EOS is ~1.5°C. The Tishchenko et al. (2005) and Duan and Sun (2006) predictions differ by less than ±0.16°C over the

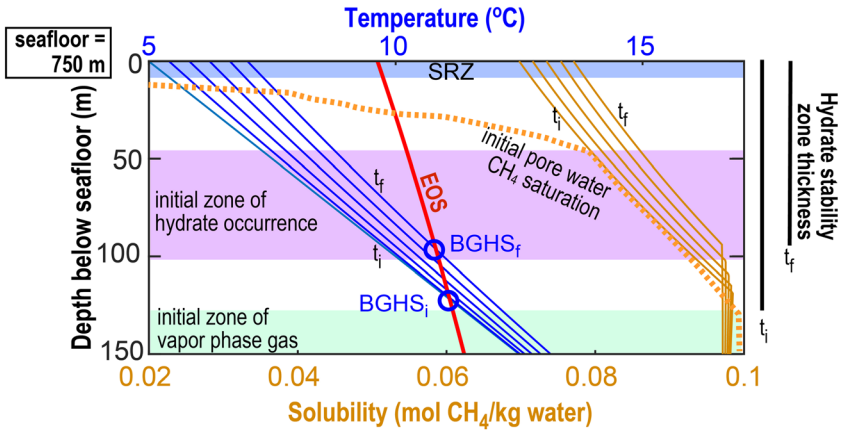

Figure 4. Schematic of the subseafloor zonation of the physical and chemical state within a homogeneous deepwater gas hydrate province, along with the evolution of geotherms (blue) and the solubility of methane in the pore waters (orange) as the bottom water temperature increases by 2°C over 1,000 years. Calculations depend on pressure and temperature and thus are keyed to a specific water depth, here taken as 750 m. The schematic assumes no in situ methane generation. The top of gas hydrate stability (TGHS) is in the water column, hundreds of meters above the seafloor. The base of gas hydrate stability (BGHS) is determined by the intersection of the evolving geotherms with the hydrate stability curve (equations of state, EOS), which is shown in red. Subscripts *i* and *f*, respectively, refer to initial and final times (*t*) for geotherms, solubility, and hydrate stability zone thickness, as well as BGHS depth. The sulfate reduction zone (SRZ) near the seafloor has no detectable methane. The initial pore water methane saturation (orange dashed curve) is at the solubility limit within only part of the stability zone, which would be the nominal zone where gas hydrate might occur (purple). With time, hydrate within the purple zone would dissolve due to the increased solubility of methane in pore space. If any hydrate remained from these dissolution processes, hydrate would dissociate at the base of the purple zone as the geotherm intersects the EOS. Initially, the saturation of methane below the BGHS exceeds solubility, meaning that vapor phase gas would be present. As warming progresses, the solubility limit decreases beneath the BGHS, meaning more of the existing methane will be in the vapor phase.

range in which the former study is considered valid. As long as researchers are not focused on reservoir temperature differences at this scale, either EOS could be used.

Since CSMGem is so widely available and implemented, it is also instructive to compare the CSMGem EOS to that of Duan and Sun (2006) for 35‰ seawater. The difference is greater than 0.2°C at lower pressures and exceeds 0.4°C at 25 MPa. For low geotherms, which would cross the EOS curves in Figure 3 at low angles, the disparity between these EOS could translate to a difference of fractions of MPa (tens of meters) in the position of the predicted base of hydrate stability (e.g., Waite et al., 2019). In general, deviations of a few meters between the depth to the base of gas hydrate stability (BGHS) as predicted from the EOS and inferred from field conditions are not significant given other factors (e.g., pore water composition and capillary effects) that can affect stability conditions in natural reservoirs. Thus, we recommend that any of the EOS discussed here can be applied with confidence in most studies.

Methane solubility (Zatsepina & Buffett, 1997, 1998) is a critical parameter controlling the dissolution of gas hydrate as well as the availability of methane for hydrate formation and the driving force for dissociation outside the stability zone (Figure 4). Calculating methane solubility can be daunting due to the need to include complex physical chemistry parameters. Waite (2012) provides a Matlab code that combines the solubility formulation of Tishchenko et al. (2005) within the hydrate stability zone and that of Duan, Moeller, Greenberg, and Weare (1992) and Duan and Mao (2006) outside hydrate stability conditions. The code can be applied to either pure water systems or systems with various user-determined salinities. Because the code combines two slightly different solubility formulations to generate a complete solubility curve for the hydrate and hydrate-free zones, we caution that the triple point (i.e., P-T for coexistence of methane in the aqueous phase, vapor phase, and hydrate phase) predicted by the code will not agree exactly with the P-T for the hydrate to vapor phase gas transition predicted by the EOS. The disparity can amount to several tens of meters in a typical marine reservoir. It is also important to remember that the combined phase boundary and solubility curve diagram as presented in Figure 1 of Xu and Ruppel (1999) and other papers (e.g., Davie & Buffett, 2001; Dickens, 2001) and shown in an updated version in Figure 4 collapses two

slices (P-T for the phase change and P-T solubility for a given geotherm) through a three-dimensional space (P-T solubility). Presenting this in three dimensions in general form is complicated by the fact that solubility will always be a function of the specific P-T conditions (geothermal regime; Figure 4 of Henry et al., 1999), pore sizes, and other factors in a reservoir (e.g., Davie et al., 2004; Liu & Flemings, 2011; Malinverno, 2010; Rempel, 2011).

2.4. Gas Hydrate in Porous Media

EOS derivations in the physical chemistry literature typically assume gas hydrate forms in bulk water rather than in the restricted space of sediment pores. The primary impact of pore size on gas hydrate formation is that methane solubility increases as pore size decreases (Clennell et al., 1999; Henry et al., 1999). This inhibits gas hydrate formation by limiting the availability of methane. Using their own EOS and a range of experimental results, Sun and Duan (2007) show that gas hydrate stability deviates from the bulk water EOS predictions for pore sizes below ~100 nm, a pore-size threshold that has also been discussed by others (Henry et al., 1999; Liu & Flemings, 2011). Sun and Duan (2007) find that the inhibition caused by gas hydrate growth in 31 nm-diameter pores instead of bulk water is roughly equivalent to the inhibition caused by replacing pure water with seawater (35‰), as shown in Figure 3b.

To provide a sense for the importance of this capillary inhibition effect, note that Uchida and Tsuji (2004) document pore sizes of ~100 nm in fine-grained marine sediments in the Nankai Trough, which is similar to the typical size (~60–70 nm) of pores in Blake Ridge sediments (Henry et al., 1999). For sands, 500–1,500 nm pore sizes have been reported in the Nankai Trough (Uchida & Tsuji, 2004) and 10^4 nm pore sizes in the Mackenzie Delta area (Uchida et al., 2009), which was the site of the Mallik permafrost hydrate well. Using the bulk water EOS for analysis of hydrate phase changes in sediments is a good approximation for even some fine-grained homogeneous reservoirs, but capillary pressure inhibition should be considered when analyzing the equilibrium state of reservoirs that contain considerable fines, even if the overall matrix is coarser grained. In Table 1 and Figure 3b, some of the capillary inhibition EOS curves provided by Duan et al. (2011) were fit with mathematical functions.

3. Definitions

This paper focuses on rates of gas hydrate formation and breakdown relevant to natural systems. Before considering the rates themselves, we define the processes and discuss common approaches to defining the phase boundaries for the gas hydrate system. Here we adopt the term breakdown to be consistent with the physical chemistry literature and to include both dissolution and dissociation.

3.1. Gas Hydrate Formation

Gas hydrate formation is controlled by three processes that are often collectively referred to as the kinetics of hydrate formation. These processes are summarized by Sloan and Koh (2007), Schicks (2018), and Yin et al. (2018) and can be divided into intrinsic kinetics, heat transfer, and mass transfer.

3.1.1. Hydrate Nucleation

The first step in the hydrate formation process is the nucleation of crystals, which can only occur in a system that is supersaturated with respect to the hydrate former. Hydrate nucleation and subsequent growth are controlled by intrinsic kinetics, which has been exhaustively reviewed by Yin et al. (2018). As summarized by these authors, most kinetic models apply to systems lacking porous media and are based either on the chemical reactions among hydrate constituents, mass transfer, or heat transfer. Models of gas hydrate growth in porous media generally neglect intrinsic kinetics, which is orders of magnitude faster than the timescales of interest in geologic systems, most flow assurance problems, and even laboratory experiments (Sloan & Koh, 2008).

Nucleation can be either homogeneous, in which only water and dissolved phase methane are present, or heterogeneous, in which salts, sediment grains, microbes, or other biological organisms or byproducts serve as "third surface" nucleation sites. Heterogeneous nucleation is always the predominant mechanism in natural systems (Knott et al., 2012) because it is far more energetically favorable than spontaneous nucleation of gas hydrate within the liquid phase. However, many laboratory synthesis experiments and MD studies continue to focus on descriptions of homogeneous nucleation.

Hydrate nucleation requires an induction time for the water and gas molecules to become organized as crystals. The induction time should not be confused with the actual kinetics of crystal formation, which, once started, proceeds so rapidly that most MD simulations track only a few nanoseconds of the system's evolution. For pure systems that lack nucleation sites, induction times for homogeneously nucleating gas hydrate, even in the entire volume of the world's oceans, have been described as being longer than the age of the universe (Knott et al., 2012). This characterization particularly refers to MD simulations that are not a priori formulated to nucleate hydrate crystals. Very long induction times have also been observed in laboratory experiments that lack impurities (Knott et al., 2012). On the other hand, Vatamanu and Kusalik (2010) and Jiménez-Ángeles and Firoozabadi (2014) describe nanosecond-scale homogeneous nucleation of gas hydrate in an extremely supercooled, methane supersaturated system used for their MD simulations. Supercooling is an important factor in the formation and long-term stability of gas hydrate and refers to a system cooled far below the phase boundary at a given pressure. The analysis of Guo and Rodger (2013) shows that, for supercooled methane solutions at supersaturation greater than 0.05 mole fraction CH_4, corresponding to 2.77 mol CH_4/kg, which is many orders of magnitude greater than supersaturations thought possible in nature, gas hydrate forms from liquid with aqueous phase methane without any induction time.

Even if induction scenarios for homogeneous hydrate nucleation have little bearing on natural systems, a finite induction time, which can range from less than a second to hours (Buffett & Zatsepina, 2000; Chaouachi et al., 2015; Jin et al., 2012; Tohidi et al., 2001), is still observed in laboratory experiments that track heterogeneous nucleation in systems containing porous media, water that is not ultrapure, or any other impurities. Induction time increases if P-T conditions are close to the stability boundary (e.g., mixture is not strongly supercooled), if fluid advection is limited (e.g., mass transport is low) or if the liquid is only minimally supersaturated with the hydrate-former (e.g., water activity limitation).

Models for homogeneous nucleation of gas hydrate crystals probably have little applicability to the heterogeneous nucleation that dominates in natural systems and are only briefly mentioned here. A recent review by Khurana et al. (2017) and brief discussion in Arjun et al. (2019) provide a modern perspective on homogeneous nucleation phenomena. Two of the simpler nucleation models are the labile clustering model, in which proto-hydrate water cage structures first form without the involvement of dissolved gas (Sloan & Fleyfel, 1991), and the local structuring model, in which dissolved gas molecules organize prior to formation of the proto-hydrate crystals (Radhakrishnan & Trout, 2002). In the cage structuring model (Guo et al., 2009), the formation of the small-site water cages precedes direct involvement of the gas molecules. Jacobson et al. (2011) postulate the blob model, in which gas molecules and proto-water cages agglomerate before becoming structured as gas hydrates.

Regardless of the most appropriate hydrate crystal nucleation model for homogeneous systems, the key factors relevant to natural systems are the locus and duration of hydrate nucleation. For an idealized system containing only water plus vapor phase and/or aqueous phase gas and no third surfaces to act as heterogeneous nucleation sites, nucleation is always most energetically favorable at the liquid-vapor interface. In a multiphase system that already contains some gas hydrate and where a vapor phase is lacking, nucleation of new hydrate crystals on the existing gas hydrate, which acts as a third surface in this case, is more energetically favorable than formation of new hydrate within the liquid. This is also the case for any other natural system lacking vapor phase gas and preexisting gas hydrate. Heterogeneous nucleation on the abundant third surfaces in natural systems is always more energetically favorable for hydrate initiation than is homogeneous nucleation within the liquid.

Even in laboratory experiments with ultraclean equipment and ultrapure water (no expected third surfaces), the induction time for hydrate nucleation is sometimes faster where gas hydrate has previously existed and then dissociated compared to systems where gas hydrate is nucleating anew. The phenomenon responsible for more rapid nucleation in the former case is known as the memory effect, and a succinct recent review of the issue is given by Ripmeester and Alavi (2016). Researchers have long postulated that dissociation of first generation hydrate leaves behind structured water containing incomplete hydrate cages (Vysniauskas & Bishnoi, 1983). The existence of these cages is thought to promote rapid crystallization of new hydrate once the thermodynamics (especially cooling; Uchida et al., 2000) is again favorable for hydrate formation. Substantial research has now also been conducted to investigate whether gas hydrate dissociation leaves behind not structured water cages, but gas nanobubbles (Bagherzadeh et al., 2015; Maeda, 2018; Uchida

et al., 2016; Zhang et al., 2019). A subsequent episode of hydrate formation would then be initiated by rapid nucleation of a hydrate film at the nanobubble's liquid-vapor interface. A third mechanism discussed by Ripmeester and Alavi (2016)—namely, the imprinted impurity hypothesis advanced for systems with hydrate inhibitors—implies that dissociation leaves behind impurities that can be sites for heterogeneous nucleation.

Detection of the memory effect would be difficult in natural systems since it would require (a) a method of delineating the occurrence or lack of gas hydrate at high spatial resolution; (b) an understanding of the types of reservoir forcing that might cause repeated formation and breakdown of gas hydrate on a temporal and spatial scale that could be monitored; and (c) a sense of how persistent the memory effect might be in pore fluids and whether advective circulation of these fluids would erase the effect. The BGHS in marine sediments might be one candidate for a reservoir location where the memory effect may play a role. As conditions there shift back and forth across the stability threshold, hydrate may break down and re-form on timescales far shorter than geologic processes. Less dramatically, the memory effect may also operate within the gas hydrate stability zone. Hydrate there can dissolve and then form again to maintain equilibrium with changing aqueous phase methane concentrations in pore waters.

3.1.2. Gas Hydrate Growth

The primary processes controlling hydrate growth are intrinsic growth kinetics, mass transfer, and heat transfer. As shown in section 4.1.1, intrinsic growth kinetics, which can be taken as the rate at which gas hydrate cages can form, are so fast relative to mass and heat transfer in natural systems that kinetics will not be considered further here.

Mass transfer of methane to the gas hydrate formation front is driven by gradients in concentration of dissolved gas in aqueous systems or is associated with the movement of gas and water molecules to the liquid-vapor interface for hydrate formation from the vapor phase. Hydrate formation from dissolved phase methane probably dominates most deepwater marine hydrate provinces, and, as noted in section 4.1, sediment pore waters must be locally supersaturated for hydrate to grow in equilibrium with the pore fluids. Mass transfer rates that carry methane to the gas hydrate formation front by either pore water advection, diffusion through the pore water, or diffusion through existing hydrate tend to be slow, as explored further in section 4. Growing hydrate from dissolved phase gas in porous media can require thousands of years for hydrate accumulations to reach saturations that are readily detectable by geophysical methods (e.g., VanderBeek & Rempel, 2018; Xu & Ruppel, 1999).

Although both diffusion and advection are normally slow transport mechanisms in nature (rates of mm/year to cm/year), advection should be more efficient than diffusion at delivering hydrate constituents to the hydrate formation front. Hydrate should grow more rapidly where fluids can circulate (Xu & Ruppel, 1999), and minimal rates of advection may be required for hydrate formation in most settings. Due to their elevated advection rates, settings with higher permeability (e.g., coarse-grained sediments and faults) and forced fluid flow (e.g., dewatering associated with compaction and fluid migration driven by temperature or pressure gradients) should be more prone to hydrate formation. However, VanderBeek and Rempel (2018) document a situation in which permeability clogging by hydrate halts advection but enhances diffusion along strong concentration gradients. In this case, diffusion is more efficient than advection in spawning the growth of new gas hydrate.

Hydrate formation at the liquid-vapor interface is the most energetically favorable formation mechanism when a vapor phase is present within the stability zone. Such formation is driven by gas fugacity between the hydrate and vapor phase, and the resulting mass transfer rates discussed in section 4.1.2 are substantially higher than can be obtained via dissolved-phase advection or diffusion. In natural systems, vapor phase gas can exist as discrete bubbles at and near the seafloor (which usually lies within the stability field) or emitted into the water column; as gas that has invaded the hydrate stability zone; in nanobubbles released by gas hydrate breakdown (see previous section); and just beneath the BGHS. Gas hydrate growth on a bubble begins at the liquid-vapor interface, forming a shell that separates the gas and water. As discussed in sections 4.1.3 and 4.2, this creates an arrangement where free gas, gas hydrate, and dissolved phase gas coexist within the P-T stability field for hydrate, marking it as a nonequilibrium thermodynamic condition (Fu et al., 2018).

Gas hydrate that forms from vapor phase gas within porous sediments initially coats gas bubble menisci between sediment grains, leading to different physical properties for the bulk medium than if hydrate

forms from dissolved phase gas (Lee et al., 2010; Waite et al., 2009). With enough vapor-phase methane, gas hydrate formation in porous media can consume all available pore waters, halting hydrate formation. Through salt exclusion that accompanies gas hydrate formation, this process can also render remaining water too saline for additional gas hydrate to form at given P-T conditions (e.g., Liu & Flemings, 2006). The absence of water that can be used for additional gas hydrate formation may then make it possible to pass gas through migration pathways within the hydrate stability zone without forming additional gas hydrate (Liu & Flemings, 2006; Smith et al., 2014). After many years in which the natural hydrates community focused primarily on formation of hydrate from aqueous phase gas in porous media (see discussion in Ruppel et al., 2019), more research is now being undertaken on hydrate formation from vapor phase. On the other hand, some researchers (e.g., VanderBeek & Rempel, 2018) have challenged the need to routinely invoke hydrate formation from vapor phase gas within the stability zone to explain high-saturation hydrate-bearing deposits.

Heat transfer is a more complicated aspect to incorporate into hydrate growth discussions since formulations must include the thermal properties of hydrate, water, and other constituents (e.g., porous media) and the exothermic heat of hydrate formation (Handa, 1986), which is ~18 kJ/mole CH_4. Just as mass transfer can involve diffusional and advective components, heat transfer can also have both conductive and advective aspects.

The heat of hydrate formation poses a particular challenge for inferring the impact of heat transfer processes in hydrate systems. For supercooled conditions, the exothermic heat of formation will slightly increase temperatures near the hydrate front, but this minor heating does not generally exercise a practical limit on hydrate growth. For systems with P-T conditions closer to the phase boundary, the exothermic heat release can play a more important role. The heat released as hydrate forms must be mitigated rapidly enough that it does not inhibit further hydrate growth. In low-permeability sediments or those with low rates of pore fluid advection, hydrate formation could be a self-regulating process due to the accumulation of heat from the formation process itself.

3.2. Gas Hydrate Breakdown

Gas hydrate can degrade either by dissolution or dissociation. Each process has its own kinetic controls that are very rapid with respect to other timescales in natural systems. Dissociation directly releases vapor phase gas and water, while dissolution should produce only aqueous phase gas and water. When P-T conditions are not conducive to gas hydrate stability, dissociation is the physical process that describes gas hydrate degradation. Dissolution occurs at P-T conditions where hydrate should be stable but where the pore fluid is undersaturated in the hydrate forming gas. In the vernacular, some researchers may refer to melting of gas hydrate, but this terminology is not strictly an accurate portrayal of the breakdown processes, which always involve the release of gas in either vapor or aqueous phase.

Most of the literature discussing gas hydrate breakdown in laboratory or field settings focuses on dissociation. Gas hydrate can be dissociated by either depressurizing or warming the system until conditions are outside those required for gas hydrate stability. Gas hydrate can also be dissociated by using chemical inhibitors to shift the gas hydrate stability conditions enough for the existing pressure and temperature to be outside the gas hydrate stability conditions.

Hydrate dissolution is more widespread than dissociation in natural systems because it can occur throughout the hydrate stability zone, not only at phase boundaries. Regardless of where gas hydrate is within the hydrate stability zone, surficial hydrate cages are constantly opening and closing, exchanging gas molecules with the pore fluid. Hydrate dissolution resulting in net loss of hydrate will occur wherever the surrounding fluid is undersaturated in aqueous methane. In this scenario, concentration gradients between the hydrate and the surrounding fluid drive gas out of hydrate lattices and into the dissolved phase (Rehder et al., 2004), reducing the local volume of gas hydrate. Like hydrate stability, gas solubility in pore fluids in the presence of hydrate is also a function of pressure and especially temperature conditions. Within the hydrate stability zone, an increase in temperature will increase solubility, leading to more gas hydrate dissolution. Conversely, cooling will reduce the solubility limit, allowing additional gas hydrate to grow from the excess methane (e.g., Servio & Englezos, 2002; Subramanian & Sloan, 2002).

Table 2
Order-of-Magnitude Gas Hydrate Growth Rate Estimates in Porous Media

Formation process	Time to saturate 1% of the pore space
Intrinsic kinetics (Molecular model) (Vatamanu & Kusalik, 2006)	0.1 s
Gas/water interface (Active injection or mixing) (Vysniauskas & Bishnoi, 1983)	Minutes
Dissolved phase fluid flow (laboratory flow rates) (Waite & Spangenberg, 2013)	~ 1 day
Gas flow (3 cm/yr, Hydrate Ridge) (Torres et al., 2004)	~20 years
Dissolved phase fluid flow (180 mm/year, Hydrate Ridge) (Nimblett & Ruppel, 2003)	1,000 years
Short-range dissolved-phase diffusion (<10 m through water) (Cook & Malinverno, 2013)	~10,000 years
Dissolved phase fluid flow (3–6 mm/year, Blake Ridge) (Nimblett & Ruppel, 2003)	20,000 years
Dissolved phase fluid flow (1–2 mm/year, general case) (Rempel & Buffett, 1997)	100,000 years

Note. Where possible, relevant flow rates are given.

4. Rates of Hydrate Phase Transitions

Actual rates of gas hydrate formation and breakdown are strongly tied to the details of the environmental conditions and imposed driving forces. Nonetheless, certain order-of-magnitude guidelines can assist researchers in assessing probable rates of gas hydrate phase change. This section discusses rates associated with gas hydrate formation and breakdown (dissolution and dissociation) through an examination of molecular modeling, laboratory, and field experiments.

4.1. Gas Hydrate Formation

This section covers the hierarchy of gas hydrate formation rates. As indicated in Table 2, the intrinsic kinetic rates of gas hydrate formation exceed the rates of hydrate formation observed in laboratory and field settings, which are in turn limited by rates of heat and mass transfer. The fastest natural rates apply to active systems with rapid heat and mass transfer. The slowest rates are associated with passive systems in which heat and mass transfer are conductive and diffusive, respectively, causing gas hydrate growth to become self-limiting. A framework for evaluating the measured rates of gas hydrate formation discussed in this section is shown schematically in Figure 5 to provide intuition about growth behavior under various conditions.

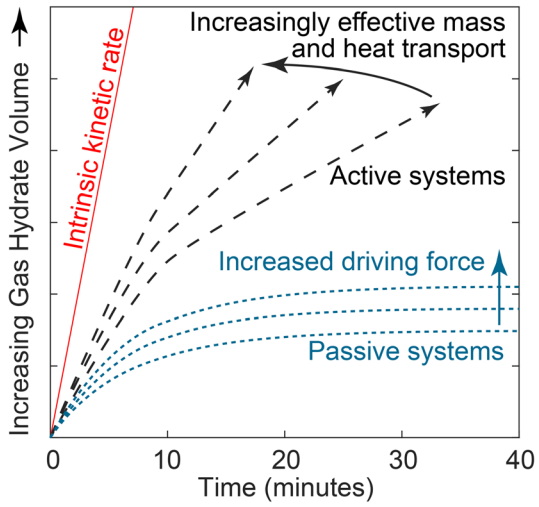

Figure 5. Schematic comparison of gas hydrate formation over time for intrinsic kinetics, active and passive systems. Gas hydrate is assumed to nucleate at time $t = 0$. Dashed black curves represent systems with active heat and mass transport. Formation rates are higher in systems that more effectively supply methane and remove heat (e.g., higher stirring speeds in batch reactors), but they do not reach the intrinsic kinetic formation rate (red solid line). Blue dotted curves represent passive systems where gas hydrate film growth separates the gas and water supplies. Formation rates and gas hydrate volumes increase with increased driving force (e.g., increased gas pressure). Though the curves are illustrative only, the crossover from rapid to slower growth near 10 min has been observed in both active and passive systems as explained in the text.

4.1.1. Molecular Modeling

As noted in section 3.1.2, gas hydrate formation rates should depend on the rates of heat and mass transfer, as well as on the intrinsic kinetics of the phase transformation. MD simulations can isolate the effect of intrinsic kinetic rates from the effects of heat and mass transfer rates. To promote gas hydrate growth within the nanosecond to microsecond durations of MD models, researchers artificially increase the concentration of available methane to several hundred times the saturation limit for methane dissolved in water (e.g., Jiménez-Ángeles & Firoozabadi, 2014; Vatamanu & Kusalik, 2006). Combined with imposed P-T conditions far within the gas hydrate stability field (Khurana et al., 2017), these MD simulations investigate gas hydrate growth at rates that are limited by neither methane availability nor the accumulation of heat. The MD results indicate that cage structures on the free surface of methane gas hydrate form on nanosecond (ns) timescales (Vatamanu & Kusalik, 2006; Walsh et al., 2009). With a surface growth (thickening) rate of ~0.1–0.4 nm/ns, gas hydrate may grow approximately four times faster than water ice (Vatamanu & Kusalik, 2006) and could theoretically fill the pore space of a fictitious standard specimen (1 m^3, 50% porosity) at a rate of 10–40% per second. Formation rates obtained from MD simulations are realistic only in the regime where mass and heat transport can be ignored and are thus not applicable to laboratory or natural systems (Table 2).

An additional observation from MD simulations is that hydrate cages are constantly opening and closing on the same nanosecond timescales on which they form (Vatamanu & Kusalik, 2006). Observations of rapid cage dynamics at gas hydrate surfaces have two important implications for gas hydrate formation and longevity in nature. The first is that nearly all gas hydrate formation rates in nature and in most laboratory experiments will be limited by mass and/or heat transfer rates rather than intrinsic kinetics. A second implication is that gas hydrate will only persist when the water in contact with the hydrate has methane concentration at or exceeding methane solubility in local pore waters, a factor discussed in section 3.1.2 and again in section 4.2.

4.1.2. Active Mass and Heat Transport

In natural systems, transport of mass, not heat, typically exercises the primary control on gas hydrate formation rates. The significance of mass transport can be anticipated from the concentrations of methane (~0.15–0.18 mole fraction) and water molecules (~0.82 mole fraction) in sI methane hydrate (Sloan, 2004; Sloan & Koh, 2007). These mole fractions are several orders of magnitude larger than the mole fraction of methane in bulk water $0.8–3.5 \times 10^{-3}$ (Lu et al., 2008; Sloan, 2004; Sloan & Koh, 2007) and the concentration of vapor-phase water in methane gas, $\sim 3.5 \times 10^{-3}$ (Sloan, 2004; Sloan & Koh, 2007). Attaining the relatively high mole fractions necessary for forming gas hydrate consumes all the methane available in adjacent water or all the water surrounding a methane gas bubble. Prolonged gas hydrate growth therefore requires methane or water to be replenished via transport to the formation front.

Figure 5 demonstrates that effective transport processes (black dashed curves) can yield formation rates approaching the intrinsic growth rate, with rapid initial growth giving way to a slower, linear increase in the amount of hydrate grown over time. The rapid initial growth phase will be discussed in greater detail in section 4.1.3 (passive systems). The constant growth rate phase is quasi-linear but does not continue indefinitely. Factors such as permeability reduction due to gas hydrate growth (Dai & Seol, 2014; Kang et al., 2016; Nimblett & Ruppel, 2003; VanderBeek & Rempel, 2018) often impose limits on methane transport and cause the growth rate to decrease.

As observed by Maini and Bishnoi (1981), Long and Sloan (1996), Tohidi, Østergaard, et al. (2001), and others (see overview by Sloan & Koh, 2007), gas hydrate formation is most energetically favorable at the gas/water interface, where high concentrations of both methane and water are available. To avoid the growth rate decreasing once gas hydrate formation has separated the gas and liquid phases, batch reactor experiments (e.g., Vysniauskas & Bishnoi, 1983, and others; also reviewed by Yin et al., 2018), which prevent constituents from entering or leaving the vessel during the reaction, use an impeller to draw gas hydrate away from the gas/water interface. This allows the gas and liquid phases to remain in contact to fuel further hydrate growth. By increasing the impeller speed to more effectively remove gas hydrate from the gas/water interface (Englezos et al., 1987; Vysniauskas & Bishnoi, 1983), the nearly linear gas hydrate growth rate can be somewhat increased. Although the peak formation rate observed during such experiments has been interpreted as the intrinsic formation rate (Englezos et al., 1987; Pangborn & Barduhn, 1970; You et al., 2019), Skovborg and Rasmussen (1994) demonstrate that this interpretation is incorrect. Even in the presence of an ideally maintained gas/water interface, gas hydrate growth is limited by the rate at which gas can be transferred into the liquid water phase from the vapor phase. This means that the observed rate in batch reactor experiments is limited by mass transport and does not represent the intrinsic kinetic growth rate (Skovborg & Rasmussen, 1994).

Actual peak gas hydrate formation rates vary with the P-T conditions (degree of subcooling) and reactor size. Even considering the mass transfer rate limitation, batch reactors are typically capable of forming methane hydrate at a rate of tens of grams per hour (Englezos et al., 1987; Skovborg & Rasmussen, 1994; Vysniauskas & Bishnoi, 1983). Considering the 500 cubic centimeter (cc) chamber used by Vysniauskas and Bishnoi (1983) as a porous sediment and approximating the porosity as being the 300 cc water volume (60% porosity), the batch reactor experiments could achieve gas hydrate growth rates of ~1% of the pore space every 5–10 min (Table 2). This estimate assumes a stoichiometry of $CH_4 \cdot 5.99H_2O$ (Circone et al., 2005a) and gas hydrate density of 0.925 g/cc (Helgerud et al., 2009).

One variation of the stirred batch reactor approach to creating fresh gas/water interfacial area for gas hydrate formation is to propagate a free gas phase through an otherwise fluid-saturated medium in a laboratory chamber. In a laboratory test of this process, Meyer et al. (2018) saturated ~11% of the pore space in their

coarse-grained sand with methane hydrate at a rate of ~1% per minute by allowing gas to invade their specimen at a rate of 0.18 ml/hr. This growth rate is similar to that estimated based on batch reactor experiments (Table 2).

These "percent per minute" gas hydrate formation rates on gas/water interfaces have implications for field-scale experiments. At the Ignik-Sikumi site on the Alaskan North Slope, injection of vapor phase CO_2 into a permafrost-associated methane hydrate reservoir was intended to displace water and drive CO_2 into the hydrate, thereby releasing the methane (Ohgaki et al., 1996). Due to hydrate formation at the interface between the injected gas and the reservoir water, the CO_2 injection rate decreased over the first 50 hr, even though researchers used a nitrogen-rich gas mixture that should have limited the rate of gas hydrate growth (Anderson et al., 2014; Boswell et al., 2017; Schoderbek et al., 2013). Anderson et al. (2014) conclude that rapid gas hydrate formation between the injected gas phase and reservoir pore water can be partially mitigated but is unavoidable.

A second variation of the stirred batch reactor is a two-chamber laboratory setup (e.g., Spangenberg et al., 2005; Priegnitz et al., 2013, 2015) that is designed to study hydrate formation from dissolved phase gas, a formation process that also relies on mass transport. The first chamber mixes water with vapor phase methane and is kept too warm for hydrate formation. The second chamber holds a water-saturated porous medium with P-T conditions within the hydrate stability field. In the warm chamber, methane is dissolved into water at temperatures near where solubility peaks. That methane-rich water is then pumped into a growth chamber held just above the freezing temperature of water, where the solubility of methane in equilibrium with gas hydrate is much lower (Priegnitz et al., 2013, 2015; Spangenberg et al., 2005; Waite & Spangenberg, 2013). The large methane solubility difference between the warm chamber and the cool gas hydrate growth chamber permits rapid (1–2% per day; Table 2) pore space gas hydrate growth (Priegnitz et al., 2013, 2015; Spangenberg et al., 2005; Waite & Spangenberg, 2013). For this laboratory setup, the rate-limiting factor for dissolved-phase growth is the rate at which methane gas can be dissolved into the bulk water in the warm chamber (Waite & Spangenberg, 2013).

4.1.3. Passive Mass and Heat Transport

The terminology of passive gas hydrate formation is used here to describe self-limiting situations in which gas hydrate growth increasingly separates the gas and water required to feed additional growth. Examples of passive natural systems include gas bubbles rising from the deep ocean floor or water droplets moving in pipelines transporting oil or gas. Gas hydrate growth in these systems typically evolves as shown by the dotted lines in Figure 5. Rapid initial growth at the gas/water interface gives way to much slower growth as the interface becomes increasingly coated with gas hydrate, forcing gas and water to diffuse through the gas hydrate layer to reach the gas hydrate growth surfaces (e.g. Taylor et al., 2007). The diffusion constant for methane through gas hydrate is 6 orders of magnitude smaller than that for methane through water (~10^{-15} m^2/s (Peters et al., 2008) compared to ~10^{-9} m^2/s (Jähne et al., 1987; Witherspoon & Bonoli, 1969; Witherspoon & Saraf, 1965)). Further slowing the growth rate is the secondary effect of the thickening gas hydrate shell, which increases the distance across which hydrate components must diffuse to sustain hydrate growth.

As in active systems, initial gas hydrate growth for passive systems occurs rapidly on a gas/water interface at observed rates of hundreds of micrometers per second (Freer et al., 2001; Liu et al., 2018; Peng et al., 2007). During this early growth stage, gas hydrate does not yet completely cover the gas/water interface, and gas hydrate simultaneously forms in the bulk water from methane that dissolves through the remaining gas/water interface (Subramanian & Sloan, 2002; Taylor et al., 2007). This bulk-water component of gas hydrate growth has important implications for why hydrate growth rate and the total amount of gas hydrate formed increase when the initial driving force is stronger (Figure 5). The driving force for gas hydrate growth can be increased by lowering the temperature (e.g., Taylor et al., 2007), which decreases methane solubility in water in the presence of hydrate (Lu et al., 2008; Servio & Englezos, 2002; Subramanian & Sloan, 2002) and thereby increases the amount of excess dissolved phase methane that can then be used for gas hydrate formation. The driving force can also be increased by raising the pressure (e.g., Lv et al., 2018), which dissolves more gas into the water. Cooling the system by a few degrees is far more effective at driving increased hydrate formation than is increasing pressure by a few MPa (1 MPa is roughly equivalent to 100 m of water in the marine environment). Gas hydrate growth from the dissolved phase methane can only continue until the

dissolved-phase methane concentration is reduced to the solubility limit. Thereafter, growth can only occur as rapidly as methane can dissolve into the water, either across the gas/water interface for the active systems discussed in section 4.1.2 or via diffusion through the gas hydrate film (Fu et al., 2019; Subramanian & Sloan, 2002; Taylor et al., 2007) for passive systems.

In both active (e.g., Englezos et al., 1987) and passive systems (e.g., Taylor et al., 2007; Fu et al., 2019), the dissolved phase methane is consumed in ~10 min, after which the growth rate drops. In active systems, for which gas hydrate formation at the constantly refreshed gas/water interface is the dominant formation mechanism, the cessation of gas hydrate formation from methane previously dissolved in the bulk water results in only a minor growth rate decrease (see Figure 4 in Vysniauskas & Bishnoi, 1983). For passive systems in which additional growth depends primarily on diffusion through an ever-thickening gas hydrate film, the growth rate decreases so significantly that Taylor et al. (2007) and Fu et al. (2019) represent the gas hydrate film thickness as constant (zero additional growth) after ~15 min.

In practice, gas hydrate growth rates even in passive systems tend to be faster than would be anticipated by assuming growth occurs only via diffusion of methane or water through the full thickness of the gas hydrate film. Several studies have shown that the gas hydrate interfaces tend to crack as they form (Jin et al., 2012; Lei et al., 2019; Tohidi, Østergaard, et al., 2001; Warzinski et al., 2014), creating pathways for more rapidly combining methane and water to form additional gas hydrate.

Initially, gas hydrate formation rates in a passive system can be rapid enough for heat dissipation to become a controlling factor. At the gas/water interface, gas hydrate coats the interface fast enough that the exothermic heat of formation must be dissipated by conduction and/or by advective flow. Such flow could itself be triggered by the temperature gradients between the advancing hydrate formation front and the surrounding medium (Freer et al., 2001; Liu et al., 2018; Mori, 2001).

The growth morphology of gas hydrate forming from dissolved-phase methane in bulk water depends on the efficiency of heat dissipation. Subramanian and Sloan (2002) and Ohmura et al. (2005) observed the formation of dendritic- or blade-shaped gas hydrate in supercooled experiments. At higher temperatures (lower subcooling), heat cannot be dissipated quickly, so formation favors polyhedral gas hydrate morphologies, which have lower surface to volume ratios (Ohmura et al., 2005; Subramanian & Sloan, 2002).

Heat transport has also been observed to limit gas hydrate formation in laboratory studies with large gas/water or gas/ice interfacial areas relative to the overall system volume. In these cases, gas hydrate growth in the initial stages can produce so much heat that the temperatures near the formation front reach the gas hydrate stability temperature (Shen et al., 2019). Continued gas hydrate growth requires dissipating heat to drop the temperature back within the stability field.

Heat transport is seldom the rate-limiting factor in natural systems because the mass transport-limited formation rates are typically low enough that heat can be sufficiently dissipated. Heat transport can be a critical consideration for industrial systems however. When a pipeline or well is intentionally shut in, flow is stopped, and fluids recovered from depths too deep and warm for gas hydrates to form have a chance to cool to near-seafloor temperatures. Hancock et al. (2019) indicate that shut-in times exceeding a few hours will likely be enough time for gas hydrates to start growing and potentially block boreholes or pipelines.

4.2. Gas Hydrate Dissolution

Rehder et al. (2004) demonstrate that gas hydrate dissolution is a diffusive process driven by the difference between the local solubility in the presence of gas hydrate (C_{eq}; solid curves in Figure 4) and the local dissolved phase concentration (C_0; dashed curve in Figure 4) of the hydrate-forming gas: $C_{eq} - C_0$. Their seafloor dissolution measurements for methane hydrate and for CO_2 hydrate, carried out where C_0 was effectively zero for both methane and CO_2, show CO_2 hydrate dissolves approximately eleven times faster than methane hydrate, in agreement with the solubility ratio: $C_{eq,\ CO2}/C_{eq,\ CH4} = 10.4$ (Rehder et al., 2004). Importantly, this study shows hydrate will continue dissolving until $C_0 = C_{eq}$. An analogous situation occurs on the free-gas/gas hydrate interface. If the partial pressure of water in the vapor phase is below the water's vapor pressure, gas hydrate will dissolve as water molecules from the gas hydrate are lost to the vapor phase (Hammerschmidt, 1934).

Table 3
Order-of-Magnitude Gas Hydrate Dissociation Rate Estimates

Dissociation process	Time to dissociate ~75% of the gas hydrate
Intrinsic kinetics (molecular model) (Windmeier & Oellrich, 2013)	0.1 second
Core recovery (conventional core) (Kowalsky & Moridis, 2007)	tens of minutes
Reservoir production (Nankai Trough, 1 m radius) (Yamamoto et al., 2017)	6 days
Reservoir production (Mt. Elbert, 450 m radius) (Kurihara et al., 2011)	50 years

Note. Gas hydrate is assumed to be filling a 1 m^3 sediment with 50% pore space for the molecular and core-scale models. Characteristic radial distance for 75% loss of gas hydrate is given for reservoir production models, both of which assume dissociation via depressurization.

In the absence of gas hydrate, dissolution rates of vapor phase methane in bulk water can be measured by tracking the size of a gas bubble over time. Bubble radius shrinkage rates of ~1 μm/s were observed in laboratory tests (Warzinski et al., 2014) and 4–7 μm/s were observed in open-ocean studies (Rehder et al., 2002, 2009). These dissolution rates provide important controls on gas hydrate formation on bubbles rising through the water column because the solubility limit for stabilizing gas hydrate is typically 4–5 orders of magnitude higher than seawater methane concentrations (Anderson et al., 2012) and gas hydrate cannot begin forming on a gas/water interface within the hydrate stability zone if the dissolved-phase methane concentration in the pore water is too low. This restriction is related to the fact that methane molecules from the gas phase dissolve into the water faster than a gas hydrate structure can develop to encage the methane (Chen et al., 2013; Maini & Bishnoi, 1981). The loss of methane from an ascending bubble to the surrounding water can, however, elevate the microscale methane concentration around the bubble to levels at which a gas hydrate shell can begin forming on the bubble's surface (Boewer et al., 2012; Chen et al., 2013; Rehder et al., 2009; Warzinski et al., 2014). Bubble dissolution rates are fast enough that bubbles released from seafloor within the hydrate stability field may only need to rise 1–5 m before developing a gas hydrate shell (Anderson et al., 2012; Wang et al., 2016).

Once a gas hydrate shell forms, observed bubble dissolution rates drop by a factor of 2–5 (Rehder et al., 2009; Warzinski et al., 2014). Rehder et al. (2009) suggest the rate reduction is due to the local solubility limit dropping from the gas/water solubility limit (no gas hydrate) to the solubility limit for methane in the presence of gas hydrate (e.g., Figures 3 and 1 in Subramanian & Sloan, 2002, and Waite et al., 2009, respectively). Reduced dissolution rates allow gas hydrate-coated bubbles to persist for longer than their uncoated counterparts. Dissolution effects are most obvious on rapidly evolving bubbles in the water column, but dissolution processes are also significant for seafloor gas hydrates exposed to seawater (section 5.1.3) and even for subsurface gas hydrate occurrences (section 5.1.1.2).

4.3. Gas Hydrate Dissociation

The rate of gas hydrate dissociation depends primarily on heat transport near the dissociation front. Yin et al. (2016) review dissociation rate models from molecular to field scales. Here, the focus is on building intuition for estimating dissociation rates at laboratory and field scales and on understanding why dissociation rates, like formation rates, are strongly dependent on experimental or site specific conditions.

4.3.1. Molecular Modeling

In the absence of mass or heat transport limitations, molecular modeling studies suggest that the intrinsic gas hydrate dissociation rate is equivalent to the intrinsic formation rate, with dissociation rates of 300–4,000 moles $CH_4/s/m^2$ possible on the gas hydrate surface (Windmeier & Oellrich, 2013). In terms of the fictitious example used for Table 3, the intrinsic dissociation rate is ~5–50% pore-space loss of gas hydrate per second (20–200 ms per 1% gas hydrate saturation). Even at the nanometer and nanosecond timescales used in molecular modeling, mass transport limitations are apparent. Methane, once liberated from the gas hydrate structure, must be dispersed into and through the water layer on the dissociating gas hydrate surface (English & Phelan, 2009; Kamath & Holder, 1987; Windmeier & Oellrich, 2013). Windmeier and Oellrich (2013) show the dissociation rate slows by 2–3 orders of magnitude as the concentration of methane builds in the adjacent water layer.

4.3.2. Laboratory and Core-Scale Processes

At the laboratory and core scale, heat transport becomes the rate-limiting factor for gas hydrate dissociation. Two heat sources are available to drive the endothermic dissociation of gas hydrate: sensible heat, meaning

the thermal energy stored in the gas hydrate, pore fluid, and sediment in the immediate vicinity of the gas hydrate dissociation front, and heat supplied from external sources via conduction or advection. For the 70% gas hydrate saturation in a medium with 40% porosity considered by Yamamoto et al. (2017), gas hydrate could supply only 5% of the sensible heat required for complete dissociation, and the surrounding pore fluid and sediment could supply 33%. Consequently, 62% of the heat necessary for full dissociation must be transported to the dissociation front from elsewhere.

For laboratory and core-scale dissociation of gas hydrate, which generally involve pure gas hydrate plugs or sediments with high saturations of gas hydrate in cylindrical pressure chambers, the heat transport requirement means dissociation occurs radially, moving inward from where the sample contacts the vessel wall (e.g., images in Ebinuma et al., 2008; Gupta, 2007; Seol & Kneafsey, 2009; Sloan, 2004; Waite et al., 2008). Even for specimens that are depressurized, meaning that the entire specimen is subjected to pressures outside the gas hydrate stability field, dissociation occurs most rapidly at the chamber walls, which act as thermal reservoirs supplying heat for dissociation.

Dissociation rates always depend strongly on the configuration of the experimental system. In a study by Waite et al. (2008), a 20-min excursion from the gas hydrate stability conditions yielded roughly a 5% decrease in gas hydrate saturation, with the dissociation occurring primarily on the outer diameter of the specimen. If a strong driving force (e.g., pressure drop far below gas hydrate stability pressure) is imposed, gas hydrate dissociation rates can be relatively constant in the early stages (Kamath & Holder, 1987; Yousif & Sloan, 1991). As dissociation continues or as conditions get closer to the gas hydrate phase boundary, dissociation rates slow and become nonlinear (e.g., Circone et al., 2004, 2005b; Li et al., 2012; Oyama et al., 2009; Yousif & Sloan, 1991) as the driving forces for heat transport decrease.

Several physical processes affect the rate of gas hydrate dissociation. Since gas hydrate dissociation is a surficial phenomenon, the rate is proportional to the gas hydrate surface area (Kim et al., 1987). Gas hydrate dissociation also cools the surroundings, consuming the readily available sensible heat (Circone et al., 2005b; Konno et al., 2014). Dissociation slows once the sensible heat is consumed (Konno et al., 2014), and the required heat transport distance increases. Moreover, the gas phase released by dissociation can displace pore water, lowering both the thermal conductivity and heat capacity (Handa, 1986; Waite et al., 2007), hindering the flow of heat to the dissociation front (Sun & Mohanty, 2006).

There are several practical implications of hydrate dissociation that proceeds rapidly until sensible heat is consumed and then continues more slowly. Disseminated, low-saturation hydrate in sediment usually dissociates rapidly because ample sensible heat is available to drive dissociation. Thus, recovering samples of hydrate-bearing sediments with disseminated hydrate intact is challenging. For higher gas hydrate saturations in sands or for nearly pure gas hydrate chunks thicker than ~1 cm in fine-grained sediment, dissociation can take several tens of minutes even at ocean surface conditions. This has allowed researchers to visually identify or thermally image gas hydrate in recovered cores (Figure 2).

When gas hydrate is rapidly depressurized to atmospheric conditions, the gas hydrate's surface temperature drops below the freezing point for water, and ice can form (Kowalsky & Moridis, 2007; Oyama et al., 2009; Paull et al., 1996; Yang et al., 2012; Yousif & Sloan, 1991). The presence of ice directly on the gas hydrate can retard dissociation by slowing the escape of methane from the dissociating gas hydrate surface (Kuhs et al., 2004; Liang et al., 2005; Stern et al., 2003). As noted by Bohrmann et al. (2007), the coating of ice created by initially rapid gas hydrate dissociation during depressurization of sediment cores in the field can slow subsequent dissociation and help preserve the underlying gas hydrate long enough for specimens to be recovered from the sediment core.

4.3.3. Reservoir Scale

The same rate-limiting processes observed for dissociation at the laboratory and core scale are significant at the reservoir scale. This section reviews lessons learned about the influence of sensible heat, heat transport, and ice formation on dissociation from field-scale gas hydrate production testing.

The importance of sensible heat as a driver for gas hydrate dissociation during reservoir production activities was demonstrated by the first International Gas Hydrate Code Comparison Project, which derived production rate predictions for the Mt. Elbert permafrost-associated gas hydrate reservoir (Anderson et al., 2011). In one scenario, production was from a hydrate-bearing sediment layer with the base at ~723 m depth and 4°C. The second

scenario was from the same layer, but farther downdip, so its base was at 822 m and 12°C. The pressure difference due to the depth change was not considered significant, but the 8°C temperature increase led to approximately an order of magnitude higher average production rate being predicted over 10 years (Anderson et al., 2011).

In the Mt. Elbert model case, sensible heat increased as the production location shifted to a warmer portion of the reservoir, but additional sensible heat can also be brought in from gas hydrate-free layers contacting the gas hydrate reservoir. The same observation about sensible heat coming from gas hydrate-free layers interbedded within a gas hydrate occurrence was made in a model for the primary NGHP-02, Area B gas hydrate reservoir offshore eastern India (Myshakin et al., 2019). With fine-scale modeling, Myshakin et al. (2019) found that gas hydrate was dissociating most readily along the gas hydrate reservoir interfaces with the gas hydrate free intervals. The Nankai Trough gas hydrate reservoir offshore eastern Japan also contains thin layers of gas hydrate-bearing sediment that are separated by thin layers of fine-grained, essentially gas hydrate-free sediment (Konno et al., 2017; Yamamoto et al., 2017). For the 6-day gas hydrate production test in the Nankai Trough, history matching to downhole data indicates dissociation could utilize the gas hydrate-free layers to draw on available sensible heat (Yamamoto et al., 2017).

As noted by Yousif and Sloan (1991), rapid, constant rate dissociation behavior occurs when the system is driven more than 1 MPa below the stability pressure, but driving the pressure too low can drive the local temperature low enough to induce ice formation (Circone et al., 2005b). Conceptually, ice formation has the potential to accelerate gas hydrate dissociation because heat released as water freezes can be used in dissociating the adjacent gas hydrate (Feng et al., 2017; Konno et al., 2014). To accelerate gas hydrate dissociation, ice must form so as not to inhibit gas release from dissociating gas hydrate, nor block pathways for recovering methane at the production well. Reservoir modeling studies typically indicate that ice formation does reduce the reservoir permeability and limit gas production rates at the well (e.g., Kowalsky & Moridis, 2007; Moridis et al., 2019; Moridis & Reagan, 2007), so maintaining a dissociation pressure high enough to avoid ice formation is typically recommended (Yin et al., 2016). In Figure 3a, this would correspond to maintaining the dissociation pressure above ~3 MPa, although this value will fluctuate based on salinity changes.

For longer-term dissociation, heat can be delivered to the gas hydrate dissociation front via conduction, as well as convection, as warmer pore water from beyond the dissociation front is pulled past the dissociation front and into the production well (Yamamoto et al., 2017). Here again, there may be constraints on how large the pressure drawdown should be, although intuitively one might assume that larger drawdowns would provide a larger driving force for dissociation, and hence a higher dissociation rate.

As detailed in experimental and modeling studies from NGHP-02 marine reservoir studies, the pore pressure drawdown required to initiate gas hydrate dissociation in the reservoir also imposes an elevated effective stress that can cause the reservoir formation to compact, dramatically reducing the overall permeability even as solid gas hydrate is dissociating to gas and water and freeing up paths for fluid flow (Dai et al., 2019; Myshakin et al., 2019; Yoneda et al., 2019). As summarized by Boswell, Myshakin, et al. (2019), optimizing the overall gas extraction rate may require balancing the competing effects of pore pressure reduction (which increases the dissociation driving force) and minimizing the applied effective stress (which preserves reservoir permeability). Permeability reduction lowers not only the rate at which gas can migrate to the production well but also the rate at which warm fluid can be drawn in to supply heat to the dissociation front.

To date, most gas hydrate production tests have endured only a few days, with a single 2-month test having been run (Yang et al., 2017; Ye et al., 2018). Given that dissociation rates do not scale linearly with the amount of gas hydrate (Table 3), it is not clear that reservoir models are fully accounting for intricately coupled processes governing long-term dissociation, some of which may only become apparent after many months or years. Long-term production tests, such as the planned test on the Alaskan North Slope (Boswell, Marsteller, et al., 2019), are vital for providing not only the site-specific dissociation rate results, but for shedding light on which physical processes exert dominant controls on gas hydrate dissociation rates during long-term production activities.

5. Hydrate Phase Transitions in Geologic Settings

This section places the information discussed in sections 2 through 4 in the context of hydrate formation and breakdown processes at the bulk scale for geologic occurrences of gas hydrates, as summarized in Table 4.

Journal of Geophysical Research: Solid Earth

10.1029/2018JB016459

Table 4
Gas Hydrate Formation and Degradation in Marine Settings: Controls and Processes

	Location	Control	Processes
Deepwater marine hydrates			
Top of hydrate stability (P-T conditions)	In the water column, ~300 to ~700 m below ocean surface in most places Note: The seafloor is far within the P-T conditions for hydrate stability for most of the world's continental marine margins.	Local thermocline	Methane within bubbles emitted from the seafloor is stripped from rising bubbles and dissolves in surrounding waters (McGinnis et al., 2006). Hydrate shells may form rapidly around bubbles and then undergo coupled growth and dissolution processes until hydrate-coated bubbles reach the top of the hydrate stability zone (Fu et al., 2018; Wang et al., 2016)
Top of hydrate occurrence in sediments	Usually centimeters (high flux) to tens of meters below seafloor; shallowest limit controlled by sulfate reduction zone	Thickness of sulfate reduction zone, rate of advective flux of pore waters, saturation of hydrate forming gas in pore waters, rate of in situ methane generation, and availability of water	Can move shallower via hydrate formation from dissolved phase methane or move deeper from dissolution of hydrate
Zone of hydrate occurrence	Usually from depths of tens of meters to hundreds of meters in porous sediments on marine continental margins; typically occurs at low saturations (<5% of pore space) except in certain lithologies or geologic settings	Rate of advective flux of pore waters, saturation of hydrate-forming gas in pore waters, external forcing processes (e.g., sedimentation, erosion, changing bottom water temperatures), rate of in situ methane generation, pore water chemistry and lithology	• Continuous, nanosecond-scale exchange of gas molecules between hydrate cages and pore waters where hydrate is in contact with pore waters (dynamic equilibrium) • Bulk dissolution of hydrate if local pore waters are undersaturated in methane • Bulk formation of hydrate from dissolved phase methane if local pore waters are oversaturated in methane • Special case: rapid formation (timescale of days) of hydrate from vapor phase gas, possibly accompanied by complete consumption of local pore waters, if gas invades this zone
Base of hydrate stability zone (P-T conditions)	Tens to hundreds of meters below the seafloor	Local P-T conditions, which are mostly controlled by external forcing (see entry above)	• Bulk formation from vapor phase gas (most energetically favorable if free gas is available) • Bulk degradation is mostly by dissociation
Upper continental slopes			
Top of hydrate stability (P-T conditions)	Very close to the seafloor at water depths of 300–700 m (Figure 11). Top of stability may be within the seafloor for small seaward slopes and low geothermal gradients (Gorman & Senger, 2010)	Local thermocline	Bubbles emitted at seafloor may rise outside of P-T stability conditions too rapidly to form hydrate shells
Top of hydrate occurrence in sediments	Predicted to be similar to deepwater marine settings, with sulfate reduction extending tens of meters in sediments with low fluid advection; possible that thick zone of sulfate reduction could eliminate the possibility of hydrate forming	Same as deepwater marine settings	Can move shallower via hydrate formation from dissolved phase methane or move deeper from dissolution of hydrate Timescale of forcing function (primarily bottom water temperature change and small fluctuations in pressure): days to months, but hydrate zone may not remain in equilibrium with these changes

Table 4
Continued

	Location	Control	Processes
Zone of hydrate occurrence	Predicted to be a thin zone (tens of meters maximum thickness)	Same as deepwater marine hydrates, but bottom water temperature changes are larger and more frequent at these water depths, potentially causing hydrate to form or degrade more rapidly than in deepwater settings. Pressure fluctuations even on the timescale and amplitude of storms and tides may also perturb the reservoir	• P-T conditions throughout the zone are close to the stability boundary, making it more difficult to form and maintain hydrate • Hydrate degradation could sometimes occur via dissociation, not dissolution, in the rare case when the top of hydrate zone is within sediments (instead of the overlying water column)
Base of hydrate stability zone (P-T conditions)	Predicted to be tens of meters maximum depth below seafloor; note that upper slope BSRs are typically not detected in seismic data		
Seafloor hydrate	On or just below the seafloor, often at the outlet of seafloor gas seeps, under overhangs that trap water with high saturations of gas, or within seafloor mounds that form above a gas pipe	Pressure-temperature conditions far within stability zone at the seafloor and local dissolved gas saturation high enough to form and maintain seafloor hydrate	• Rapid formation of hydrate at the vapor-water interface and subsequent accumulation of hydrate-coated bubbles • Dissolution where hydrate is in contact with seawater undersaturated in gas

Note. In this table, methane is assumed to exist in the dissolved phase, and special situations involving vapor phase methane are explicitly identified.

Here, we focus on marine and cryospheric hydrates and exclude discussion of rare freshwater lake gas hydrates in Lake Baikal (Granin et al., 2019; Kida et al., 2006; Scholz et al., 1993). Many processes characteristic of marine reservoirs will operate in Lake Baikal, although pore water salinity and sulfate dynamics are different in the freshwater setting.

5.1. Marine Reservoirs

5.1.1. Deepwater Marine Settings

Deepwater marine settings may host over 95% of Earth's gas hydrate deposits (McIver, 1981; Ruppel, 2015) if the poorly constrained amounts beneath large ice sheets (e.g., Antarctica and Greenland; Lamarche-Gagnon et al., 2019; Wadham et al., 2012) are excluded from the inventory. Here we use deepwater gas hydrates to refer to hydrates in the sediments of continental margins at water depths at least 100 m greater than the shallowest limit for gas hydrate stability, which is typically 450 to 700 m for temperate and tropical latitudes (Figure 6). Those upper continental slope hydrates are the focus of section 5.1.2.

The emphasis on continental margins in delineating deepwater hydrate provinces arises from the requirement that sufficient sedimentary organic carbon exists to fuel past or present methane production by microbes. Microbial methane—often referred to as biogenic methane in the older literature—is the most common source for methane sequestered in gas hydrates that have so far been recovered, although the sampling may be biased by the geographic location of sampling and the concentration of samples at shallow depths in the sedimentary section. Gas hydrate can also form from methane that is not generated in situ or that is not attributable to microbial processes. Additional sources for methane that becomes bound in gas hydrate may include (a) older microbial methane that has accumulated in situ or migrated from elsewhere; (b) thermogenic methane generated in conventional reservoirs at PT conditions greater than those associated with gas hydrate stability and migrated into the hydrate stability zone; and, possibly, (c) abiotic methane generated in hydrothermal settings (Johnson et al., 2015; Klein et al., 2019). The physical processes associated with gas hydrate formation and breakdown in deepwater settings are not a function of the gas source. However, where it occurs, in situ methanogenesis can supply new gas (Malinverno, 2010; VanderBeek & Rempel, 2018; Xu & Ruppel, 1999), thereby increasing methane saturation in pore waters and increasing hydrate formation rates or decreasing dissolution rates within the stability zone.

Gas hydrate reservoirs in deepwater settings should be the most stable and longest lived of the marine gas hydrate occurrences. Most of the depth extent of these reservoirs exists at P-T conditions well within the gas hydrate stability field (supercooled) and is expected to remain stable for thousands of years into the future, even under scenarios of warming ocean-bottom waters (Ruppel, 2011; Ruppel & Kessler, 2017). The top of the gas hydrate stability (TGHS) zone and the BGHS are in theory the most dynamic parts of marine hydrate reservoirs (Figure 4). In marine locations deeper than the upper continental slopes, the TGHS always occurs within the water column, not at the seafloor (Figures 4 and 6). The seafloor itself is therefore within the P-T conditions for gas hydrate stability, even though gas hydrate usually will not form there since ocean bottom waters are undersaturated in methane (section 5.1.3).

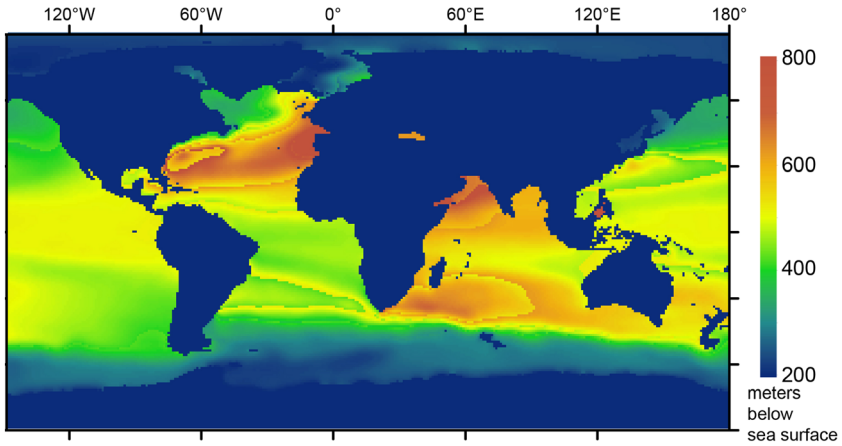

Figure 6. The depth from the sea surface to the top of the gas hydrate stability (TGHS) calculated by intersecting the CSMGem (Sloan & Koh, 2007) hydrate stability curve for sI methane hydrate with ocean temperatures to depths of 1,000 m in 1° × 1° blocks (Locarnini et al., 2010). The landward limit of gas hydrate stability on a given margin occurs where the TGHS meets the seafloor on the upper continental slope, mostly in the range of 450–700 m except at high latitudes. The TGHS will always be within the water column (not the sediments) except for a certain specific combination of a low geotherm and shallow dip to the upper continental slope (Gorman & Senger, 2010). Gas hydrate rinds that form on bubbles emitted from the seafloor will not dissociate (but may dissolve) before the ascending bubbles reach the TGHS. Most of the world's deep ocean basins do not contain sufficient organic carbon to generate methane for hydrates and are distant from thermogenic basins that could supply gas for hydrate formation.

5.1.1.1. Gas Hydrate Formation

Formation of new gas hydrate in deepwater systems is thought to primarily consume dissolved phase methane, which must exist in concentrations exceeding the local solubility limit in order to supply new gas hydrate growth (Xu & Ruppel, 1999). Unlike laboratory systems in which large, stepwise drops in solubility can be imposed to increase gas hydrate growth rates, the in situ solubility gradient in homogeneous sediments does not change dramatically with depth within the gas hydrate stability zone (Figure 4). Thus, in an equilibrium system, only a small fraction of the pore-water methane will be in excess of solubility as pore water migrates upward through each depth increment. You et al. (2019) estimate that ~2,000 pore volumes of methane-rich fluid flowing through a pore may be required to collect enough methane in excess of the solubility limit to fill ~1% of the pore space with gas hydrate. As shown in Table 2, pore water advection rates and thus gas hydrate formation rates can vary by orders of magnitude between sites. Forming gas hydrates in sediments from dissolved phase methane generally requires thousands and even more than a million years (Malinverno, 2010; Nimblett & Ruppel, 2003; VanderBeek & Rempel, 2018).

In the absence of fluid flow, methane can still migrate through pore fluid to the gas hydrate growth front via diffusion. In the gas hydrate formation model developed by Malinverno (2010), methane generated by microbes in fine-grained sediment diffuses into nearby coarser-grained sediment. Cook and Malinverno (2013) note that this type of diffusive migration is slow, requiring ~1 Myr to transport methane 100 m. However, on the scale of meters, diffusion could supply methane at rates comparable to slow to moderate advection and may even overtake advection as the primary control on gas hydrate formation in some locations (VanderBeek & Rempel, 2018). Cook and Malinverno (2013) calculate that over a 10 m migration path from fine-grained sediment into adjacent thin, coarse-grained sand at Walker Ridge 313H in the Gulf of Mexico, diffusion could supply methane fast enough to develop 33–45% gas hydrate saturation in ~300 ky, yielding an estimated bulk growth rate of 1% per 10 ky (Table 2). For the same site, the modeling of VanderBeek and Rempel (2018) also shows that hundreds of thousands of years would be required to accumulate more than 10% gas hydrate in a system where methane is supplied by methanogenesis.

Factors other than mass transport mechanisms (i.e., advection and diffusion) govern how shallow in the stability zone gas hydrates can actually form. The top of the zone of potential hydrate occurrence is usually controlled by pore water chemistry and microbial processes and rarely coincides with the seafloor. If methane is

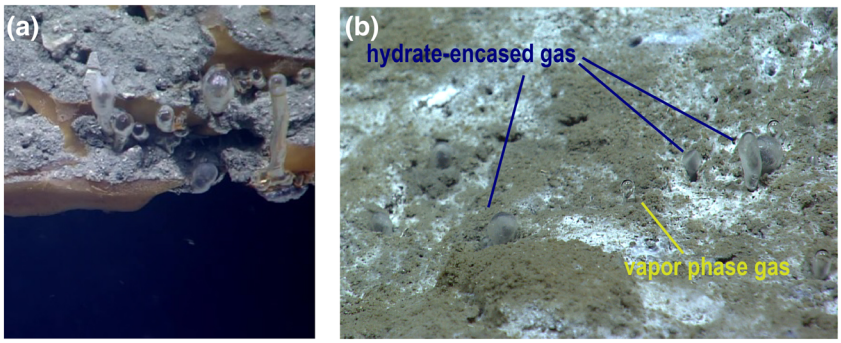

Figure 7. Photographs (see the supporting information for corresponding videos) of hydrate forming around vapor phase gas chimneys in open water at locations on the seafloor of the northern Gulf of Mexico. This process is similar to that envisioned to occur as vapor phase gas invades the hydrate stability zone in porous media (Meyer, Flemings, & DiCarlo, 2018). For these hydrate-encrusting processes to operate at these locations requires seafloor waters to be supersaturated in the hydrate former. Otherwise, the bubbles would dissolve as they emerge, or the hydrate might form and then quickly dissolve. Field of view for photos estimated to be less than 5 cm across. (a) Gas emitted at the edge of a carbonate overhang where sediment (gray) is interspersed with orange hydrate was filmed in 2017. The orange color is likely attributable to the inclusion of petroleum in the gas hydrate. The gas emerges as free bubbles, as bubbles that become coated in hydrate while attached to the seafloor, or as bubbles from hydrate chimneys or tubes. Some tubes have stopped emitting gas and have a frozen bubble at the top. The long tube on the right breaks off in the video, as shown in the supporting information. High-resolution video available from Kennedy et al. (2019). (b) Some bubbles emitted from bare seafloor immediately form a rind of gas hydrate, as filmed in 2014. As more pressure builds, the hydrate eventually detaches from the seafloor, and a new bubble is emitted and is encased in a hydrate rind. Photograph is from video acquired by the NOAA's Ocean Exploration and Research using the remotely operated vehicle Deep Discover 2 (D2), as given in low-resolution in the supporting information, and is in the public domain. High-resolution video available from Lobecker et al. (2019).

supplied mostly from below and sulfate infiltrates the seafloor from the overlying seawater, sulfate concentration normally decreases from the seafloor to near-zero at the so-called sulfate-methane interface or transition (SMT), whose depth is controlled by the rate of vertical advective flux (Borowski et al., 1996). The SMT may be only millimeters deep at active methane seeps (Joye et al., 2004), centimeters deep where methanogenesis is very active, and meters to tens of meters in the deep ocean in low advection rate regimes (Borowski et al., 1996). As methane migrates upward from below, it is almost entirely consumed by the anaerobic oxidation of methane (AOM) by microbes within the sulfate reduction zone (SRZ; Reeburgh, 2007). Even when methane enters the SRZ above the SMT, the existing pore waters are strongly undersaturated in methane, and there is not enough excess methane to drive hydrate formation.

Where vapor phase methane invades the hydrate stability zone (e.g., the Cascadia Margin; Torres et al., 2004), gas hydrate formation can proceed rapidly at the gas/liquid interface (Meyer et al., 2018). In their model, gas pressure building from below would enable a gas chimney to advance into the gas hydrate stability zone. The chimney would advance episodically, breaking through gas hydrate that formed on the gas/liquid interface as pressure built in this cyclic process of gas advance and hydrate formation. The supporting information contains videos linked to Figure 7, which shows photos of a similar process occurring on the seafloor of the northern Gulf of Mexico as free gas invades bottom waters saturated in the hydrate-forming gas and within the hydrate stability zone. Within the sediments, gas hydrate formation rates via the gas invasion mechanism would ultimately be limited by the advancement rate of the gas front itself, which may be relatively slow (e.g., 3 cm/year inferred for the Cascadia Margin by Torres et al., 2004; Table 2) when compared to laboratory rates (e.g., gas advances 3 cm in only 80 hr [0.01 year] in the gas percolation experiment of Meyer, Flemings, and DiCarlo (2018)).

Gas hydrate can also grow outward into surrounding sediments from gas hydrate-coated chimney walls, although much more slowly than growth occurs at the gas/liquid interface. Meyer, Flemings, and DiCarlo (2018) contend that once the chimney's gas/water interface is coated in gas hydrate, subsequent gas hydrate growth in the surrounding sediment would have to occur by methane transport through the gas hydrate chimney wall via diffusion or other processes. Such processes would juxtapose gas hydrate

formed rapidly from vapor phase methane within a chimney and gas hydrate that grows slowly from dissolved phase methane over thousands of years in the surrounding sediments.

5.1.1.2. Dissolution

Most of the deepwater gas hydrate reservoir is well within the gas hydrate stability conditions (supercooled relative to the stability boundary), meaning dissociation will not occur. Dynamic processes do affect gas hydrate at the microscale level throughout the gas hydrate stability zone over short timescales though. As mentioned in section 4.1.1, gas hydrate surfaces exposed to pore waters in this zone are constantly releasing and taking up gas molecules on nanosecond scales (Vatamanu & Kusalik, 2006) even when gas hydrate is in equilibrium with the pore water methane concentration. Dissolution acting at a larger scale can permanently erode gas hydrate within the stability zone if pore waters in contact with gas hydrate do not remain saturated in methane (Figure 4). Such a dissolution mechanism has been proposed to explain the existence of gas hydrate-free, water-bearing intervals within otherwise highly gas hydrate-saturated reservoirs (Boswell et al., 2012; Collett et al., 2019). Given typical pore-water advection rates, this intrareservoir dissolution process would likely require thousands of years to complete.

Gas hydrate in sediments that end up within the SRZ (e.g., due to seafloor erosion or deepening of the SMT during slowing of advection) will also be destroyed by dissolution. Pore waters in this zone contain very low concentrations of methane, and gas hydrate will release methane molecules to the pore waters, where the methane becomes available to fuel further AOM.

5.1.1.3. Dissociation

When dissociation occurs in marine reservoirs, it should be confined to a relatively narrow depth range near the BGHS, which is defined by the triple point where methane coexists in hydrate, vapor phase, and dissolved phase (Figure 4). As noted in sections 2.3 and 2.4, the theoretical BGHS for natural systems is often inferred based on bulk properties, as if the reservoir contained hydrate in equilibrium with water, even though capillary forces, water activity, and other factors can shift the BGHS. The BGHS is referred to as a thermodynamic triple point and often appears to be a discrete line in the sediments when researchers identify bottom simulating reflections (BSRs) that separate hydrate-bearing sediments from underlying gas. However, the BGHS and the BSR (where it exists) are more properly considered as finite-thickness zones (Wood et al., 2002) in which methane may persist in all three phases. Although the BGHS is often described as the locus of dissociation, gas hydrate could form, dissolve, or dissociate at this depth, depending on the driving process. The driving processes rarely operate in isolation, which complicates analysis of the net response of the reservoir to perturbations.

5.1.1.4. Formation and Breakdown Processes in Natural Systems

Tectonic, sedimentary, climate, and fluid flow processes can lead to bulk hydrate formation, dissolution, or dissociation in different parts of deepwater marine reservoirs. Understanding the full impact of these processes on the state of the hydrate reservoir (thickness and hydrate saturation) and the persistence of hydrate within any given sediment parcel requires an approach that incorporates all the complexities of multiphase fluid flow (Stranne et al., 2016). To build intuition, we here use a simple model that tracks only P-T and solubility in a homogeneous system to illustrate the first-order effects of geologic and climate-related processes.

As a simple example, sustained cooling of ocean bottom water (e.g., cooling lagging the onset of a global glaciation) changes the thermal boundary condition at the seafloor and produces cooling of the near-seafloor sediments at a rate controlled by their thermal diffusivity. The cooling in turn causes a decrease in the solubility of methane in pore waters within the gas hydrate stability field, making more methane available for hydrate formation. Thus, in addition to bottom water cooling thickening the stability zone (migration of BGHS to greater depths), cooling also leads to an increased hydrate accumulation throughout the reservoir. Bottom water warming has the opposite effect, as shown in Figure 4 and in the temperature and solubility plots in Figure 5 of Ruppel and Kessler (2017).

On contemporary Earth, relative sea level on many continental margins is rising at rates of several millimeters a year (Cazenave & Llovel, 2010). If the corresponding pressure increase were propagated elastically through incompressible, homogeneous sediments in the deep ocean, this would cause formation of new gas hydrate at the BGHS via consumption of vapor phase or dissolved gas beneath the BGHS, assuming enough methane and water were present (Figure 5b of Ruppel & Kessler, 2017).

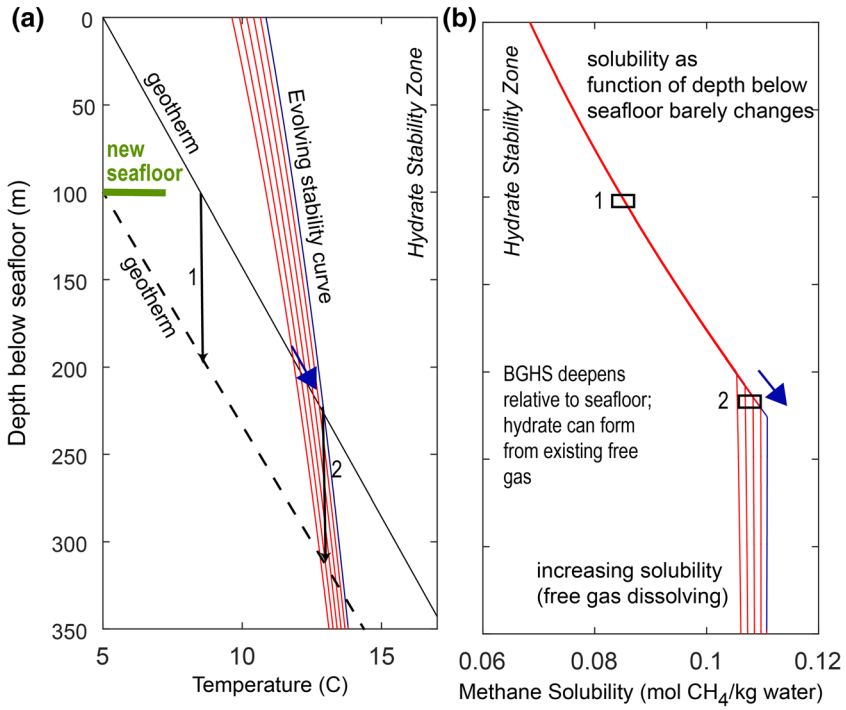

Figure 8. The impact of pressure increases (sea level rise or subsidence) on P-T and solubility in a marine reservoir. Figure modified from Figure 5b of Ruppel and Kessler (2017) and uses different initial conditions than Figures 9 and 10. Pressure corresponding to the addition of 100 m of water or 100 m of subsidence is added over 1,000 years, with no change in bottom water temperature. (a) The geotherm (black line) remains constant relative to the seafloor in this scenario, but the phase boundary for gas hydrate stability evolves from left (red curves) to right (blue), deepening the base of gas hydrate stability (BGHS; intersection of geotherm and stability curve). Note that the addition of ~1 MPa of pressure to the reservoir produces <30 m deepening of the BGHS due to the morphology of the stability curve in P-T space. A parcel of sediment (shown as black lines with arrows) remains at a constant depth relative to the seafloor (new seafloor shown schematically in green along with dashed line to indicate that the geotherm remains unchanged relative to the seafloor) during a simple subsidence or sea level rise event. Parcel 1 starts within the hydrate stability zone and ends up more supercooled relative to the phase boundary during the subsidence event. Parcel 2 starts outside the stability zone and ends up within it during the event. (b) This plot of methane solubility is drawn relative to the seafloor, regardless of its depth relative to the sea surface. Thus, the reference frame (see section 5.1.1.4) is different than that used to illustrate the evolving P-T conditions at the phase boundary in (a). Here, increased pressure does not noticeably alter solubility within the hydrate stability zone. Solubility increases within the vapor phase zone, meaning that more free gas dissolves. Because the solubility curve is affected only by pressure in the scenario described here, Parcel 1 starts and maintains its original point on the solubility curve relative to the seafloor. Parcel 2 also maintains this point, but the solubility field evolves through the parcel so that it experiences first the changes in the vapor phase solubility constraint and then ends up within the stability zone near the BGHS.

Subsidence, which increases the depth of the seafloor relative to the sea surface, rarely occurs without sedimentation. Rapid deposition of large volumes of sediment can drive subsidence (sedimentation preceding subsidence), or sedimentation can fill the "hole" produced during subsidence (subsidence preceding sedimentation). Acting on its own, subsidence increases hydrostatic pressure in the reservoir by increasing the distance between the original reservoir and the sea surface and can appear to have the same impact as sea level rise (Figure 8). However, in the subsidence scenario, the geotherm moves through the original stability curve (seafloor is moving), while in the sea level rise scenario, the stability curve moves relative to the geotherm (sea surface is moving). Solubility is so weakly dependent on pressure within the hydrate stability zone that processes affecting the depth of the seafloor relative to the sea surface barely change the solubility. In the subsidence scenario, a sediment parcel initially within the hydrate stability zone is carried isothermally to greater pressure (Parcel 1 in Figure 8) and ends up farther inside the stability field, but with the same solubility constraint as before. A parcel (Parcel 2 of Figure 8) originally just outside the stability zone can end up within the stability zone during the isothermal pressure increase. The solubility curve moves

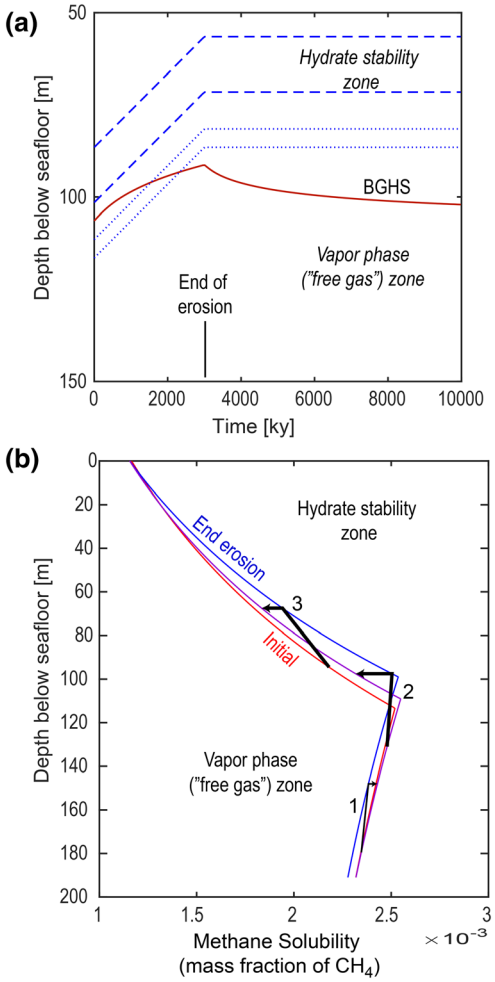

Figure 9. Tracking the impact of an erosional event on a parcel of seafloor sediment. To make this model as general as possible, we assume homogeneous 35‰ NaCl pore waters (even when hydrate dissociates and freshens pore waters) and incorporate no endothermic heat of dissociation or exothermic heat of formation. The former assumption implies rapid advection to keep pore waters homogeneous, while the latter assumption implies rapid heat transfer in the vicinity of the formation/dissociation front. While neither assumption is realistic, the goal of this model is to underscore that not only fluid but also sediment is moving through the P-T solubility space that dictates hydrate stability. The initial geotherm was assigned to be nearly 90°C/km to bring the base of gas hydrate stability (BGHS) for this water depth (1,000 m) to ~100 m below the seafloor for convenience in plotting and to ensure propagation of some seafloor temperature effects to the depth of the BGHS during these short model runs. (a) For an erosional event of 10 mm/year for 3 ky followed by a 7 ky period of re-equilibration, the BGHS first shoals then deepens (red curve). Parcels that are originally immediately below the BGHS (dotted blue curves) end up within the hydrate stability zone. Parcels within the hydrate stability zone (dashed blue curves) are carried closer to the seafloor and to colder equilibrium temperatures. (b) The red, blue, and purple curves indicate the solubility as a function of depth below the seafloor (which is eroding) at the initial time, the end of erosion, and after 7 ky of equilibration, respectively. The black paths show how parcels at different depths experience solubility changes during and after the erosional event. Parcel 1 (below the BGHS) experiences reduced solubility conditions during erosion, which creates more vapor phase gas. As the system equilibrates, some of the vapor phase gas would again move into the dissolved phase. Methane solubility in pore waters is nearly the same before and at the end of the erosional event for Parcel 2, which moves from below the BGHS to the hydrate stability zone. During re-equilibration, solubility decreases significantly, which would encourage the formation of hydrate. Parcel 3 experiences reduced solubility for the entire event, meaning that hydrate formation is likely. See section 5.1.1.4 for more explanation.

through this parcel as it evolves, first with solubility increasing in the vapor phase zone and then the parcel ending up within the stability zone just above the BGHS.

Uplift, such as that accompanying the formation of compressional ridges on the subducting plate of active margins or rebound of seafloor following melting of a grounded ice sheet, has an impact opposite to that

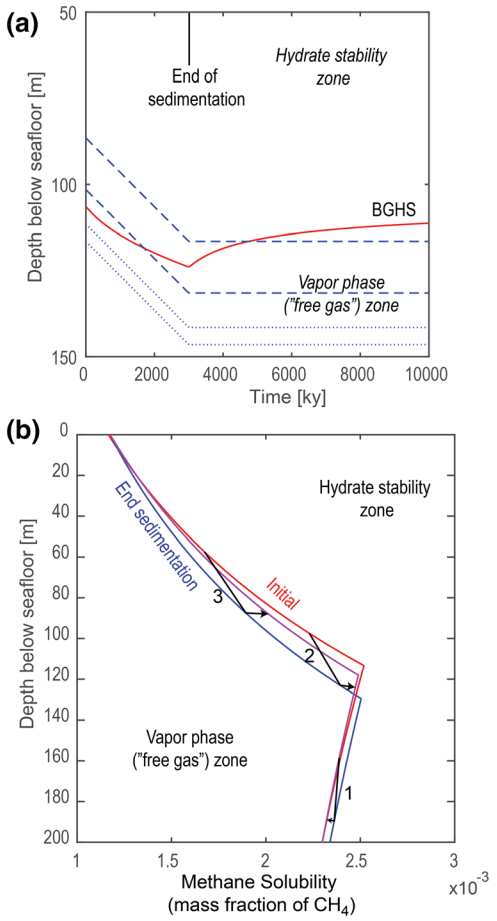

Figure 10. Same as Figure 9 but for a 3 ky sedimentation event at 10 mm/year followed by 7 ky of equilibration. (a) The base of gas hydrate stability (BGHS) first deepens and then shoals (red curve). Gas hydrate in parcels that are originally immediately above the BGHS (dashed blue curves) experiences dissociation as these parcels end up below the BGHS. Parcels originally within the vapor phase zone (dotted blue curves) are carried deeper. (b) The red, blue, and purple curves indicate the solubility as a function of depth below the seafloor (which is receiving sediment) at the initial time, the end of erosion, and after 7 ky of equilibration, respectively. The black paths show how parcels at different depths experience solubility changes during and after the erosional event. Parcel 1 (below the BGHS) experiences decreased solubility conditions during sedimentation, which increases vapor phase gas. Methane solubility in pore waters increases during sedimentation for Parcel 2, which moves from above the BGHS to the vapor phase zone during equilibration. Solubility always increases, meaning that gas hydrate would first dissolve and then dissociate as the parcel crosses into the vapor phase zone. Parcel 3 experiences increased solubility for the entire event, meaning that hydrate dissolution is likely. See section 5.1.1.4 for more explanation.

of subsidence. Uplift decreases pressure within the hydrate reservoir, leading to shoaling of the BGHS relative to the seafloor. Solubility in the free gas zone decreases as pressure diminishes, causing the accumulation of more vapor phase gas beneath the BGHS.

Erosional processes —slow erosion associated with continuous scouring of the seafloor, more rapid erosion associated with episodic events, or sudden removal of a thickness of seafloor due to turbidity currents or submarine slide formation—can lead to new hydrate in the reservoir and at the BGHS as the BGHS migrates to greater depths relative to the new seafloor (Figure 9). Normal geotherms increase as a function of depth in the shallow sedimentary section, and equilibrium geotherms have a boundary condition equivalent to the bottom water temperature at the seafloor. Erosional removal of material exposes formerly deeper, warmer sediments to cold seafloor temperatures. As the geotherm re-equilibrates, the solubility of methane in pore water in the hydrate reservoir decreases, making more methane available for hydrate formation. After some lag time, the temperature at the BGHS also starts decreasing, causing the BGHS to migrate deeper. Below the BGHS, solubility increases slightly, consuming some of the free gas that may previously have been contained there.

Sedimentation ultimately increases temperatures within a specific parcel of sediment in the reservoir and leads to hydrate dissociation at the original BGHS (Figure 10). Sedimentation occurs at slow rates on many continental margins, but the emplacement of landslide deposits can be cast as a more catastrophic form of sedimentation. For the hydrostatic assumption, sedimentation does not change the pressure in the reservoir. Thus, the impact of sedimentation should in theory be related only to the associated perturbation in temperatures and hence solubility. Sedimentation adds material at the temperature, salinity, and sulfate concentration of bottom waters to the seafloor. Re-equilibration of geotherms in response to this addition leads to increasing temperatures for a given parcel within the hydrate zone, increasing local methane solubility, and thus dissolution of hydrate that may previously have been in equilibrium with the pore waters. The BGHS will end up at its initial depth relative to the new seafloor but migrates (upward) to that depth through dissociation of gas hydrate between the original (now more deeply buried) and new BGHS. Sedimentation also delivers new organic carbon to the seafloor, thus providing more fuel for methanogenic microbes that can produce methane in situ in the reservoir.

A potential point of confusion in assessing the impact of geologic processes on deepwater marine reservoirs is the appropriate frame of reference when seafloor depth is changing. For example, the BGHS will be at the same depth relative to the seafloor before an erosional process and after complete re-equilibration if other factors (e.g., bottom water temperature) remain the same. However, parcels of sediment that were previously below the BGHS may now be within the hydrate stability zone, having shoaled relative to the seafloor (Figure 9a). Thus, it is important to remember that not only are fluids moving through the reservoir via migration processes, but sediment parcels also end up in different positions relative to the seafloor for processes that add or remove sediment from the seafloor.

Another issue is accounting for the addition or removal of sediment in terms of the height of the water column. In theory, the addition of 1 m of sediment should reduce the amount of water above a spot on the seafloor by 1 m. The seafloor becomes shallower relative to the sea surface, but the overall pressure in the reservoir remains the same if the hydrostatic assumption is adopted, as is the norm for calculating the

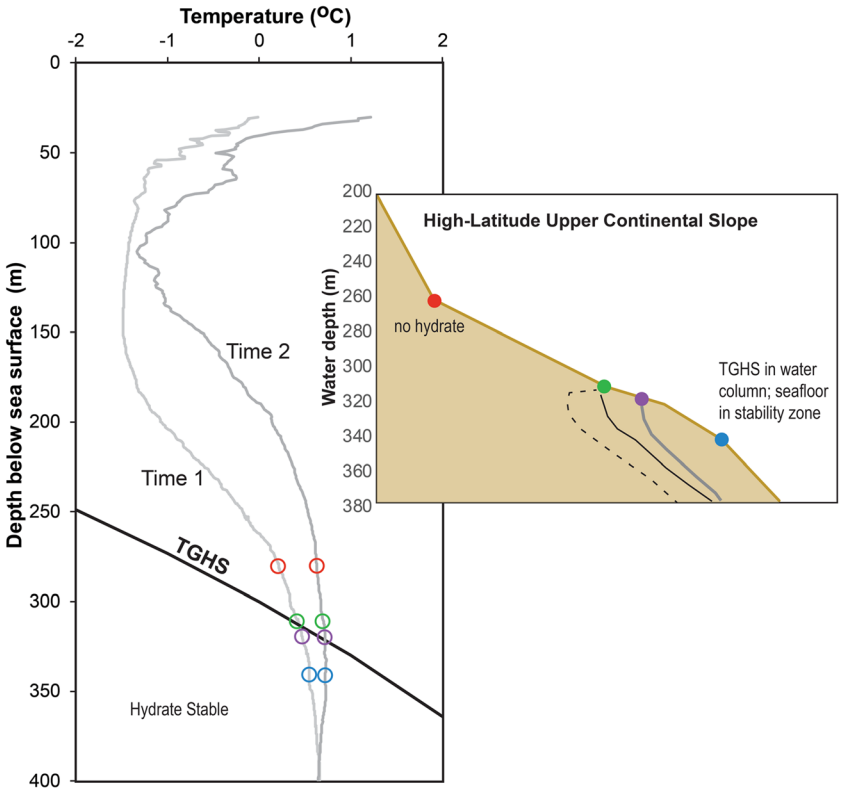

Figure 11. Gas hydrate on upper continental slopes exists in a dynamic environment. This diagram shows the case of a high-latitude upper continental slope where gas hydrate is stable nearly as shallow as ~300 m water depth at just above 0° C bottom water temperature. The general principle illustrated here is applicable to other upper continental slopes. The main diagram shows water column temperatures recorded as a function of depth during measurements in July and October 2012 on the Beaufort Sea upper continental slope. The pressure corresponding to the top of gas hydrate stability (TGHS) changes ~0.1 MPa (~10 m) over that time. On a shallow upper continental slope, a 10 m change in bathymetry could translate to hundreds of meters or more along the slope. It is important not to view the TGHS boundary on the diagram as a proxy for the upper continental slope since the temperatures within the sediments follow a geotherm, not the water column thermocline. The colored circles on the diagram correspond to the positions on the inset diagram. No hydrate exists shallower than the landward limit of stability (red circles). The green and purple circles mark the landward limit of stability at Times 1 and 2, respectively. The blue circle marks a location that is similar to normal deepwater marine hydrate provinces: The TGHS is in the water column, and the seafloor lies within the hydrate stability zone. The black and dashed curves in the seafloor below the green point are schematic BGHS for normal conditions and the condition described by Gorman and Senger (2010), respectively. The gray curve is the schematic BGHS for the landward gas hydrate limit associated with the purple circle. It is unlikely that hydrate formation and breakdown at the landward limit of stability keep pace with the changes in the temperatures of bottom waters in the overlying ocean.

hydrate stability zone in deep marine sediments. In this scenario, a basin would eventually fill with sediment, but the pressure experienced by any parcel would remain constant throughout sedimentation. In an alternate, endmember formulation, the addition of 1 m of sediment would be accommodated by 1 m of subsidence (local isostatic compensation) so that the height of the water column above the seafloor remains constant. In this case, pressure increases in the reservoir as sedimentation continues (~0.1 MPa for every 10 m of sedimentation).

Figures 8 through 10 highlight particle tracking, namely, following a specific parcel of sediment through the solubility and P-T changes that affect the reservoir during and following erosion and sedimentation. For the scenario illustrated here, the seafloor adjusted to the removal or addition of the 30 m of sediment, meaning that the pressure changed by ~0.3 MPa for these cases. Figures 8a and 10a are plotted relative to the seafloor. The BGHS re-equilibrates to nearly its starting depth by 7 ky after the end of the erosion/sedimentation event, but parcels of sediment that started in the hydrate stability zone or beneath the BGHS end up in different positions relative to these components of the reservoir. The solubility curves in Figures 9b and

10b are plotted relative to the seafloor, regardless of its depth relative to the sea surface at any time. The particle tracks shown in black arrows on the solubility curves demonstrate schematically how a parcel moving through changing solubility conditions in the reservoir will experience different regimes during and after the erosion/sedimentation events.

5.1.2. Upper Continental Slopes

Uppermost continental slopes bracket the landward limit of gas hydrate stability and are roughly estimated to include ~3.5% of the marine area where gas hydrates might occur (Ruppel, 2011). The landward limit of gas hydrate stability can be as shallow as 300 m in the Arctic Ocean in winter months or more than 700 m deep on continental margins at tropical latitudes (Figure 6). On most of the world's temperate margins, the landward limit of stability, determined by intersecting the theoretical TGHS zone with seafloor bathymetry, lies at ~450 to 700 m.

Because upper continental slopes have P-T conditions close to the hydrate phase boundaries (top and/or bottom), any hydrate that exists there would be particularly susceptible to changing ocean conditions, an issue that has been investigated on numerous margins and with various models (Berndt et al., 2014; Biastoch et al., 2011; Brothers et al., 2014; Darnell & Flemings, 2015; Kvenvolden, 1988; Phrampus et al., 2014; Phrampus & Hornbach, 2012; Ruppel, 2011; Ruppel & Kessler, 2017). Note that the amount of hydrate actually present on upper continental slopes is uncertain. For various reasons, classic BSRs are typically undetectable at these water depths, meaning that few hard constraints exist to determine an upper boundary to vapor phase gas beneath the theoretical BGHS. In addition, if the BGHS is predicted to lie only a few meters to tens of meters below the seafloor, the SRZ would overlap with much of the stability zone and prevent the development of hydrate. If hydrate is present, even a small decrease in pressure or increase in temperature could theoretically drive dissociation. Once dissociation begins, several factors might limit further gas hydrate breakdown though. First, the endothermic heat of dissociation acts as a thermodynamic brake on continued destabilization of the deposits. Second, dissociation releases fresh water into pore space, which shifts the phase boundary to higher temperature at any given pressure, thereby stabilizing hydrate. Only when heat or mass transfer processes overcome the barriers to further dissociation can upper slope gas hydrate degradation proceed.

Hydrate dissociation on upper continental slopes may not keep pace with processes such as intermediate ocean warming. Ocean waters immediately overlying the upper continental slope could be out of equilibrium with the state of hydrate in the sediments. Brothers et al. (2014) highlight a case in which gas hydrate may have been stranded beneath the upper slope landward of the present-day stability boundary in the U.S. Mid-Atlantic Bight owing to the time lag in hydrate dissociation in response to temperature forcing. In the U.S. sector of the Beaufort Sea in the Arctic Ocean, seasonal warming and cooling of intermediate waters impinging on the upper continental slope could in theory cause migration of the landward limit of gas hydrate stability by ~10 m in depth and hundreds of meters along the slope during a few-month period, as shown schematically in Figure 11. While intrinsic kinetics does not play a role in limiting the capacity of the zone of hydrate occurrence to remain in thermal equilibrium with the overlying ocean water, mass and heat transfer limitations could mean that hydrate does not re-form quickly enough each autumn for the hydrate zone to keep pace with the thermal changes in the ocean water.

Where the seafloor on upper continental slopes dips seaward by only a few degrees and geothermal gradients in the sediments are small, a peculiar situation could develop in the gas hydrate reservoir. As described by Gorman and Senger (2010) and illustrated schematically in the inset to Figure 11, the TGHS and BGHS may both occur within the sediments for this special case. Landward of the point at which gas hydrate first becomes stable at the seafloor, gas hydrate could form within the sediments over an updip distance of tens of meters in a feature that Gorman and Senger (2010) call a bulge.

5.1.3. Seafloor Hydrate

Gas hydrate exposed at the seafloor represents a special case related to formation and breakdown processes. While not considered volumetrically important in global gas hydrate inventories (Boswell & Collett, 2011), seafloor gas hydrate is the only naturally occurring hydrate that is visible without disturbing sediments and therefore garners outsized attention. Seafloor hydrate can exist in areas of active gas seepage at water depths (pressures) and bottom water temperatures where hydrate should be stable, even if the surrounding ocean waters are too undersaturated with methane for the seafloor hydrate to be maintained long term.

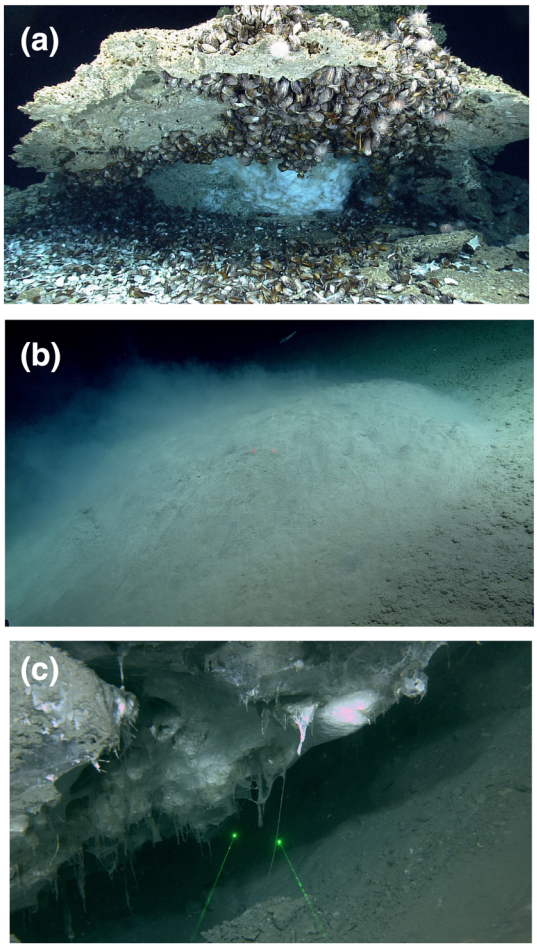

Figure 12. Seafloor hydrate examples. (a) Photograph published by Ruppel and Kessler (2017), showing white hydrate beneath a mussel-encrusted carbonate cap in the northern Gulf of Mexico. This feature may represent a mound whose sides have collapsed and exposed the hydrate, or the hydrate may have formed in this way due to seepage from a seafloor vent. Pits in the hydrate may be caused by dissolution processes. Photograph by NOAA's Ocean Exploration and Research Program in 2014 (Lobecker et al., 2019). (b) Low-relief mound set within the Norfolk Seep field (Skarke et al., 2014), as photographed by NOAA's D2 ROV in 2019 (Cantwell et al., 2019). The mound is several meters across and ~1 m high and inferred to have a core of gas hydrate. The cloud of sediment in the water column is entrained as the current flows across small jets of dense fluid (brine) mixed with sediment being emitted out of the side of the mound, as shown in the video in the supporting information. In other areas, these seafloor mounds have a more peaked morphology or may expose hydrate where the side of the mound has been eroded. (c) Gas hydrate "inverted snowcone" formed beneath a carbonate overhang. The remnants of hydrate-encrusted bubbles that merged to form this feature are visible on the right side of the feature. Photograph by the Global Explorer ROV on the mid-Atlantic margin during a USGS-led cruise in 2017. Lasers separated by 10 cm.

One habit for seafloor gas hydrate (Figure 12) is exposed mounds, which are often capped by a thin veneer of sediment, oil, or bacterial biofilm (Lapham et al., 2014). Such mounds were first described on the seafloor of the northern Gulf of Mexico, where they are habitat for "ice worms" (Fisher et al., 2000). The surface coatings often observed on seafloor gas hydrate mounds may act as physical barriers to hydrate dissolution in the surrounding ocean water, which is undersaturated with respect to hydrate-forming gases. Without such physical barriers, dissolution can be rapid. Gas hydrate dissolution experiments at the seafloor by Rehder et al. (2004) measured dissolution rates of several millimeters of methane hydrate per day, and the gas hydrate dissolution model of Egorov et al. (1999) suggests that a 30 cm-thick seafloor outcropping of gas hydrate would dissolve within a year. Lapham et al. (2014) measure dissolution rates of 15 cm/year for a seafloor hydrate mound that may have been buffered from faster dissolution by a residual oily layer. At some locations, hydrate mounds may be dissolving from above where they are in contact with ocean waters, but also forming new hydrate underneath as methane bubbles ascending through the underlying sediments encounter sufficient water (Anderson et al., 2012; Egorov et al., 1999; Roberts, 2001). With fast enough bubble delivery, rapid vapor phase hydrate formation may keep pace with or even exceed (leading to mound inflation) the slower rate of dissolution from above. Even when most of the seafloor deposit is protected from dissolution, the scoop-shaped pits sometimes observed on some seafloor gas hydrate (Figure 12a) may arise as dissolution erodes the surface hydrate.

Low relief seafloor mounds (Figure 12b) encountered during remotely operated vehicle (ROV) explorations of seep fields on the U.S. Atlantic margin, the Cascadia margin (Chapman et al., 2004), and the northern Gulf of Mexico are also inferred to be manifestations of seafloor gas hydrate, even when gas hydrate is not visible. Whether such mounds should be described as gas hydrate pingos (Serié et al., 2012) or whether such terminology should be confined to mounds of a certain morphology and in association with high-latitude settings (Paull et al., 2007; Serov et al., 2015; Waage et al., 2019) has not yet been resolved. On the northern Cascadia margin, the thinly sedimented mounds are described as pingo like and ~3 m high with exposed hydrate (Chapman et al., 2004). On the U.S. Atlantic margin and southern Cascadia margin, the low, hummocky mounds are sometimes entirely mantled by sediment and set within seep fields (Figure 12b). Further investigation will be required to verify the origin of the mounds and determine if they are cored by gas hydrate and inflate as gas hydrate forms. In the case of a mound encountered in 2019 on the U.S. Atlantic margin at ~1,500 m water depth within the Norfolk Seep field (Figure 12b), video footage (supporting information) revealed the flow of dense fluid (presumed to be brine) from holes on the surface of the mound. Gas migrating into the mound from below could combine with water to form gas hydrate, and the volume increase associated with that phase transition could lead to further inflation of the mound. At the same time, exclusion of salts during hydrate formation, coupled with consumption of some pore water during hydrate formation, would increase the salinity of the remaining fluids trapped in interstitial spaces between hydrate-encased bubbles.

Another commonly observed habit for seafloor gas hydrate is as an inverted, rounded mound of seemingly homogeneous hydrate beneath overhangs such as those formed by authigenic carbonate outcrops

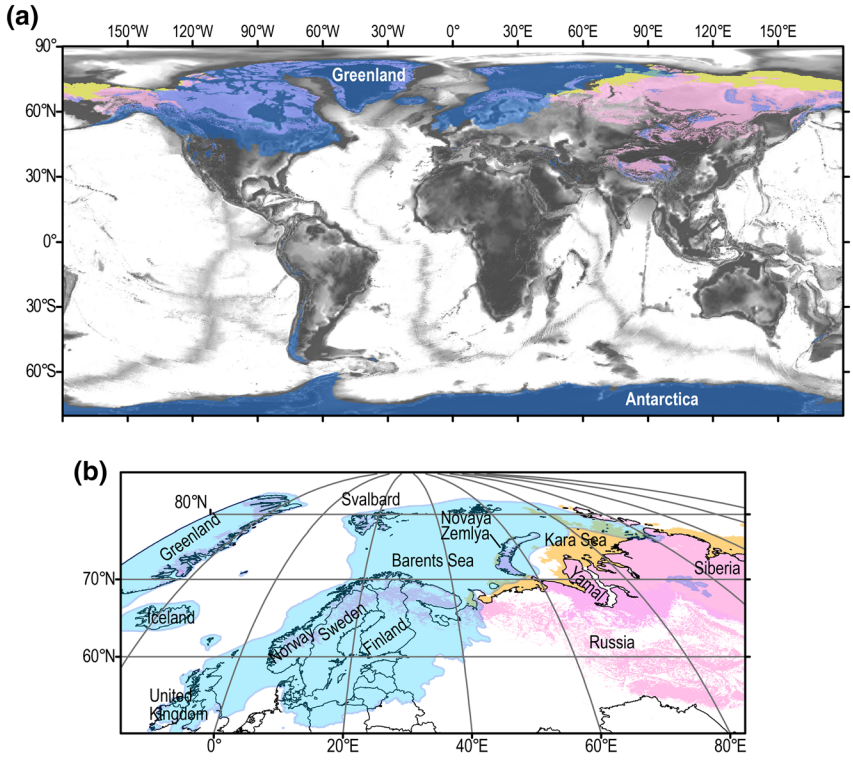

Figure 13. The maximum potential extent of temperature conditions suitable for cryospheric gas hydrates to have formed in the past (i.e., at the Last Glacial Maximum [LGM] at ~21.5 ka) or be present now. Note that for terrestrial locations, gas hydrates are frequently located above thermogenic reservoirs (e.g., Collett et al., 2011; Ruppel, 2015) and are not as ubiquitous as in marine settings. Blue indicates the extent of ice sheets at the LGM from Ehlers et al. (2011). Pink marks the contemporary distribution of continuous, discontinuous, and isolated permafrost from the model of Obu et al. (2019), and orange indicates the extent of contemporary subsea permafrost from Overduin et al. (2019). Land areas glaciated at the LGM, along with shallow seas where ice was grounded, could have evolved subglacial hydrates. Areas where permafrost persists today may have relict hydrates formed during glacial periods, and new hydrate may form if gas migrates into the stability zone. (a) Global map. Subglacial hydrate inventories have been estimated for Greenland and Antarctica (Lamarche-Gagnon et al., 2019; Wadham et al., 2012). (b) Map focused on Scandinavia, Russian, and the Kara and Barents Seas. The extent of the LGM ice coverage and subsea permafrost explains why gas hydrate degradation features have increasingly been described there (Andreassen et al., 2017; Portnov et al., 2013, 2016; Serov et al., 2015, 2017).

(Figure 12c). The first description of such a feature, which is popularly termed an inverted snowcone, may have been on a 2001 *DSV Alvin* dive (Van Dover et al., 2003) on the Blake Ridge at a seep/salt diapir location that had been drilled in 1995 (Paull et al., 1996). Since then, such hydrate snowcones have been observed by ROVs at several other locations. The inverted snowcone habit of these seafloor hydrate deposits originates when a methane seep emits a bubble beneath a physical barrier that interferes with the bubble's continued rise. The physical barrier also protects trapped bottom water from having its accumulated dissolved methane swept away into the surrounding ocean. The bubble emerges into ocean water that is already locally saturated with methane and rapidly acquires a hydrate shell. As the bubble continues to rise, it encounters the previous accumulation of gas hydrate-encased bubbles. The buoyancy of the newly hydrate-encased bubble causes it to remain attached to the previous accumulation, which may (a) become compressed as more hydrate-encased bubbles are added (Egorov et al., 2014); (b) transform into more massive hydrate if enough water is present; or (c) retain porosity even as the hydrate shells collapse. The snowcones of gas hydrate under carbonate ledges would dissolve rapidly if exposed to normal ocean water undersaturated in methane or if conduits stop supplying gas (possibly due to clogging by gas hydrate; e.g., Nimblett & Ruppel, 2003) for too long. In the case of the Blake Ridge snowcone, the feature observed in 2001 (Van Dover et al., 2003) was largely absent during a return visit by *DSV Alvin* in 2003.

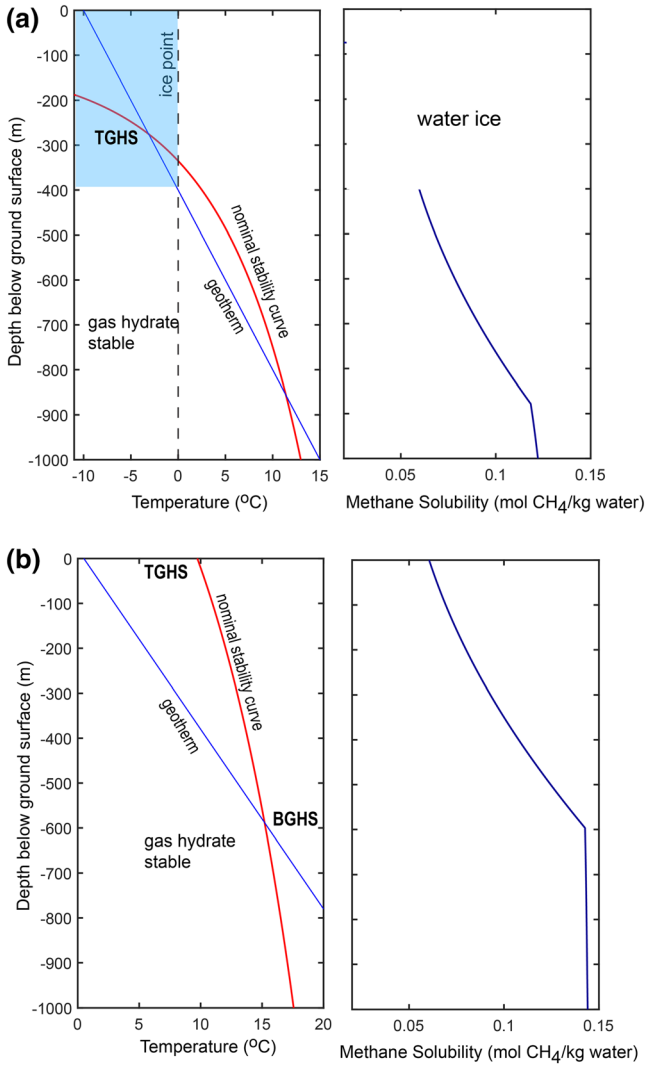

Figure 14. Cryospheric hydrate stability and solubility conditions. (a) Permafrost-associated hydrate (PAH) situation for a surface temperature of −10°C and a constant 25°C/km geotherm. The geotherm is usually lower within the permafrost zone (blue shading) than in the underlying sediments due to difference in thermal conductivity associated with the presence of water ice. Hydrate is stable from several hundred meters depth in the sediment (top of gas hydrate stability zone; TGHS) to hundreds of meters below the base of permafrost. The stability curve here is schematic since the pure water curve fit given in Table 1 is not valid below 0°C. CSMGem (Sloan & Koh, 2007) can be used to calculate the equation of state (EOS) under these cold conditions. The solubility curve on the right stops at the base of the water ice zone. The role of small amounts of free water in hydrate dynamics within the intrapermafrost zone has not been investigated, but hydrate is also considered more rare in this zone than in the subpermafrost. (b) Stability considerations and solubility beneath a 770 m-thick warm base (0.5°C at ground surface) glacier with the same geotherm as in (a). The TGHS is now at the ground surface.

The rapid accumulation of hydrate-encased bubbles beneath interfaces that block their ascent through the water column occurs not only in natural settings but also beneath some deep sea infrastructure (Anderson et al., 2012; Graham et al., 2011). During the Deepwater Horizon incident, an oil containment dome could not be placed over the leaking well because large amounts of hydrate formed rapidly around gas bubbles and accumulated under the dome, making it buoyant and difficult to control the oil (Deepwater Horizon Trustees, 2016; Graham et al., 2011).

5.2. Gas Hydrates in Cryospheric Settings

Gas hydrates that occur in settings associated with water ice or that exist because an area was glaciated are termed cryospheric hydrates. These include permafrost-associated gas hydrates, hydrate that forms beneath ice sheets (whether or not the subglacial regime is permafrost), and pingo-like features (section 5.1.3) found on some high-latitude continental shelves and not discussed further here.

Figure 13 shows the distribution of contemporary Northern Hemisphere ice-bearing permafrost (Obu et al., 2019) and subsea permafrost (Overduin et al., 2019) and the extent of the continental ice sheets at the Last Glacial Maximum (LGM) from Ehlers et al. (2011). Any of these areas is a candidate for the presence of present-day cryospheric hydrates although it is important to remember that such hydrates are not as ubiquitous as those in marine settings (see discussion in Ruppel & Kessler, 2017).

5.2.1. Permafrost-Associated Hydrate

If the global gas hydrate inventory consists only of deepwater marine and permafrost-associated hydrates (PAHs), less than 2% is estimated to occur in areas of continuous permafrost (McIver, 1981; Ruppel, 2015). The top of the methane hydrate stability zone in areas of continuous permafrost would typically be encountered at ~200 m (depending on the geothermal gradient) below the tundra surface and would therefore lie within the permafrost layer (Figure 14a). The BGHS could be several hundreds of meters below the base of the permafrost in the underlying unfrozen ground. Here we use the terminology of PAH to refer to gas hydrates that have formed in and beneath subaerial permafrost at high latitudes or in high plateaux. This designation includes hydrates associated with subsea permafrost that is currently offshore beneath some high-latitude continental shelves (Brothers et al., 2012, 2016; Hu et al., 2013; Overduin et al., 2019; Portnov et al., 2013; Rachold et al., 2007; Rekant et al., 2015; Ruppel et al., 2016) since this permafrost formed subaerially. Gas hydrates that have formed beneath ice sheets (subglacial) may or may not be associated with a permafrost regime and are discussed in section 5.2.2.

Most PAHs that exist now formed during Pleistocene Ice Ages (Majorowicz et al., 2008). During global cooling that accompanied major glaciations, cold temperatures propagated into the ground, leading to the development of thick (hundreds of meters) subaerial permafrost in locations such as the Alaskan North Slope and Siberia. Depending on preexisting thermal conditions, the rapidity of surface cooling, and the thermal properties of the sediments, the formation of the first gas hydrate (probably from vapor phase gas) could have preceded the formation of water ice within the zone that eventually became permafrost (Dai et al., 2011). Cooling of pore waters in contact with hydrate makes gas less soluble, which in turn also promotes additional formation of gas hydrate under these conditions. The gas hydrate zone may expand upward and downward simultaneously as the geotherm cools in response to surface temperature forcing. After the ice point is reached in the permafrost

zone, further hydrate formation could be limited if water is mostly consumed by ice formation. Ice formation also leaves behind more saline pore waters that would inhibit the formation of new hydrate and may lead to the dissociation of existing hydrates.

The most common driver for dissolution or dissociation of PAH is the downward propagation of warming temperatures from the ground surface. For hydrates associated with subsea permafrost, which ended up beneath high-latitude inner continental shelves as coastal regions were inundated during sea level rise starting at the end of the LGM, the slight increase in pressure owing to inundation (typically less than 1 MPa or ~100 m of water) is not enough to overcome the destabilizing effect of ocean bottom temperatures that are warmer than average annual air temperatures to which the new seafloor had previously been exposed (e.g., Ruppel & Kessler, 2017).

As discussed in section 5.1.1.2, dissolution is the most important process affecting the integrity of hydrate in deepwater marine sediment. In contrast, the lack of free water means that dissolution is not significant within the permafrost part of the PAH stability zone. Beneath the permafrost, dissolution processes are similar to those in deepwater reservoirs.

For all PAH, dissociation driven by ground (which includes the now-seafloor above subsea permafrost) warming commences at the TGHS and eventually occurs simultaneously at both the TGHS and BGHS (e.g., Taylor et al., 2013). Due to the nearly isobaric morphology of the phase diagram at low pressures and at temperatures below 0°C, a temperature increase at the TGHS will result in hydrate dissociation in a smaller thickness of the reservoir than will the same magnitude temperature increase at the BGHS. Temperatures will of course increase faster at the shallower depth of the TGHS relative to the BGHS; however, PAHs are more common deeper in the stability zone (closer to the BGHS) in locations studied so far (Collett et al., 2011). The relatively large depths for most PAH are related to the fact that they are believed to be formed mostly from gas that had migrated from deeper, thermogenic, conventional reservoirs prior to Pleistocene cooling events (Collett et al., 2011; Ruppel, 2015). Coalbed methane or methane and CO_2 that had been generated in situ by microbial processes may mix with thermogenic gases to form rarer gas hydrates within the shallower permafrost zone (Dai et al., 2011; Dallimore & Collett, 1995), as illustrated in Figure 10 of Ruppel and Kessler (2017). Near the BGHS, gas released by PAH dissociation may migrate upward but would be prone to re-form hydrate on the vapor phase interfaces in the subpermafrost zone if free water is available. Gas released by dissociation at the TGHS is already in the permafrost zone, and existing water ice can act as a permeability seal that impedes further migration. Water released during hydrate dissociation at the TGHS at temperatures below the ice point (Melnikov et al., 2009) would also freeze, further increasing the amount of water ice and lowering the permeability of the formation.

5.2.2. Subglacial Hydrate

Subglacial hydrate, which is hydrate formed in the ground beneath ice sheets, has only started to receive significant attention in the past decade with studies of possible hydrates beneath the Antarctic (Wadham et al., 2012) and Greenland (Lamarche-Gagnon et al., 2019) ice sheets and with field and modeling studies that link contemporary methane release to post-LGM deglaciation of other areas (e.g., Andreassen et al., 2017; Portnov et al., 2013, 2016; Serov et al., 2017). Serov et al. (2017) in particular provide a detailed discussion of the impact of deglacial episodes on subglacial gas hydrate reservoirs.

As summarized schematically in Figure 11 of Ruppel and Kessler (2017), gas hydrate is stable beneath both warm base and cold base ice sheets if sufficient methane and (unfrozen) pore water are available. Only cold base ice sheets have a permafrost zone, and shallow hydrates in these settings have affinities with PAH. For both warm and cold base ice sheets, the elevated pressures caused by the weight of the ice can plunge a substantial thickness of the ground into the hydrate stability zone (Figure 14b). Hydrate could theoretically be stable at the ground surface and form from vapor phase gas trapped in surficial features like wetlands or in near-surface basin sediments. As the ground cools during glacial episodes, solubility of gas in pore space decreases, contributing to hydrate formation deeper in the section. Once evolved, warm base ice sheets have underlying hydrate systems that have similarities with deepwater marine systems in terms of drivers for hydrate dissociation and dissolution. Warm base glaciers can also have well-developed basal drainage systems though, and such drainage may keep methane concentrations below solubility limits and impede the development of hydrate systems at shallower depths in the ground surface. For cold base ice sheets,

permafrost evolution also factors into the hydrate dynamics. Hydrates beneath these ice sheets have affinities with PAH (section 5.2.1) except that the reservoir is more controlled by pressure than temperature.

6. Recommendations and Conclusions

This paper has focused on the Grand Challenge related to the rates of gas hydrate phase changes, with particular emphasis on results relevant to the natural environment. A summary of the key findings and recommendations is as follows:

- Despite the tendency to view gas hydrate stability only through the prism of pressure and temperature, more than 25 years of geoscience literature emphasizes the role of gas solubility in controlling the thermodynamic stability of hydrates and in determining the relative importance of formation, dissolution, and dissociation processes in various parts of natural systems. Formulations focusing only on the impact of P-T on hydrate deposits inherently assume that the adjacent water phase is always in equilibrium with the hydrate or vapor phase. In other words, the water phase has to be exactly saturated (at the limit of methane solubility for a given P-T condition) for solubility to be ignored. Such formulations miss the dynamic nature of gas hydrate within the hydrate stability zone, including the potential to gain or lose gas hydrate based solely on fluctuations in the available pore-water methane content. As discussed in sections 4 and 5, evaluating intrastability zone dynamics is important for understanding a variety of natural and industrial systems.
- Researchers can adopt any of the most widely used EOS (Table 1) for most studies, as long as the focus is not a detailed analysis of P-T conditions requiring an accuracy of better than 0.5°C. For all but the finest grained reservoirs or coarser-grained reservoirs known to contain significant volumes of fines in pore space, including the capillary inhibition effect in the EOS calculation is probably not necessary for first-order analyses of reservoir conditions in homogeneous sediments. The inhibition of hydrate stability in the presence of saline pore waters is greater than early estimates by Dickens and Quinby-Hunt (1994), and researchers should use one of the EOS that correctly incorporates salinity (Table 1) to ensure accurate determination of stability conditions, particularly in marine systems.
- Of the three processes—intrinsic kinetics, mass transfer, and heat transfer—involved in hydrate formation and dissociation, intrinsic kinetics can be ignored even in systems undergoing rapid phase changes. Mass transfer is often the most important process in formation of gas hydrate, although heat transfer is critical since the exothermic heat of formation means that heat must always be removed before hydrate formation can continue. Heat transfer typically plays a more significant role for dissociation, which is an endothermic process, but mass transfer is necessary to move the byproducts of dissociation (especially vapor phase gas) away from the dissociation front so that pressures remain below the gas hydrate stability requirement and dissociation can continue. Further complicating the process is that mass transfer (advection) can also contribute to the transfer of heat to the dissociation front.
- Mass transfer rates limit gas hydrate formation rates in many natural settings. For example, because fluid advection and diffusion rates are slow in natural sediments, hydrate formation proceeds slowly from the aqueous phase methane available in excess of methane solubility, with timescales of thousands of years or more required to form significant hydrate saturations. Hydrate formation from the vapor phase can be very rapid due to the abundance of methane and water available for forming hydrate at the liquid-gas interface. Vapor phase formation processes can occur at the seafloor and in the ocean water column (in less than a second), where free gas invades the hydrate stability zone (probably in days), at the base of the stability zone under some conditions, and where freezing fronts (e.g., from major glaciations) pass through ground containing vapor phase gas and free water.
- In terms of the volume of gas hydrates affected in natural porous systems, dissolution, not hydrate formation or dissociation, is the most widespread process since it is the one driven by disequilibrium in the methane concentrations between gas hydrate and adjacent pore waters. Dissolution can operate within the entire hydrate stability zone, even within systems that are seemingly at equilibrium according to P-T considerations. Dissolution of hydrate within reservoirs would proceed slowly in most cases, requiring thousands of years to erode preexisting gas hydrate.
- Dissociation is confined only to the phase boundaries in hydrate systems. In the marine setting, where the TGHS is always in the water column except in a special combination of geothermal gradient and seafloor slope on upper continental slopes, dissociation in the sediments occurs only at the BGHS. For PAHs and

formations beneath cold base ice sheets, dissociation can sometimes occur simultaneously at the TGHS and BGHS, both of which are within the formation. The endothermic nature of dissociation acts as a thermodynamic brake that prevents runaway dissociation of gas hydrate; however, endothermic dissociation also presents a challenge for hydrate production testing, where additional heat must sometimes be supplied to provoke continued release of gas from reservoir hydrates. Dissociation should not be viewed as an instantaneous process. In other words, once a parcel of sediment attains a P-T condition outside the hydrate stability field, the hydrate does not instantly dissociate. A useful, although imprecise, analogy is an ice cube removed from a freezer. The ice cube does not instantly become water but rather requires finite time for heat transfer to trigger the phase transition of the whole ice cube. Because hydrate dissociation requires both heat and mass transfer, there is always a lag between attaining disequilibrium P-T conditions and breakdown. Though small concentrations of gas hydrate can be dissociated in seconds to days via rapid depressurization or heating, heat transport requirements begin to dominate for larger concentrations of gas hydrate. Gas hydrate-bearing reservoirs tapped as energy resources are anticipated to productively dissociate for decades (Hancock et al., 2019). For most geologic systems, bulk dissociation likely requires thousands of years in response to typical tectonic, sedimentary, or climate triggers.

Data Availability Statement

The database plotted in Figure 1 is available online at https://doi.org/10.5066/P9LLFVJM.

Acknowledgments

Both authors have received nearly two decades of support from the U.S. Geological Survey's (USGS's) Energy Resources Program and the Coastal/Marine Hazards and Resources Program and from numerous DOE-USGS Interagency Agreements, most recently DE-FE0023495. C. R. acknowledges support from NOAA's Office of Ocean Exploration and Research (OER) under NOAA-USGS Interagency Agreement 16-01118. C. R. thanks OER for the opportunity to participate in many telepresence-based remotely operated vehicle dives that imaged hydrate phenomena discussed in this paper, as shown in Figures 7 and 12 and highlighted in the movies included as supporting information. We thank L. Stern and an anonymous reviewer for insights that improved the paper and L.-G. Boze, B. Buczkowski, and K. McMullen for help with maintaining the database of gas hydrate locations originally started by K. Kvenvolden and T. Lorenson. Any use of trade, firm, or product name is for descriptive purposes only and does not imply endorsement by the U.S. Government.

References

Anderson, B., Boswell, R., Collett, T. S., Farrell, H., Ohtsuki, S., White, M., & Zyrianova, M. (2014). *Review of the findings of the Ignik Sikumi CO_2-CH_4 gas hydrate exchange field trial*. Paper presented at the 8th International Conference on Gas Hydrates (ICGH8-2014), ICGH, Beijing, China, 28 Jul.–1 Aug.

Anderson, B., Hancock, S., Wilson, S., Enger, C., Collett, T., Boswell, R., & Hunter, R. (2011). Formation pressure testing at the Mount Elbert Gas Hydrate Stratigraphic Test Well, Alaska North Slope: Operational summary, history matching, and interpretations. *Marine and Petroleum Geology*, *28*(2), 478–492. https://doi.org/10.1016/j.marpetgeo.2010.02.012

Anderson, K., Bhatnagar, G., Crosby, D., Hatton, G., Manfield, P., Kuzmicki, A., et al. (2012). Hydrates in the ocean beneath, around, and above production equipment. *Energy & Fuels*, *26*(7), 4167–4176. https://doi.org/10.1021/ef300261z

Andreassen, K., Hubbard, A., Winsborrow, M., Patton, H., Vadakkepuliyambatta, S., Plaza-Faverola, A., et al. (2017). Massive blow-out craters formed by hydrate-controlled methane expulsion from the Arctic seafloor. *Science*, *356*(6341), 948. https://doi.org/10.1126/science.aal4500

Archer, D. (2007). Methane hydrate stability and anthropogenic climate change. *Biogeosciences*, *4*(4), 521–544. https://doi.org/10.5194/bg-4-521-2007

Arjun, Berendsen, T. A., & Bolhuis, P. G. (2019). Unbiased atomistic insight in the competing nucleation mechanisms of methane hydrates. *Proceedings of the National Academy of Sciences*, *116*(39), 19305. https://doi.org/10.1073/pnas.1906502116

Bagherzadeh, S. A., Alavi, S., Ripmeester, J., & Englezos, P. (2015). Formation of methane nano-bubbles during hydrate decomposition and their effect on hydrate growth. *The Journal of Chemical Physics*, *142*(21), 214701. https://doi.org/10.1063/1.4920971

Bangs, N., Musgrave, R. J., & Tréhu, A. M. (2005). Upward shifts in the southern Hydrate Ridge gas hydrate stability zone following postglacial warming, offshore Oregon. *Journal of Geophysical Research*, *110*, B03102. https://doi.org/10.1029/2004JB003293

Beaudoin, Y. C., Waite, W., Boswell, W., & Dallimore, S. R. (Eds.) (2014). *Frozen Heat-A UNEP Global Outlook on Methane Gas Hydrates, Volume 1: United Nations Environment Programme, GRID-Arendal*. https://wedocs.unep.org/bitstream/handle/20.500.11822/9355/GasHydrates_Vol1_screen.pdf

Berndt, C., Feseker, T., Treude, T., Krastel, S., Liebetrau, V., Niemann, H., et al. (2014). Temporal constraints on hydrate-controlled methane seepage off Svalbard. *Science*, *343*(6168), 284–287. https://doi.org/10.1126/science.1246298

Biastoch, A., Treude, T., Rüpke, L. H., Riebesell, U., Roth, C., Burwicz, E. B., et al. (2011). Rising Arctic Ocean temperatures cause gas hydrate destabilization and ocean acidification. *Geophysical Research Letters*, *38*, L08602. https://doi.org/10.1029/2011gl047222

Boewer, L., Nase, L., Paulus, M., Lehmkühler, F., Tiemeyer, S., Holz, S., Pontoni, D., & Tolan, M. (2012). On the spontaneous formation of clathrate hydrates at water–guest interfaces. *The Journal of Physical Chemistry C*, *116*, 8548–8553. https://www.doi.org/10.1021/jp211784w

Bohrmann, G., Kuhs, W. F., Klapp, S. A., Techmer, K. S., Klein, H., Murshed, M. M., & Abegg, F. (2007). Appearance and preservation of natural gas hydrate from Hydrate Ridge sampled during ODP Leg 204 drilling. *Marine Geology*, *244*, 1–14. https://doi.org/10.1016/j.margeo.2007.05.003

Borowski, W. S., Paull, C. K., & Ussler, W. (1996). Marine pore-water sulfate profiles indicate in situ methane flux from underlying gas hydrate. *Geology*, *24*(7), 655–658. https://doi.org/10.1130/0091-7613(1996)024%3C0655:MPWSPI%3E2.3.CO;2

Boswell, R., & Collett, T. S. (2011). Current perspectives on gas hydrate resources. *Energy & Environmental Science*, *4*(4), 1206–1215. https://doi.org/10.1039/C0EE00203H

Boswell, R., Collett, T. S., Frye, M., Shedd, W., McConnell, D. R., & Shelander, D. (2012). Subsurface gas hydrates in the northern Gulf of Mexico. *Marine and Petroleum Geology*, *34*(1), 4–30. https://doi.org/10.1016/j.marpetgeo.2011.10.003

Boswell, R., Marsteller, S., Okinaka, N., Wakatsuki, M., Collett, T. S., & Hunter, R. (2019). Viable long-term gas hydrate testing site confirmed on the Alaska North Slope Fire in the Ice: Department of Energy, Office of Fossil Energy, National Energy Technology Laboratory. *Methane Hydrate News Letter*, *19*(1), 1–5.

Boswell, R., Myshakin, E. M., Moridis, G. J., Konno, Y., Collett, T. S., Reagan, M. T., et al. (2019). India National Gas Hydrate Program Expedition 02 summary of scientific results: Numerical simulation of reservoir response to depressurization. *Marine and Petroleum Geology*, *108*. https://doi.org/10.1016/j.marpetgeo.2018.09.026

Boswell, R., Schoderbek, D., Collett, T. S., Ohtsuki, S., White, M., & Anderson, B. J. (2017). The Iġnik Sikumi Field Experiment, Alaska North Slope: Design, operations, and implications for CO_2-CH_4 exchange in gas hydrate reservoirs. *Energy & Fuels*, *31*(1), 140–153. https://doi.org/10.1021/acs.energyfuels.6b01909

Brooks, J. M., Kennicutt, M. C., Fay, R. R., McDonald, T. J., & Sassen, R. (1984). Thermogenic gas hydrates in the Gulf of Mexico. *Science*, *225*(4660), 409. https://doi.org/10.1126/science.225.4660.409

Brothers, D. S., Ruppel, C., Kluesner, J. W., ten Brink, U. S., Chaytor, J. D., Hill, J. C., et al. (2014). Seabed fluid expulsion along the upper slope and outer shelf of the U.S. Atlantic continental margin. *Geophysical Research Letters*, *41*, 96–101. https://doi.org/10.1002/2013GL058048

Brothers, L. L., Hart, P. E., & Ruppel, C. D. (2012). Minimum distribution of subsea ice-bearing permafrost on the U.S. Beaufort Sea continental shelf. *Geophysical Research Letters*, *39*, L15501. https://doi.org/10.1029/2012GL052222

Brothers, L. L., Herman, B. M., Hart, P. E., & Ruppel, C. D. (2016). Subsea ice-bearing permafrost on the U.S. Beaufort Margin: 1. Minimum seaward extent defined from multichannel seismic reflection data. *Geochemistry, Geophysics, Geosystems*, *17*, 4354–4365. https://doi.org/10.1002/2016GC006584

Buffett, B. A., & Zatsepina, O. Y. (2000). Formation of gas hydrate from dissolved gas in natural porous media. *Marine Geology*, *164*(1), 69–77. https://doi.org/10.1016/S0025-3227(99)00127-9

Cantwell, K., Wagner, A., & Weinnig, A. (2019). *Oceanographic data collected during the EX1903L2 Mid and Southeast US (ROV & Mapping) expedition on NOAA Ship OKEANOS EXPLORER in the North Atlantic Ocean from 2019-06-20 to 2019-07-12 (NCEI Accession 0195408)*. NOAA National Centers for Environmental Information. Dataset. https://doi.org/10.25921/aajk-1b71. Accessed May 16, 2020.

Cazenave, A., & Llovel, W. (2010). Contemporary sea level rise. *Annual Review of Marine Science*, *2*(1), 145–173. https://doi.org/10.1146/annurev-marine-120308-081105

Chaouachi, M., Falenty, A., Sell, K., Enzmann, F., Kersten, M., Haberthür, D., & Kuhs, W. F. (2015). Microstructural evolution of gas hydrates in sedimentary matrices observed with synchrotron X-ray computed tomographic microscopy. *Geochemistry, Geophysics, Geosystems*, *16*, 1711–1722. https://doi.org/10.1002/2015GC005811

Chapman, R., Pohlman, J., Coffin, R., Chanton, J., & Lapham, L. (2004). Thermogenic gas hydrates in the northern Cascadia margin. *Eos, Transactions American Geophysical Union*, *85*(38), 361–365. https://doi.org/10.1029/2004EO380001

Chatterjee, S., Bhatnagar, G., Dugan, B., Dickens, G. R., Chapman, W. G., & Hirasaki, G. J. (2014). The impact of lithologic heterogeneity and focused fluid flow upon gas hydrate distribution in marine sediments. *Journal of Geophysical Research: Solid Earth*, *119*, 6705–6732. https://doi.org/10.1002/2014JB011236

Chen, L., Sloan, E. D., Koh, C. A., & Sum, A. K. (2013). Methane hydrate formation and dissociation on suspended gas bubbles in water. *Journal of Chemical & Engineering Data*, *59*. https://doi.org/10.1021/je400765a

Circone, S., Kirby, S. H., & Stern, L. A. (2005a). Direct measurement of methane hydrate composition along the hydrate equilibrium boundary. *Journal of Physical Chemistry B*, *109*, 9468–9475. https://doi.org/10.1021/jp0504874

Circone, S., Kirby, S. H., & Stern, L. A. (2005b). Thermal regulation of methane hydrate dissociation: Implications for gas production models. *Energy & Fuels*, *19*(6), 2357–2363. https://doi.org/10.1021/ef0500437

Circone, S., Stern, L. A., & Kirby, S. H. (2004). The effect of elevated methane pressure on methane hydrate dissociation. *American Mineralogist*, *89*(8–9), 1192–1201. https://doi.org/10.2138/am-2004-8-905

Clennell, M. B., Hovland, M., Booth, J. S., Henry, P., & Winters, W. J. (1999). Formation of natural gas hydrates in marine sediments: 1. Conceptual model of gas hydrate growth conditioned by host sediment properties. *Journal of Geophysical Research*, *104*(B10), 22,985–23,003. https://doi.org/10.1029/1999JB900175

Collett, T., Riedel, M., Cochran, J., Boswell, R., Presley, J., Kumar, P., et al. (2015). *Indian National Gas Hydrate Program Expedition 01 report* (Scientific Investigations Report 2012-5054). Reston, VA: U.S. Geological Survey. https://doi.org/10.3133/sir20125054

Collett, T. S. (2002). Energy resource potential of natural gas hydrates. *AAPG Bulletin*, *86*(11), 1971–1992. https://doi.org/10.1306/61eeddd2-173e-11d7-8645000102c1865d

Collett, T. S., Boswell, R., Waite, W. F., Kumar, P., Roy, S. K., Chopra, K., et al. (2019). India National Gas Hydrate Program Expedition 02 Summary of Scientific Results: Gas hydrate systems along the eastern continental margin of India. *Marine and Petroleum Geology*, *108*. https://doi.org/10.1016/j.marpetgeo.2019.05.023

Collett, T. S., Johnson, A. H., Knapp, C. C., & Boswell, R. (2009). Natural gas hydrates—Energy resource potential and associated geologic hazards, edited by T. Collett, A. Johnson, C. Knapp, and R. Boswell. *AAPG Memoir*, *89*, 146–219.

Collett, T. S., Lee, M. W., Agena, W. F., Miller, J. J., Lewis, K. A., Zyrianova, M. V., et al. (2011). Permafrost-associated natural gas hydrate occurrences on the Alaska North Slope. *Marine and Petroleum Geology*, *28*(2), 279–294. https://doi.org/10.1016/j.marpetgeo.2009.12.001

Cook, A. E., & Malinverno, A. (2013). Short migration of methane into a gas hydrate-bearing sand layer at Walker Ridge, Gulf of Mexico. *Geochemistry, Geophysics, Geosystems*, *14*, 283–291. https://doi.org/10.1002/ggge.20040

Dai, S., Kim, J., Xu, Y., Waite, W. F., Jang, J., Yoneda, J., et al. (2019). Permeability anisotropy and relative permeability in sediments from the National Gas Hydrate Program Expedition 02, offshore India. *Marine and Petroleum Geology*. https://doi.org/10.1016/j.marpetgeo.2018.08.016

Dai, S., Lee, C., & Santamarina, J. C. (2011). Formation history and physical properties of sediments from the Mount Elbert Gas Hydrate Stratigraphic Test Well, Alaska North Slope. *Marine and Petroleum Geology*, *28*(2), 427–438. https://doi.org/10.1016/j.marpetgeo.2010.03.005

Dai, S., & Seol, Y. (2014). Water permeability in hydrate-bearing sediments: A pore-scale study. *Geophysical Research Letters*, *41*, 4176–4184. https://doi.org/10.1002/2014GL060535

Dallimore, S. R., & Collett, T. S. (1995). Intrapermafrost gas hydrates from a deep core-hole in the Mackenzie Delta, Northwest-Territories, Canada. *Geology*, *23*(6), 527–530. https://doi.org/10.1130/00917613(1995)023%3C0527:ighfad%3E2.3.co;2

Darnell, K. N., & Flemings, P. B. (2015). Transient seafloor venting on continental slopes from warming-induced methane hydrate dissociation. *Geophysical Research Letters*, *42*, 10,765–710,772. https://doi.org/10.1002/2015GL067012

Davie, M. K., & Buffett, B. A. (2001). A numerical model for the formation of gas hydrate below the seafloor. *Journal of Geophysical Research*, *106*(B1), 497–514. https://doi.org/10.1029/2000JB900363

Davie, M. K., Zatsepina, O. Y., & Buffet, B. A. (2004). Methane solubility in marine hydrate environments. *Marine Geology*, *203*, 177–184. https://doi.org/10.1016/s0025-3227(03)00331-1

De Roo, J. L., Peters, C. J., Lichtenthaler, R. N., & Diepen, G. A. M. (1983). Occurrence of methane hydrate in saturated and unsaturated solutions of sodium chloride and water In dependence of temperature and pressure. *AICHE Journal*, *29*(4), 651–657. https://doi.org/10.1002/aic.690290420

Deepwater Horizon Natural Resource Damage Assessment Trustees (2016). Chapter 2: Incident Overview Deepwater Horizon oil spill. In *Final Programmatic Damage Assessment and Restoration Plan and Final Programmatic Environmental Impact Statement*, 24 pp. http://www.gulfspillrestoration.noaa.gov/restoration-planning/gulf-plan

Denman, K. L., Brasseur, G., Chidthaisong, A., Ciais, P., Cox, P. M., & Dickinson, R. E. (2007). Couplings between changes in the climate system and biogeochemistry. In S. Solomon, D. Qin, M. Manning, Z. Chen, M. Marquis, K. B. Averyt, M. Tignor, & H. L. Miller (Eds.), *Climate change 2007: The physical science basis. Contribution of Working Group I to the Fourth Assessment Report of the Intergovernmental Panel on Climate Change* (pp. 499–587). Cambridge: Cambridge University Press.

Dickens, G. R. (2001). The potential volume of oceanic methane hydrates with variable external conditions. *Organic Geochemistry*, *32*(10), 1179–1193. https://doi.org/10.1016/S0146-6380(01)00086-9

Dickens, G. R. (2003). Rethinking the global carbon cycle with a large, dynamic and microbially mediated gas hydrate capacitor. *Earth and Planetary Science Letters*, *213*(3–4), 169–183. https://doi.org/10.1016/S0012-821X(03)00325-X

Dickens, G. R., Castillo, M. M., & Walker, J. C. G. (1997). A blast of gas in the latest Paleocene: Simulating first-order effects of massive dissociation of oceanic methane hydrate. *Geology*, *25*(3), 259–262. https://doi.org/10.1130/0091-7613(1997)025%3C0259:ABOGIT%3E2.3.CO;2

Dickens, G. R., & Quinby-Hunt, M. S. (1994). Methane hydrate stability in seawater. *Geophysical Research Letters*, *21*(19), 2115–2118. https://doi.org/10.1029/94GL01858

Dickens, G. R., & Quinby-Hunt, M. S. (1997). Methane hydrate stability in pore water: A simple theoretical approach for geophysical applications. *Journal of Geophysical Research*, *102*(B1), 773–783. https://doi.org/10.1029/96JB02941

Duan, Z., Li, D., Chen, Y., & Sun, R. (2011). The influence of temperature, pressure, salinity and capillary force on the formation of methane hydrate. *Geoscience Frontiers*, *2*(2), 125–135. https://doi.org/10.1016/j.gsf.2011.03.009

Duan, Z., & Sun, R. (2006). A model to predict phase equilibrium of CH_4 and CO_2 clathrate hydrate in aqueous electrolyte solutions. *American Mineralogist*, *91*, 1346–1354. https://doi.org/10.2138/am.2006.2017

Duan, Z., & Weare, J. H. (1992). Reply to comment by J. J. Carroll on "The prediction of methane solubility in natural waters to high ionic strength from 0 to 250°C and from 0 to 1600 bar". *Geochimica et Cosmochimica Acta*, *56*(12), 4303. https://doi.org/10.1016/0016-7037(92)90271-j

Duan, Z. H., & Mao, S. D. (2006). A thermodynamic model for calculating methane solubility, density and gas phase composition of methane-bearing aqueous fluids from 273 to 523 K and from 1 to 2000 bar. *Geochimica et Cosmochimica Acta*, *70*(13), 3369–3386. https://doi.org/10.1016/j.gca.2006.03.018

Duan, Z. H., Moeller, N., Greenberg, J., & Weare, J. H. (1992). The prediction of methane solubility in natural waters to high ionic strength from 0 to 250°C and from 0 to 1,600 bar. *Geochimica et Cosmochimica Acta*, *56*(4), 1451–1460. https://doi.org/10.1016/0016-7037(92)90215-5

Duan, Z. H., Moeller, N., & Weare, J. H. (1992). An equation of state for the CH4-CO2-H20 system: I. Pure systems from 0 to 1000°C and 0 to 8000 bar. *Geochimica et Cosmochimica Acta*, *56*, 2605–2617. https://doi.org/10.1016/0016-7037(92)90347-l

Dugan, B., & Sheahan, T. C. (2012). Offshore sediment overpressures of passive margins: Mechanisms, measurement, and models. *Reviews of Geophysics*, *50*, RG3001. https://doi.org/10.1029/2011RG000379

Ebinuma, T., Oyama, H., Utiumi, T., Nagao, J., & Narita, H. (2008). *Direct observation of characteristic dissociation behaviors of hydrate-bearing cores by rapid-scanning X-ray CT imaging*. Vancouver, Canada, July 6–10: Paper presented at the 6th International Conference on Gas Hydrates. 8 p

Egorov, A. V., Crane, K., Vogt, P. R., & Rozhkov, A. N. (1999). Gas hydrates that outcrop on the sea floor: Stability models. *Geo-Marine Letters*, *19*(1–2), 68–75. https://doi.org/10.1007/s003670050094

Egorov, A. V., Nigmatulin, R. I., & Rozhkov, A. N. (2014). Transformation of deep-water methane bubbles into hydrate. *Geofluids*, *14*(4), 430–442. https://doi.org/10.1111/gfl.12085

Ehlers, J., Gibbard, P. L., & Hughes, P. D. (2011). *Quaternary glaciations—Extent and chronology: A closer look* (Vol. 15, p. 1108). Amsterdam: Elsevier.

Englezos, P., Kalogerakis, N., Dholabhai, P. D., & Bishnoi, P. R. (1987). Kinetics of formation of methane and ethane gas hydrates. *Chemical Engineering Science*, *42*(11), 2647–2658. https://doi.org/10.1016/0009-2509(87)87015-X

English, N. J., & Phelan, G. M. (2009). Molecular dynamics study of thermal-driven methane hydrate dissociation. *Journal of Chemical Physics*, *131*, 074704(7). https://doi.org/10.1063/1.3211089

Feng, J.-C., Wang, Y., & Li, X.-S. (2017). Large scale experimental evaluation to methane hydrate dissociation below quadruple point by depressurization assisted with heat stimulation. *Energy Procedia*, *142*, 4117–4123. https://doi.org/10.1016/j.egypro.2017.12.334

Fisher, C. R., MacDonald, I. R., Sassen, R., Young, C. M., Macko, S. A., Hourdez, S., et al. (2000). Methane ice worms: Hesiocaeca methanicola Colonizing Fossil Fuel Reserves. *Naturwissenschaften*, *87*(4), 184–187. https://doi.org/10.1007/s001140050700

Freer, E. M., Sami Selim, M., & Sloan, E. D. (2001). Methane hydrate film growth kinetics. *Fluid Phase Equilibria*, *185*(1–2), 65–75. https://doi.org/10.1016/S0378-3812(01)00457-5

Fu, X., Cueto-Felgueroso, L., & Juanes, R. (2018). Nonequilibrium thermodynamics of hydrate growth on a gas-liquid interface. *Physical Review Letters*, *120*(14), 144501. https://doi.org/10.1103/PhysRevLett.120.144501

Fu, X., Waite, W. F., Cueto-Felgueroso, L., & Juanes, R. (2019). Xenon hydrate as an analog of methane hydrate in geologic systems out of thermodynamic equilibrium. *Geochemistry, Geophysics, Geosystems*, *20*, 2462–2472. https://doi.org/10.1029/2019GC008250

Gorman, A. R., & Senger, K. (2010). Defining the updip extent of the gas hydrate stability zone on continental margins with low geothermal gradients. *Journal of Geophysical Research*, *115*, B07105. https://doi.org/10.1029/2009JB006680

Graham, R., Reilly, W. K., Beinecke, F., Boesch, D. F., Garcia, T. D., Murray, C. A., & Ulmer, F. (2011). *Deep water—The Gulf oil disaster and the future of offshore drilling: Report to the President*. Washington D.C.: National Commission on the BP Deepwater Horizon Oil Spill and Offshore Drilling, Government Printing Office.

Granin, N. G., Aslamov, I. A., Kozlov, V. V., Makarov, M. M., Kirillin, G., McGinnis, D. F., et al. (2019). Methane hydrate emergence from Lake Baikal: direct observations, modelling, and hydrate footprints in seasonal ice cover. *Scientific Reports*, *9*, 19361. https://doi.org/10.1038/s41598-019-55758-8

Guo, G.-J., Li, M., Zhang, Y.-G., & Wu, C.-H. (2009). Why can water cages adsorb aqueous methane? A potential of mean force calculation on hydrate nucleation mechanisms. *Physical Chemistry Chemical Physics*, *11*(44), 10,427–10,437. https://doi.org/10.1039/B913898F

Guo, G.-J., & Rodger, P. M. (2013). Solubility of aqueous methane under metastable conditions: Implications for gas hydrate nucleation. *The Journal of Physical Chemistry B*, *117*(21), 6498–6504. https://doi.org/10.1021/jp3117215

Gupta, A. (2007). *Methane hydrate dissociation measurements and modeling: The role of heat transfer (doctor of philosophy)*. Golden, Colorado: Colorado School of Mines, Ph. D thesis.

Hadley, C., Peters, D., Vaughan, A., & Bean, D. (2008). *Gumusut-Kakap Project: Geohazard characterisation and impact on field development plans*. Kuala Lumpur, Malaysia: International Petroleum Technology Conference, 3–5 December.

Hammerschmidt, E. G. (1934). Formation of gas hydrates in natural gas transmission lines. *Industrial and Engineering Chemistry*, *26*(8), 851–855. https://doi.org/10.1021/ie50296a010

Hancock, S., Boswell, R., & Collett, T. (2019). *Development of deepwater natural gas hydrates*. Houston, Texas: Paper presented at the Offshore Technology Conference. May 6–9, Paper OTC-29374-MS

Handa, Y. P. (1986). Compositions, enthalpies of dissociation, and heat capacities in the range 85 to 270 K for clathrate hydrates of methane, ethane, and propane, and enthalpy of dissociation of isobutane hydrate, as determined by a heat-flow calorimeter. *Journal of Chemical Thermodynamics*, *18*, 915–921. https://doi.org/10.1016/0021-9614(1086)90149-90147

Harvey, L. D. D., & Huang, Z. (1995). Evaluation of the potential impact of methane clathrate destabilization on future global warming. *Journal of Geophysical Research*, *100*(D2), 2905–2926. https://doi.org/10.1029/94JD02829

Helgerud, M. B., Waite, W. F., Kirby, S. H., & Nur, A. (2009). Elastic wave speeds and moduli in polycrystalline ice Ih, sI methane hydrate, and sII methane-ethane hydrate. *Journal of Geophysical Research*, *114*, B02212. https://doi.org/10.01029/02008JB006132

Henry, P., Thomas, M., & Clennell, M. B. (1999). Formation of natural gas hydrate in marine sediments: 2. Thermodynamic calculations of stability conditions in porous sediments. *Journal of Geophysical Research*, *104*, 23,005–023,022. https://doi.org/10.1029/1999JB900167

Holder, G. D., Kamath, V. A., & Godbole, S. P. (1984). The potential of natural gas hydrates as an energy resource. *Annual Review of Energy*, *9*. https://doi.org/10.1146/annurev.eg.1109.110184.002235

Hornbach, M. J., Saffer, D. M., & Holbrook, W. S. (2004). Critically pressured free-gas reservoirs below gas-hydrate provinces. *Nature*, *427*(6970), 142–144. https://doi.org/10.1038/nature02172

Hu, K., Issler, Z., Chen, Z., & Brent, T. A. (2013). *Permafrost investigation by well logs, and seismic velocity and repeated shallow temperature surveys, Beaufort-Mackenzie Basin* (Geol. Surv. Can. Open File Rep., 6956, 228 pp.)

Jacobson, L. C., Matsumoto, M., & Molinero, V. (2011). Order parameters for the multistep crystallization of clathrate hydrates. *The Journal of Chemical Physics*, *135*(7), 074501. https://doi.org/10.1063/1.3613667

Jähne, B., Heinz, G., & Dietrich, W. (1987). Measurement of the diffusion coefficients of sparingly soluble gases in water. *Journal of Geophysical Research*, *92*(C10), 10,767–10,776. https://doi.org/10.1029/JC092iC10p10767

Jain, A. K., & Juanes, R. (2009). Preferential mode of gas invasion in sediments: Grain-scale mechanistic model of coupled multiphase fluid flow and sediment mechanics. *Journal of Geophysical Research*, *114*, B08101. https://doi.org/10.1029/2008JB006002

Jiménez-Ángeles, F., & Firoozabadi, A. (2014). Nucleation of methane hydrates at moderate subcooling by molecular dynamics simulations. *The Journal of Physical Chemistry C*, *118*(21), 11,310–11,318. https://doi.org/10.1021/jp5002012

Jin, Y., Konno, Y., & Nagao, J. (2012). Growth of methane clathrate hydrates in porous media. *Energy & Fuels*, *26*(4), 2242–2247. https://doi.org/10.1021/ef3001357

Johnson, J. E., Mienert, J., Plaza-Faverola, A., Vadakkepuliyambatta, S., Knies, J., Bünz, S., et al. (2015). Abiotic methane from ultraslow-spreading ridges can charge Arctic gas hydrates. *Geology*, *43*(5), 371–374. https://doi.org/10.1130/G36440.1

Joye, S. B., Boetius, A., Orcutt, B. N., Montoya, J. P., Schulz, H. N., Erickson, M. J., & Lugo, S. K. (2004). The anaerobic oxidation of methane and sulfate reduction in sediments from Gulf of Mexico cold seeps. *Chemical Geology*, *205*(3–4), 219–238. https://doi.org/10.1016/j.chemgeo.2003.12.019

Kamath, V. A., & Holder, G. D. (1987). Dissociation heat transfer characteristics of methane hydrates. *AICHE Journal*, *33*(2), 347–350. https://doi.org/10.1002/aic.690330228

Kang, D. H., Yun, T. S., Kim, K. Y., & Jang, J. (2016). Effect of hydrate nucleation mechanisms and capillarity on permeability reduction in granular media. *Geophysical Research Letters*, *43*, 9018–9025. https://doi.org/10.1002/2016GL070511

Kennedy, B., Messing, C., & Amon, D. (2019). *Oceanographic data collected during the EX1711 Gulf of Mexico Mapping (ROV & Mapping) expedition on NOAA Ship OKEANOS EXPLORER in the Gulf of Mexico from 2017-11-29 to 2017-12-21 (NCEI Accession 0170751)*. NOAA National Centers for Environmental Information Dataset.

Khurana, M., Yin, Z., & Linga, P. (2017). A review of clathrate hydrate nucleation. *ACS Sustainable Chemistry & Engineering*, *5*(12), 11,176–11,203. https://doi.org/10.1021/acssuschemeng.7b03238

Kida, M., Jin, Y., Watanabe, M., Konno, Y., Yoneda, J., Egawa, K., et al. (2015). Chemical and crystallographic characterizations of natural gas hydrates recovered from a production test site in the eastern Nankai Trough. *Marine and Petroleum Geology*, *66*, 396–403. https://doi.org/10.1016/j.marpetgeo.2015.02.019

Kida, M., Jin, Y., Yoneda, J., Oshima, M., Kato, A., Konno, Y., et al. (2019). Crystallographic and geochemical properties of natural gas hydrates accumulated in the National Gas Hydrate Program Expedition 02 drilling sites in the Krishna-Godavari Basin off India. *Marine and Petroleum Geology*, *108*, 471–481. https://doi.org/10.1016/j.marpetgeo.2018.10.012

Kida, M., Khlystov, O., Zemskaya, T., Takahashi, N., Minami, H., Sakagami, H., et al. (2006). Coexistence of Structure I and II gas hydrates in Lake Baikal suggesting gas sources from microbial and thermogenic origin. *Geophysical Research Letters*, *33*, L24603. https://doi.org/10.1029/2006GL028296

Kim, H. C., Bishnoi, P. R., Heidemann, R. A., & Rizvi, S. S. H. (1987). Kinetics of methane hydrate decomposition. *Chemical Engineering Science*, *42*(7), 1645–1653. https://doi.org/10.1016/0009-2509(87)80169-0

Klapp, S. A., Murshed, M. M., Pape, T., Klein, H., Bohrmann, G., Brewer, P. G., & Kuhs, W. F. (2010). Mixed gas hydrate structures at the Chapopote Knoll, southern Gulf of Mexico. *Earth and Planetary Science Letters*, *299*(1), 207–217. https://doi.org/10.1016/j.epsl.2010.09.001

Klein, F., Grozeva, N. G., & Seewald, J. S. (2019). Abiotic methane synthesis and serpentinization in olivine-hosted fluid inclusions. *Proceedings of the National Academy of Sciences*, *116*(36), 17666. https://doi.org/10.1073/pnas.1907871116

Knott, B. C., Molinero, V., Doherty, M. F., & Peters, B. (2012). Homogeneous nucleation of methane hydrates: Unrealistic under realistic conditions. *Journal of the American Chemical Society*, *134*(48), 19,544–19,547. https://doi.org/10.1021/ja309117d

Konno, Y., Fujii, T., Sato, A., Akamine, K., Naiki, M., Masuda, Y., et al. (2017). Key findings of the world's first offshore methane hydrate production test off the coast of japan: toward future commercial production. *Energy & Fuels*, *31*(3), 2607–2616. https://doi.org/10.1021/acs.energyfuels.6b03143

Konno, Y., Jin, Y., Shinjou, K., & Nagao, J. (2014). Experimental evaluation of the gas recovery factor of methane hydrate in sandy sediment. *RSC Advances*, *4*(93), 51,666–51,675. https://doi.org/10.1039/C4RA08822K

Kowalsky, M. B., & Moridis, G. J. (2007). Comparison of kinetic and equilibrium reaction models in simulating gas hydrate behavior in porous media. *Energy Conversion and Management*, *48*(6), 1850–1863. https://doi.org/10.1016/j.enconman.2007.01.017

Kuhs, W. F., Genov, G., Staykova, D. K., & Hansen, T. (2004). Ice perfection and onset of anomalous preservation of gas hydrates. *Physical Chemistry Chemical Physics*, *6*(21), 4917–4920. https://doi.org/10.1039/B412866D

Kurihara, M., Sato, A., Funatsu, K., Ouchi, H., Masuda, Y., Narita, H., & Collett, T. S. (2011). Analysis of formation pressure test results in the Mount Elbert methane hydrate reservoir through numerical simulation. *Marine and Petroleum Geology*, *28*, 502–516. https://doi.org/10.1016/j.marpetgeo.2010.01.007

Kvenvolden, K. A. (1988). Methane hydrates and global climate. *Global Biogeochemical Cycles*, *2*(3), 221–229. https://doi.org/10.1029/GB002i003p00221

Lamarche-Gagnon, G., Wadham, J. L., Sherwood Lollar, B., Arndt, S., Fietzek, P., Beaton, A. D., et al. (2019). Greenland melt drives continuous export of methane from the ice-sheet bed. *Nature*, *565*(7737), 73–77. https://doi.org/10.1038/s41586-018-0800-0

Lapham, L. L., Wilson, R. M., MacDonald, I. R., & Chanton, J. P. (2014). Gas hydrate dissolution rates quantified with laboratory and seafloor experiments. *Geochimica et Cosmochimica Acta*, *125*, 492–503. https://doi.org/10.1016/j.gca.2013.10.030

Lee, J. Y., Francisca, F. M., Santamarina, J. C., & Ruppel, C. (2010). Parametric study of the physical properties of hydrate-bearing sand, silt, and clay sediments: 2. Small-strain mechanical properties. *Journal of Geophysical Research*, *115*, B11105. https://doi.org/10.1029/2009JB006670

Lei, L., Seol, Y., & Myshakin, E. M. (2019). Methane hydrate film thickening in porous media. *Geophysical Research Letters*, *46*, 11,091–11,099. https://doi.org/10.1029/2019GL084450

Li, X.-S., Xu, C.-G., Zhang, Y., Ruan, X., Li, G., & Wang, Y. (2016). Investigation into gas production from natural gas hydrate: A review. *Applied Energy*, *172*, 286–322. https://doi.org/10.1016/j.apenergy.2016.03.101

Li, X. S., Yang, B., Zhang, Y., Li, G., Duan, L. P., Wang, Y., et al. (2012). Experimental investigation into gas production from methane hydrate in sediment by depressurization in a novel pilot-scale hydrate simulator. *Applied Energy*, *93*, 722–732. https://doi.org/10.1016/j.apenergy.2012.01.009

Liang, M. Y., Chen, G. J., Sun, C. Y., Yan, L. J., Liu, J., & Ma, Q. L. (2005). Experimental and modeling study on decomposition kinetics of methane hydrates in different media. *Journal of Physical Chemistry B*, *109*(40), 19,034–19,041. https://doi.org/10.1021/jp0526851

Liu, X., & Flemings, P. B. (2006). Passing gas through the hydrate stability zone at southern Hydrate Ridge, offshore Oregon. *Earth and Planetary Science Letters*, *241*, 211–226. https://doi.org/10.1016/j.epsl.2005.10.026

Liu, X., & Flemings, P. B. (2007). Dynamic multiphase flow model of hydrate formation in marine sediments. *Journal of Geophysical Research*, *112*, B03101. https://doi.org/10.1029/2005JB004227

Liu, X., & Flemings, P. B. (2011). Capillary effects on hydrate stability in marine sediments. *Journal of Geophysical Research*, *116*. https://doi.org/10.1029/2010JB008143

Liu, Z., Li, H., Chen, L., & Sun, B. (2018). A new model of and insight into hydrate film lateral growth along the gas–liquid interface considering natural convection heat transfer. *Energy & Fuels*, *32*(2), 2053–2063. https://doi.org/10.1021/acs.energyfuels.7b03530

Lobecker, E., Austin, J., & Farrington, S. (2019). *Oceanographic data and ROV dive-related multimedia and information collected during the EX1402L3 (Gulf of Mexico Mapping and ROV Exploration) expedition on NOAA Ship OKEANOS EXPLORER in the Gulf of Mexico from 2014-04-10 to 2014-05-01 (NCEI Accession 0157088)*. NOAA National Centers for Environmental Information. https://doi.org/10.7289/v5nc5z7d

Locarnini, R. A., Mischonov, A. V., Antonov, J. I., Boyer, T. P., Garcia, H. E., Baranova, O. K., Zweng, M. M., & Johnson, D. R. (2010). World Ocean Atlas 2009, Volume 1: Temperature. In S. Levitus (Ed.), *NOAA Atlas NESDIS 68* (p. 184). Washington DC: U.S. Government Printing Office.

Long, J. P., & Sloan, E. D. (1996). Hydrates in the ocean and evidence for the location of hydrate formation. *International Journal of Thermophysics*, *17*(1), 1–13. https://doi.org/10.1007/BF01448204

Lu, W., Chou, I. M., & Burruss, R. C. (2008). Determination of methane concentrations in water in equilibrium with sI methane hydrate in the absence of a vapor phase by in situ Raman spectroscopy. *Geochimica et Cosmochimica Acta*, *72*, 412–422. https://doi.org/10.1016/j.gca.2007.11.006

Lv, X., Shi, B., Zhou, S., Peng, H., Lei, Y., & Yu, P. (2018). Study on the growth rate of natural gas hydrate in water-in-oil emulsion system using a high-pressure flow loop. *RSC Advances*, *8*(64), 36484–36492. https://doi.org/10.1039/C8RA07571A

Maeda, N. (2018). Interfacial nanobubbles and the memory effect of natural gas hydrates. *The Journal of Physical Chemistry C*, *122*(21), 11399–11406. https://doi.org/10.1021/acs.jpcc.8b02416

Maekawa, T. (2001). Equilibrium conditions for gas hydrates of methane and ethane mixtures in pure water and sodium chloride solution. *Geochemical Journal*, *35*(1), 59–66. https://doi.org/10.2343/geochemj.35.59

Maini, B. B., & Bishnoi, P. R. (1981). Experimental investigation of hydrate formation behaviour of a natural gas bubble in a simulated deep sea environment. *Chemical Engineering Science*, *36*, 183–189. https://doi.org/10.1016/0009-2509(81)80062-0

Majorowicz, J. A., Osadetz, K., & Safanda, J. (2008). *Onset and stability of gas hydrates under permafrost in an environment of surface climactic change-past and future*. Vancouver BC: Paper presented at the Proceedings of the 6th International Conference on Gas Hydrates.

Malinverno, A. (2010). Marine gas hydrates in thin sand layers that soak up microbial methane. *Earth and Planetary Science Letters*, *292*(3–4), 399–408. https://doi.org/10.1016/j.epsl.2010.02.008

McGinnis, D. F., Greinert, J., Artemov, Y., Beaubien, S. E., & Wuest, A. (2006). Fate of rising methane bubbles in stratified waters: How much methane reaches the atmosphere? *Journal of Geophysical Research*, *111*, C09007. https://doi.org/10.1029/2005JC003183

McIver, R. D. (1981). Gas hydrates. In R. F. Meyer, & J. C. Olson (Eds.), *Long-term energy resources* (pp. 713–726). Boston, MA: Pitman.

Mehta, A. P., & Sloan, E. D. (1996). *Structure H hydrates*. Denver, Colorado: Paper presented at the SPE Annual Technical Conference and Exhibition.

Melnikov, V. P., Nesterov, A. N., Reshetnikov, A. M., & Zavodovsky, A. G. (2009). Evidence of liquid water formation during methane hydrates dissociation below the ice point. *Chemical Engineering Science*, *64*(6), 1160–1166. https://doi.org/10.1016/j.ces.2008.10.067

Meyer, D. W., Flemings, P. B., & DiCarlo, D. (2018). Effect of gas flow rate on hydrate formation within the hydrate stability zone. *Journal of Geophysical Research: Solid Earth*, *123*, 6263–6276. https://doi.org/10.1029/2018JB015878

Meyer, D. W., Flemings, P. B., DiCarlo, D., You, K., Phillips, S. C., & Kneafsey, T. J. (2018). Experimental investigation of gas flow and hydrate formation within the hydrate stability zone. *Journal of Geophysical Research: Solid Earth*, *123*, 5350–5371. https://doi.org/10.1029/2018JB015748

Mienert, J., Vanneste, M., Bünz, S., Andreassen, K., Haflidason, H., & Sejrup, H. P. (2005). Ocean warming and gas hydrate stability on the mid-Norwegian margin at the Storegga Slide. *Marine and Petroleum Geology*, *22*(1–2), 233–244. https://doi.org/10.1016/j.marpetgeo.2004.10.018

Mori, Y. H. (2001). Estimating the thickness of hydrate films from their lateral growth rates: application of a simplified heat transfer model. *Journal of Crystal Growth*, *223*(1–2), 206–212. https://doi.org/10.1016/S0022-0248(01)00614-5

Moridis, G. J., Reagan, M. T., Queiruga, A. F., & Boswell, R. (2019). Evaluation of the performance of the oceanic hydrate accumulation at site NGHP-02-09 in the Krishna-Godavari Basin during a production test and during single and multi-well production scenarios. *Marine and Petroleum Geology*, *108*. https://doi.org/10.1016/j.marpetgeo.2018.12.001

Moridis, G. J., & Reagan, T. (2007). *Strategies for gas production from oceanic Class 3 hydrate accumulations, OTC 18865*. Houston, Texas: Paper presented at the Offshore Technology Conference. 30 April - 3 May, 2007

Myshakin, E. M., Seol, Y., Lin, J. S., Uchida, S., Collett, T. S., & Boswell, R. (2019). Numerical simulations of depressurization-induced gas production from an interbedded turbidite gas-hydrate-bearing sedimentary section in the offshore of India: Site NGHP-02-16 (Area-B). *Marine and Petroleum Geology*, *108*. https://doi.org/10.1016/j.marpetgeo.2018.10.047

Nimblett, J., & Ruppel, C. (2003). Permeability evolution during the formation of gas hydrates in marine sediments. *Journal of Geophysical Research*, *108*(B9), 2420. https://doi.org/10.1029/2001JB001650

Obu, J., Westermann, S., Bartsch, A., Berdnikov, N., Christiansen, H. H., Dashtseren, A., et al. (2019). Northern Hemisphere permafrost map based on TTOP modelling for 2000–2016 at 1 km2 scale. *Earth-Science Reviews*, *193*, 299–316. https://doi.org/10.1016/j.earscirev.2019.04.023

Ohgaki, K., Takano, K., Sangawa, H., Matsubara, T., & Nakano, S. (1996). Methane exploitation by carbon dioxide from gas hydrates—Phase equilibria for CO_2-CH_4 mixed hydrate system. *Journal of Chemical Engineering of Japan*, *29*(3), 478–483. https://doi.org/10.1252/jcej.29.478

Ohmura, R., Matsuda, S., Uchida, T., Ebinuma, T., & Narita, H. (2005). Clathrate hydrate crystal growth in liquid water saturated with a guest substance: Observations in a methane plus water system. *Crystal Growth & Design*, *5*(3), 953–957. https://doi.org/10.1021/Cg049675u

Overduin, P. P., Schneider von Deimling, T., Miesner, F., Grigoriev, M. N., Ruppel, C., Vasiliev, A., et al. (2019). Submarine Permafrost Map in the Arctic Modeled Using 1-D Transient Heat Flux (SuPerMAP). *Journal of Geophysical Research: Oceans*, *124*, 3490–3507. https://doi.org/10.1029/2018JC014675

Oyama, H., Konno, Y., Masuda, Y., & Narita, H. (2009). Dependence of depressurization-induced dissociation of methane hydrate bearing laboratory cores on heat transfer. *Energy & Fuels*, *23*(10), 4995–5002. https://doi.org/10.1021/ef900179y

Paganoni, M., Cartwright, J. A., Foschi, M., Shipp, R. C., & Van Rensbergen, P. (2016). Structure II gas hydrates found below the bottom-simulating reflector. *Geophysical Research Letters*, *43*, 5696–5706. https://doi.org/10.1002/2016GL069452

Pangborn, J. B., & Barduhn, A. J. (1970). Kinetics of methyl bromide hydrate formation. *Desalination*, *8*(1), 35–68. https://doi.org/10.1016/S0011-9164(00)82013-5

Paull, C. K., Matsumoto, R., & Wallace, P. J. (1996). *Proceedings of the Ocean Drilling Program, Initial Reports* (Vol. 164). College Station, TX: Ocean Drilling Program.

Paull, C. K., Ussler, W., Dallimore, S. R., Blasco, S. M., Lorenson, T. D., Melling, H., et al. (2007). Origin of pingo-like features on the Beaufort Sea shelf and their possible relationship to decomposing methane gas hydrates. *Geophysical Research Letters*, *34*, L01603. https://doi.org/10.1029/2006GL027977

Pecher, I. A., Henrys, S. A., Wood, W. T., Kukowski, N., Crutchley, G. J., Fohrmann, M., et al. (2010). Focussed fluid flow on the Hikurangi Margin, New Zealand—Evidence from possible local upwarping of the base of gas hydrate stability. *Marine Geology*, *272*(1–4), 99–113. https://doi.org/10.1016/j.margeo.2009.10.006

Peng, B. Z., Dandekar, A., Sun, C. Y., Luo, H., Ma, Q. L., Pang, W. X., & Chen, G. J. (2007). Hydrate film growth on the surface of a gas bubble suspended in water. *The Journal of Physical Chemistry B*, *111*(43), 12485–12493. https://doi.org/10.1021/jp074606m

Peters, B., Zimmermann, N. E. R., Beckham, G. T., Tester, J. W., & Trout, B. L. (2008). Path sampling calculation of methane diffusivity in natural gas hydrates from a water-vacancy assisted mechanism. *Journal of the American Chemical Society*, *130*(51), 17342–17350. https://doi.org/10.1021/ja802014m

Phrampus, B. J., & Hornbach, M. J. (2012). Recent changes to the Gulf Stream causing widespread gas hydrate destabilization. *Nature*, *490*(7421), 527–530. https://doi.org/10.1038/nature11528

Phrampus, B. J., Hornbach, M. J., Ruppel, C. D., & Hart, P. E. (2014). Widespread gas hydrate instability on the upper U.S. Beaufort margin. *Journal of Geophysical Research: Solid Earth*, *119*, 8594–8609. https://doi.org/10.1002/2014JB011290

Pitzer, K. S. (1991). Ion interaction approach: theory and data correlation. In K. S. Pitzer (Ed.), *Activity coefficients in electrolyte solutions* (pp. 75–153). Boca Raton, Florida: CRC Press.

Portnov, A., Cook, A. E., Sawyer, D. E., Yang, C., Hillman, J. I. T., & Waite, W. F. (2019). Clustered BSRs: Evidence for gas hydrate-bearing turbidite complexes in folded regions, example from the Perdido Fold Belt, northern Gulf of Mexico. *Earth and Planetary Science Letters*, *528*, 115843. https://doi.org/10.1016/j.epsl.2019.115843

Portnov, A., Smith, A. J., Mienert, J., Cherkashov, G., Rekant, P., Semenov, P., et al. (2013). Offshore permafrost decay and massive seabed methane escape in water depths %3E20m at the South Kara Sea shelf. *Geophysical Research Letters*, *40*, 3962–3967. https://doi.org/10.1002/grl.50735

Portnov, A., Vadakkepuliyambatta, S., Mienert, J., & Hubbard, A. (2016). Ice-sheet-driven methane storage and release in the Arctic. *Nature Communications*, *7*. https://doi.org/10.1038/ncomms10314

Priegnitz, M., Thaler, J., Spangenberg, E., Rucker, C., & Schicks, J. M. (2013). A cylindrical electrical resistivity tomography array for three-dimensional monitoring of hydrate formation and dissociation. *Review of Scientific Instruments*, *84*(10). https://doi.org/10.1063/1.4825372

Priegnitz, M., Thaler, J., Spangenberg, E., Schicks, J. M., Schrotter, J., & Abendroth, S. (2015). Characterizing electrical properties and permeability changes of hydrate bearing sediments using ERT data. *Geophysical Journal International*, *202*(3), 1599–1612. https://doi.org/10.1093/gji/ggv245

Qian, J., Wang, X., Collett, T. S., Guo, Y., Kang, D., & Jin, J. (2018). Downhole log evidence for the coexistence of Structure II gas hydrate and free gas below the bottom simulating reflector in the South China Sea. *Marine and Petroleum Geology*, *98*, 662–674. https://doi.org/10.1016/j.marpetgeo.2018.09.024

Rachold, V., Bolshiyanov, D. Y., Grigoriev, M. N., Hubberten, H.-W., Junker, R., Kunitsky, V. V., et al. (2007). Nearshore Arctic subsea permafrost in transition. *Eos, Transactions American Geophysical Union*, *88*, 149. https://doi.org/10.1029/2007eo130001

Radhakrishnan, R., & Trout, B. L. (2002). A new approach for studying nucleation phenomena using molecular simulations: Application to CO_2 hydrate clathrates. *The Journal of Chemical Physics*, *117*(4), 1786–1796. https://doi.org/10.1063/1.1485962

Ranieri, U., Koza, M. M., Kuhs, W. F., Klotz, S., Falenty, A., Gillet, P., & Bove, L. E. (2017). Fast methane diffusion at the interface of two clathrate structures. *Nature Communications*, *8*(1), 1076–1076. https://doi.org/10.1038/s41467-017-01167-2

Reeburgh, W. S. (2007). Oceanic methane biogeochemistry. *Chemical Reviews*, *107*(2), 486–513. https://doi.org/10.1021/cr050362v

Rehder, G., Brewer, P. W., Peltzer, E. T., & Friederich, G. (2002). Enhanced lifetime of methane bubble streams within the deep ocean. *Geophysical Research Letters*, *29*(15). https://doi.org/10.1029/2001GL013966

Rehder, G., Kirby, S. H., Durham, W. B., Stern, L. A., Peltzer, E. T., Pinkston, J., & Brewer, P. G. (2004). Dissolution rates of pure methane hydrate and carbon-dioxide hydrate in undersaturated seawater at 1000-m depth. *Geochimica et Cosmochimica Acta*, *68*(2), 285–292. https://doi.org/10.1016/j.gca.2003.07.001

Rehder, G., Leifer, I., Brewer, P. G., Friederich, G., & Peltzer, E. T. (2009). Controls on methane bubble dissolution inside and outside the hydrate stability field from open ocean field experiments and numerical modeling. *Marine Chemistry*, *114*(1–2), 19–30. https://doi.org/10.1016/J.Marchem.2009.03.004

Rekant, P., Bauch, H. A., Schwenk, T., Portnov, A., Gusev, E., Spiess, V., et al. (2015). Evolution of subsea permafrost landscapes in Arctic Siberia since the Late Pleistocene: A synoptic insight from acoustic data of the Laptev Sea. *Arktos*, *1*(1), 11. https://doi.org/10.1007/s41063-015-0011-y

Rempel, A. W. (2011). A model for the diffusive growth of hydrate saturation anomalies in layered sediments. *Journal of Geophysical Research*, *116*, B10105. https://doi.org/10.1029/2011JB008484

Rempel, A. W., & Buffett, B. A. (1997). Formation and accumulation of gas hydrate in porous media. *Journal of Geophysical Research*, *102*, 10,151–10,164. https://doi.org/10.1029/97JB00392

Ripmeester, J. A., & Alavi, S. (2016). Some current challenges in clathrate hydrate science: Nucleation, decomposition and the memory effect. *Current Opinion in Solid State and Materials Science*, *20*(6), 344–351. https://doi.org/10.1016/j.cossms.2016.03.005

Ripmeester, J. A., Tse, J. S., Ratcliffe, C. I., & Powell, B. M. (1987). A new clathrate hydrate structure. *Nature*, *325*(6100), 135–136. https://doi.org/10.1038/325135a0

Roberts, H. H. (2001). Fluid and gas expulsion on the Northern Gulf of Mexico continental slope: Mud-prone to mineral-prone responses. In C. K. Paull, & W. P. Dillon (Eds.), *Natural gas hydrates: Occurrence, distribution and detection* (Vol. 124, pp. 145–161). Washington D. C.: American Geophysical Union, Geophysical Monograph.

Ruppel, C., Dickens, G. R., Castellini, D. G., Gilhooly, W., & Lizarralde, D. (2005). Heat and salt inhibition of gas hydrate formation in the northern Gulf of Mexico. *Geophysical Research Letters*, *32*, L04605. https://doi.org/10.1029/2004GL021909

Ruppel, C. D. (2011). Methane hydrates and contemporary climate change. *Nature Education Knowledge*, *3*(10), 29. Available at http://www.nature.com/scitable/knowledge/library/methane-hydrates-and-contemporary-climate-change-24314790

Ruppel, C. D. (2015). Permafrost-associated gas hydrate: Is it really approximately 1% of the global system? *Journal of Chemical & Engineering Data*, *60*(2), 429–436. https://doi.org/10.1021/je500770m

Ruppel, C. D., Herman, B. M., Brothers, L. L., & Hart, P. E. (2016). Subsea ice-bearing permafrost on the U.S Beaufort Margin: 2 Borehole constraints. *Geochemistry, Geophysics, Geosystems*, *17*, 4333–4353. https://doi.org/10.1002/2016GC006582

Ruppel, C. D., & Kessler, J. D. (2017). The interaction of climate change and methane hydrates. *Reviews of Geophysics*, *55*(1), 126–168. https://doi.org/10.1002/2016RG000534

Ruppel, C. D., Lee, J. Y., & Pecher, I. (2019). Introduction to special issue on gas hydrate in porous media: Linking laboratory and field-scale phenomena. *Journal of Geophysical Research: Solid Earth*, *124*(8), 7525–7537. https://doi.org/10.1029/2019JB018186

Sassen, R., & MacDonald, I. R. (1994). Evidence of structure H hydrate, Gulf of Mexico continental slope. *Organic Geochemistry*, *22*(6), 1029–1032. https://doi.org/10.1016/0146-6380(94)90036-1

Schicks, J. M. (2018). Gas hydrates: Formation, structures, and properties. In H. Wilkes (Ed.), *Hydrocarbons, oils and lipids: Diversity, origin, chemistry and fate* (pp. 1–15). Cham: Springer International Publishing.

Schicks, J. M., & Ripmeester, J. A. (2004). The coexistence of two different methane hydrate phases under moderate pressure and temperature conditions: Kinetic versus thermodynamic products. *Angewandte Chemie International Edition*, *43*(25), 3310–3313. https://doi.org/10.1002/anie.200453898

Schoderbek, D., Farrell, H., Hester, K., Howard, J., Raterman, K., Silpngarmlert, S., et al. (2013). *ConocoPhillips gas hydrate production test final technical report*. Retrieved from https://www.netl.doe.gov/File%20Library/Research/Oil-Gas/methane%20hydrates/nt0006553-final-report-hydrates.pdf

Scholz, C. A., Klitgord, K. D., Hutchinson, D. R., ten Brink, U. S., Zonenshain, L. P., Golmshtok, A. Y., & Moore, T. C. (1993). Results of 1992 seismic reflection experiment in Lake Baikal. *Eos, Transactions American Geophysical Union*, *74*(41), 465–470. https://doi.org/10.1029/93EO00546

Seol, Y., & Kneafsey, T. J. (2009). X-ray computed-tomography observations of water flow through anisotropic methane hydrate-bearing sand. *Journal of Petroleum Science and Engineering*, *66*(3–4), 121–132. https://doi.org/10.1016/J.Petrol.2009.01.008

Serié, C., Huuse, M., & Schødt, N. H. (2012). Gas hydrate pingoes: Deep seafloor evidence of focused fluid flow on continental margins. *Geology*, *40*(3), 207–210. https://doi.org/10.1130/G32690.1

Serov, P., Portnov, A., Mienert, J., Semenov, P., & Ilatovskaya, P. (2015). Methane release from pingo-like features across the South Kara Sea shelf, an area of thawing offshore permafrost. *Journal of Geophysical Research: Earth Surface*, *120*, 1515–1529. https://doi.org/10.1002/2015JF003467

Serov, P., Vadakkepuliyambatta, S., Mienert, J., Patton, H., Portnov, A., Silyakova, A., et al. (2017). Postglacial response of Arctic Ocean gas hydrates to climatic amelioration. *Proceedings of the National Academy of Sciences of the United States of America*, *114*(24), 6215–6220. https://doi.org/10.1073/pnas.1619288114

Servio, P., & Englezos, P. (2002). Measurement of dissolved methane in water in equilibrium with its hydrate. *Journal of Chemical and Engineering Data*, *47*(1), 87–90. https://doi.org/10.1021/je0102255

Shen, X.-D., Liang, D.-Q., & Maeda, N. (2019). Growth kinetics of methane hydrate in a pilot-scale flow loop. *Energy & Fuels*, *33*(8), 7717–7725. https://doi.org/10.1021/acs.energyfuels.9b01643

Skarke, A., Ruppel, C., Kodis, M., Brothers, D., & Lobecker, E. (2014). Widespread methane leakage from the sea floor on the northern US Atlantic margin. *Nature Geoscience*, *7*(9), 657–661. https://doi.org/10.1038/ngeo2232

Skovborg, P., & Rasmussen, P. (1994). A mass transport limited model for the growth of methane and ethane gas hydrates. *Chemical Engineering Science*, *49*(8), 1131–1143. https://doi.org/10.1016/0009-2509(94)85085-2

Sloan, E. D. Jr. (2004). Introductory overview: Hydrate knowledge development. *American Mineralogist*, *89*, 1155–1161. https://doi.org/10.2138/am-2004-8-901

Sloan, E. D., & Fleyfel, F. (1991). A molecular mechanism for gas hydrate nucleation from ice. *AICHE Journal*, *37*(9), 1281–1292. https://doi.org/10.1002/aic.690370902

Sloan, E. D., & Koh, C. (2008). *Clathrate hydrates of natural gases* (3rd ed.). Boca Raton, FL: CRC Press.

Sloan, E. D., & Koh, C. A. (2007). *Clathrate hydrates of natural gases* (3rd ed., Vol. 119). Boca Raton: CRC Press.

Smith, A. J., Flemings, P. B., Liu, X., & Darnell, K. (2014). The evolution of methane vents that pierce the hydrate stability zone in the world's oceans. *Journal of Geophysical Research: Solid Earth*, *119*, 6337–6356. https://doi.org/10.1002/2013JB010686

Spangenberg, E., Kulenkampff, J., Naumann, R., & Erzinger, J. (2005). Pore space hydrate formation in a glass bead sample from methane dissolved in water. *Geophysical Research Letters*, *32*, L24301. https://doi.org/10.1029/2005GL024107

Stern, L. A., Circone, S., Kirby, S. H., & Durham, W. B. (2003). Temperature, pressure, and compositional effects on anomalous or "self" preservation of gas hydrates. *Canadian Journal of Physics*, *81*(1–2), 271–283. https://doi.org/10.1139/p03-018

Stern, L. A., Kirby, S. H., Circone, S., & Durham, W. B. (2004). Scanning Electron Microscopy investigations of laboratory-grown gas clathrate hydrates formed from melting ice, and comparison to natural hydrates. *American Mineralogist*, *89*(8–9), 1162–1175. https://doi.org/10.2138/am-2004-8-902

Stranne, C., O'Regan, M., & Jakobsson, M. (2016). Overestimating climate warming-induced methane gas escape from the seafloor by neglecting multiphase flow dynamics. *Geophysical Research Letters*, *43*, 8703–8712. https://doi.org/10.1002/2016GL070049

Subramanian, S., Kini, R. A., Dec, S. F., & Sloan, E. D. Jr. (2000). Structural transition studies in methane + ethane hydrates using Raman and NMR. *Annals of the New York Academy of Sciences*, *912*(1), 873–886. https://doi.org/10.1111/j.1749-6632.2000.tb06841.x

Subramanian, S., & Sloan, E. D. (2002). Solubility effects on growth and dissolution of methane hydrate needles. In *Paper presented at the 4th International Conference on Gas Hydrates, Yokohama, Japan, May 19–23, 2002* (pp. 856–861).

Sun, R., & Duan, Z. (2007). An accurate model to predict the thermodynamic stability of methane hydrate and methane solubility in marine environments. *Chemical Geology*, *244*(1–2), 248–262. https://doi.org/10.1016/j.chemgeo.2007.06.021

Sun, R., & Duan, Z. H. (2005). Prediction of CH_4 and CO_2 hydrate phase equilibrium and cage occupancy from ab initio intermolecular potentials. *Geochimica et Cosmochimica Acta*, *69*(18), 4411–4424. https://doi.org/10.1016/j.gca.2005.05.012

Sun, X. F., & Mohanty, K. K. (2006). Kinetic simulation of methane hydrate formation and dissociation in porous media. *Chemical Engineering Science*, *61*(11), 3476–3495. https://doi.org/10.1016/j.ces.2005.12.017

Taylor, A. E., Dallimore, S. R., Hill, P. R., Issler, D. R., Blasco, S., & Wright, F. (2013). Numerical model of the geothermal regime on the Beaufort Shelf, arctic Canada since the Last Interglacial. *Journal of Geophysical Research: Earth Surface*, *118*, 2365–2379. https://doi.org/10.1002/2013JF002859

Taylor, C. J., Miller, K. T., Koh, C. A., & Sloan, E. D. (2007). Macroscopic investigation of hydrate film growth at the hydrocarbon/water interface. *Chemical Engineering Science*, *62*(23), 6524–6533. https://doi.org/10.1016/j.ces.2007.07.038

Tishchenko, P., Hensen, C., Wallmann, K., & Wong, C. S. (2005). Calculation of the stability and solubility of methane hydrate in seawater. *Chemical Geology*, *219*(1–4), 37–52. https://doi.org/10.1016/j.chemgeo.2005.02.008

Tohidi, B., Anderson, R., Clennell, M. B., Burgass, R. W., & Biderkab, A. B. (2001). Visual observation of gas-hydrate formation and dissociation in synthetic porous media by means of glass micromodels. *Geology*, *29*(9), 867–870. https://doi.org/10.1130/0091-7613(2001)029%3C0867:vooghf%3E2.0.co;2

Tohidi, B., Østergaard, K. K., Danesh, A., Todd, A. C., & Burgass, R. W. (2001). Structure-H gas hydrates in petroleum reservoir fluids. *The Canadian Journal of Chemical Engineering*, *79*(3), 384–391. https://doi.org/10.1002/cjce.5450790311

Torres, M. E., Wallmann, K., Trehu, A. M., Bohrmann, G., Borowski, W. S., & Tomaru, H. (2004). Gas hydrate growth, methane transport, and chloride enrichment at the southern summit of Hydrate Ridge, Cascadia margin off Oregon. *Earth and Planetary Science Letters*, *226*(1–2), 225–241. https://doi.org/10.1016/j.epsl.2004.07.029

Tryon, M. D., Brown, K. M., & Torres, M. E. (2002). Fluid and chemical flux in and out of sediments hosting methane hydrate deposits on Hydrate Ridge, OR, II: Hydrological processes. *Earth and Planetary Science Letters*, *201*(3–4), 541–557. https://doi.org/10.1016/S0012-821X(02)00732-X

Tryon, M. D., Brown, K. M., Torres, M. E., Tréhu, A. M., McManus, J., & Collier, R. W. (1999). Measurements of transience and downward fluid flow near episodic methane gas vents, Hydrate Ridge, Cascadia. *Geology*, *27*(12), 1075–1078. https://doi.org/10.1130/0091-7613(1999)027%3C1075:MOTADF%3E2.3.CO;2

Uchida, T., Ebinuma, T., & Narita, H. (2000). Observations of CO_2-hydrate decomposition and reformation processes. *Journal of Crystal Growth*, *217*(1), 189–200. https://doi.org/10.1016/S0022-0248(00)00470-X

Uchida, T., & Tsuji, T. (2004). Petrophysical Properties of Natural Gas Hydrates-Bearing Sands and Their Sedimentology in the Nankai Trough. *Resource Geology*, *54*(1), 79–87. https://doi.org/10.1111/j.1751-3928.2004.tb00189.x

Uchida, T., Waseda, A., & Namikawa, T. (2009). Methane accumulation and high concentration of gas hydrate in marine and terrestrial sandy sediments. In T. Collett, A. Johnson, C. Knapp, & R. Boswell (Eds.), *Chapter 13, Natural gas hydrates-Energy resource potential and associated geologic hazards* (Vol. 89, pp. 401–413). Tulsa, OK: American Association of Petroleum Geologists. https://doi.org/10.1306/13201154M893351

Uchida, T., Yamazaki, K., & Gohara, K. (2016). Generation of micro- and nano-bubbles in water by dissociation of gas hydrates. *Korean Journal of Chemical Engineering*, *33*. https://doi.org/10.1007/s11814-016-0032-7

Van Dover, C. L., Aharon, P., Bernhard, J. M., Caylor, E., Doerries, M., Flickinger, W., et al. (2003). Blake Ridge methane seeps: Characterization of a soft-sediment, chemo synthetically based ecosystem. *Deep-Sea Research Part I-Oceanographic Research Papers*, *50*(2), 281–300. https://doi.org/10.1016/S0967-0637(02)00162-0

VanderBeek, B. P., & Rempel, A. W. (2018). On the importance of advective versus diffusive transport in controlling the distribution of methane hydrate in heterogeneous marine sediments. *Journal of Geophysical Research: Solid Earth*, *123*, 5394–5411. https://doi.org/10.1029/2017JB015298

Vatamanu, J., & Kusalik, P. G. (2006). Molecular insights into the heterogeneous crystal growth of sI methane hydrate. *The Journal of Physical Chemistry B*, *110*(32), 15,896–15,904. https://doi.org/10.1021/jp061684l

Vatamanu, J., & Kusalik, P. G. (2010). Observation of two-step nucleation in methane hydrates. *Physical Chemistry Chemical Physics*, *12*(45), 15,065–15,072. https://doi.org/10.1039/C0CP00551G

Vysniauskas, A., & Bishnoi, P. R. (1983). A kinetic study of methane hydrate formation. *Chemical Engineering Science*, *38*(7), 1061–1072. https://doi.org/10.1016/0009-2509(83)80027-X

Waage, M., Portnov, A., Serov, P., Bünz, S., Waghorn, K. A., Vadakkepuliyambatta, S., et al. (2019). Geological controls on fluid flow and gas hydrate pingo development on the Barents Sea Margin. *Geochemistry, Geophysics, Geosystems*, *20*, 630–650. https://doi.org/10.1029/2018GC007930

Wadham, J. L., Arndt, S., Tulaczyk, S., Stibal, M., Tranter, M., Telling, J., et al. (2012). Potential methane reservoirs beneath Antarctica. *Nature*, *488*(7413), 633–637. https://doi.org/10.1038/nature11374

Waite, W. F. (2012). *Methane solubility [computer software] MATLAB central file exchange*. Retrieved from https://www.mathworks.com/matlabcentral/fileexchange/36963-methane-solubility

Waite, W. F., Kneafsey, T. J., Winters, W. J., & Mason, D. H. (2008). Physical property changes in hydrate-bearing sediment due to depressurization and subsequent repressurization. *Journal of Geophysical Research*, *113*, B07102. https://doi.org/10.01029/02007JB005351

Waite, W. F., Ruppel, C. D., Boze, L. G., Lorenson, T. D., Buckzowski, B. J., McMullen, K., & Kvenvolden, K. A. (2020). *Preliminary global database of known and inferred gas hydrate locations*. U.S. Geological Survey data release. https://doi.org/10.5066/P9llFVJM

Waite, W. F., Ruppel, C. D., Collett, T. S., Schultheiss, P., Holland, M., Shukla, K. M., & Kumar, P. (2019). Multi-measurement approach for establishing the base of gas hydrate occurrence in the Krishna-Godavari Basin for sites cored during expedition NGHP-02 in the offshore of India. *Marine and Petroleum Geology*, *108*, 296–320. https://doi.org/10.1016/j.marpetgeo.2018.07.026

Waite, W. F., Santamarina, J. C., Cortes, D. D., Dugan, B., Espinoza, D. N., Germaine, J., et al. (2009). Physical properties of hydrate-bearing sediments. *Reviews of Geophysics*, *47*, RG4003. https://doi.org/10.1029/2008RG000279

Waite, W. F., & Spangenberg, E. (2013). Gas hydrate formation rates from dissolved-phase methane in porous laboratory specimens. *Geophysical Research Letters*, *40*, 4310–4315. https://doi.org/10.1002/grl.50809

Waite, W. F., Stern, L. A., Kirby, S. H., Winters, W. J., & Mason, D. H. (2007). Simultaneous determination of thermal conductivity, thermal diffusivity and specific heat in sI methane hydrate. *Geophysical Journal International*, *169*, 767–774. https://doi.org/10.1111/j.1365-1246X.2007.03382.x

Walsh, M. R., Koh, C. A., Sloan, E. D., Sum, A. K., & Wu, D. T. (2009). Microsecond simulations of spontaneous methane hydrate nucleation and growth. *Science*, *326*(5956), 1095–1098. https://doi.org/10.1126/science.1174010

Wang, B. B., Socolofsky, S. A., Breier, J. A., & Seewald, J. S. (2016). Observations of bubbles in natural seep flares at MC 118 and GC 600 using in situ quantitative imaging. *Journal of Geophysical Research: Oceans*, *121*, 2203–2230. https://doi.org/10.1002/2015JC011452

Warzinski, R. P., Lynn, R., Haljasmaa, I., Leifer, I., Shaffer, F., Anderson, B. J., & Levine, J. S. (2014). Dynamic morphology of gas hydrate on a methane bubble in water: Observations and new insights for hydrate film models. *Geophysical Research Letters*, *41*, 6841–6847. https://doi.org/10.1002/2014gl061665

Windmeier, C., & Oellrich, L. R. (2013). Theoretical study of gas hydrate decomposition kinetics: Model predictions. *Journal of Physical Chemistry A*, *117*(47), 12,184–12,195. https://doi.org/10.1021/jp406837q

Witherspoon, P. A., & Bonoli, L. (1969). Correlation of Diffusion Coefficients for Paraffin, Aromatic, and Cycloparaffin Hydrocarbons in Water. *Industrial and Engineering Chemistry Fundamentals*, *8*(3), 589–591. https://doi.org/10.1021/i160031a038

Witherspoon, P. A., & Saraf, D. N. (1965). Diffusion of methane, ethane, propane, and n-butane in water from 25 to 43°. *Journal of Physical Chemistry*, *69*(11), 3752–3755. https://doi.org/10.1021/j100895a017

Wood, W. T., Gettrust, J. F., Chapman, N. R., Spence, G. D., & Hyndman, R. D. (2002). Decreased stability of methane hydrates in marine sediments owing to phase-boundary roughness. *Nature*, *420*(6916), 656–660. https://doi.org/10.1038/nature01263

Xu, W., & Ruppel, C. (1999). Predicting the occurrence, distribution, and evolution of methane gas hydrate in porous marine sediments. *Journal of Geophysical Research*, *104*(B3), 5081–5095. https://doi.org/10.1029/1998JB900092

Yamamoto, K., Kanno, T., Wang, X. X., Tamaki, M., Fujii, T., Chee, S. S., et al. (2017). Thermal responses of a gas hydrate-bearing sediment to a depressurization operation. *RSC Advances*, *7*(10), 5554–5577. https://doi.org/10.1039/c6ra26487e

Yang, S., Liang, J., Lei, Y., Gong, Y., Xu, H., & Wang, H. (2017). GMGS4 gas hydrate drilling expedition in the South China Sea. *DOE/NETL Fire in the Ice Newsletter*, *17*(1), 7–11.

Yang, X., Sun, C. Y., Su, K. H., Yuan, Q., Li, Q. P., & Chen, G. J. (2012). A three-dimensional study on the formation and dissociation of methane hydrate in porous sediment by depressurization. *Energy Conversion and Management*, *56*, 1–7. https://doi.org/10.1016/j.enconman.2011.11.006

Ye, J.-L., Qin, X.-W., Qiu, H.-J., Liang, Q.-Y., Dong, Y.-F., Wei, J.-G., et al. (2018). Preliminary results of environmental monitoring of the natural gas hydrate production test in the South China Sea. *China Geology*, *1*, 202–209. https://doi.org/10.31035/cg2018029

Yin, Z., Khurana, M., Tan, H. K., & Linga, P. (2018). A review of gas hydrate growth kinetic models. *Chemical Engineering Journal*, *342*, 9–29. https://doi.org/10.1016/j.cej.2018.01.120

Yin, Z. Y., Chong, Z. R., Tan, H. K., & Linga, P. (2016). Review of gas hydrate dissociation kinetic models for energy recovery. *Journal of Natural Gas Science and Engineering*, *35*, 1362–1387. https://doi.org/10.1016/j.jngse.2016.04.050

Yoneda, J., Oshima, M., Kida, M., Kato, A., Konno, Y., Jin, Y., et al. (2019). Permeability variation and anisotropy of gas hydrate-bearing pressure-core sediments recovered from the Krishna-Godavari Basin, offshore India. *Marine and Petroleum Geology*, *108*. https://doi.org/10.1016/j.marpetgeo.2018.07.006

You, K., Flemings, P. B., Malinverno, A., Collett, T. S., & Darnell, K. (2019). Mechanisms of methane hydrate formation in geological systems. *Reviews of Geophysics*, *57*, 1146–1196. https://doi.org/10.1029/2018RG000638

Yousif, M. H., & Sloan, E. D. (1991). Experimental investigation of hydrate formation and dissociation in consolidated porous media. *SPE Reservoir Engineering*, *6*(4), 452–458. https://doi.org/10.2118/20172-PA

Zatsepina, O. Y., & Buffett, B. A. (1997). Phase equilibrium of gas hydrate: Implications for the formation of hydrate in the deep-sea floor. *Geophysical Research Letters*, *24*(13), 1567–1570. https://doi.org/10.1029/97GL01599

Zatsepina, O. Y., & Buffett, B. A. (1998). Thermodynamic conditions for the stability of gas hydrate in the seafloor. *Journal of Geophysical Research*, *103*(B10), 24,127–24,139. https://doi.org/10.1029/98JB02137

Zhang, Y., Zhao, L., Deng, S., Zhao, R., Nie, X., & Liu, Y. (2019). Effect of nanobubble evolution on hydrate process: A review. *Journal of Thermal Science*, *28*(5), 948–961. https://doi.org/10.1007/s11630-019-1181-x